Preprint; cite as *Chem. Eng. Sci.* **171** (2017) 520–533

Evaporating Foam Films of Pure Liquid Stabilized via the Thermal Marangoni Effect

Javor K. Novev[1], Nikolay Panchev[2], Radomir I. Slavchov[3]*

[1]*Department of Chemistry, Physical and Theoretical Chemistry Laboratory, University of Oxford, Oxford OX1 3QZ, UK*

[2]*Institute of Physical Chemistry, Bulgarian Academy of Sciences, Sofia 1113, Bulgaria*

[3]*Department of Chemical Engineering and Biotechnology, University of Cambridge, Cambridge CB2 3RA, UK*

** Corresponding author (ris26@cam.ac.uk)*

Abstract. A foam film made of pure liquid can be stabilized by evaporation. This is demonstrated experimentally for water and alkane films formed in a Scheludko cell at controlled saturation of the ambient air. A mechanism of the stabilization is proposed – evaporation leads to a local decrease of the temperature in the centre of the film; the meniscus acts as a thermostat and maintains a higher temperature at the film periphery. The resulting temperature gradient brings about a surface tension gradient causing a stabilizing thermal Marangoni flow that carries fluid from the meniscus to the interior of the film. The film thickness is quasi-stationary and gradually decreases as the meniscus cools due to the evaporation. At a certain critical meniscus temperature, the film reaches a critical thickness at which the Marangoni effect can no longer counteract the combined action of the capillary pressure and the van der Waals attraction, and the film breaks. The lifetime of the film is estimated as a function of the film geometry and the experimental conditions (temperature, saturation, vapour pressure, capillary pressure). The theoretical and the experimental results for the lifetime and the critical thickness are in qualitative agreement for films at moderate saturation.

Keywords: Marangoni effect; evaporation; foam film stability; surfactant-free films; Scheludko cell; alkane films.

Contents

I.Introduction

The drainage and stability of thin liquid films determine the properties of a broad range of objects, including foam, bakery yeast (Exerowa and Kruglyakov, 1998), cement (Du and Folliard, 2005), water-crude oil emulsions (Sullivan and Kilpatrick, 2002), and many others. The process of evaporation is known to influence the stability of these films. In particular, there are numerous studies on evaporating *wetting films* on solid substrates due to their importance for certain technological processes, such as fibre optic coating, semiconductor chip deposition (Danov et al., 1998), fuel atomization in engines (Baumgarten, 2006), etc. Evaporation interferes with these processes primarily by causing Marangoni flows (Baumgarten, 2006; Danov et al., 1998; Sultan et al., 2005; Yiantsios and Higgins, 2006; Zuiderweg and Harmens, 1958). In contrast, the research on evaporating *foam films* is quite limited (Manev and Nguyen, 2005) and to our knowledge, only a handful of studies devote significant attention to evaporating thin films containing no surfactant, e.g. (Yaminsky et al., 2010a). The related problem for evaporation of sessile drops from pure liquids has been studied in greater depth (Chandramohan et al., 2016; Hu and Larson, 2006, 2005).

Evaporation has a twofold effect on the stability of thin films – by taking away heat and mass from the film, it brings about thermal Marangoni flows (driven by a temperature gradient) and Gibbs-Marangoni flows (driven by concentration gradients in multicomponent liquids). In the case of a wetting film, the solid substrate acts as a thermostat and reduces the magnitude of the thermal Marangoni effect. Due to the absence of this thermostating effect, it can be expected that the Marangoni flow is stronger in evaporating foam films. There are hints in the literature in support of this hypothesis. For example, Li et al. (Li et al., 2012) reported that bubbles formed from *surfactant solutions* burst under non-uniform evaporation. In their experiment, evaporation leads to a local thinning of the liquid films, as well as to a local increase of the surfactant concentration, resulting in a gradient of the surface tension σ. This gradient causes a Marangoni flux away from the thinner region of more intense evaporation and leads to the bursting of the bubble. In contrast, Manev et al. (Manev, 1975; Manev and Nguyen, 2005) studied evaporating foam films formed from surfactant solutions in a Scheludko cell and found no significant effect

of evaporation in these systems. Yaminsky et al. (Yaminsky, 2006; Yaminsky et al., 2010a, 2010b) hypothesized that evaporation-driven Marangoni effects are the cause of the stabilization of the foam films they observed in a variety of experimental setups. Their *surfactant-free* films reacted particularly strongly to evaporation. Yaminsky (Yaminsky, 2006) reported that when a small air bubble attaches to the interface between air and a *pure liquid* containing no surfactant, its behaviour is dependent upon the saturation – if the air is saturated with vapour, the bubble coalesces immediately. Conversely, in an unsaturated environment, the air|liquid|air film formed upon contact between the bubble and the surface remains stable over an indefinite period of time. Another interesting phenomenon occurring in evaporating films free of surfactant was reported by Karakashev and co-authors (Karakashev et al., 2008). Contrary to expectations based on the Derjaguin-Landau-Verwey-Overbeek theory, their foam films exhibited significant stability (lifetime ~100 s) and a complex dynamic behaviour despite being formed from *concentrated solutions of inorganic electrolytes*. This anomalous stability was only displayed when the surrounding gas was undersaturated with respect to the vapour pressure of the salt solution (Karakashev et al., 2008).

These reports suggest that evaporation plays a key role in the stabilization of surfactant-free foam films against the capillary pressure-driven drainage and generated our interest in exploring this topic. The salt films studied by Karakashev et al. (Karakashev et al., 2008) are complex systems – the observed intensive fluxes must be affected by the evaporation-induced gradient of the electrolyte concentration and the effect of the electrolyte on surface tension (Slavchov and Novev, 2012). Evidently, evaporation-driven Gibbs-Marangoni flows are also present in surfactant solutions – for this reason, trace amounts of surfactant have a *destabilizing* effect on evaporating films of pure liquid (Yaminsky et al., 2010a). Instead of tackling the complicated problem of two-component films, in this study we explore the simpler case of an evaporating film comprised of pure liquid, where only the thermal Marangoni effect is present.

Even in this case, however, the behaviour of the film is influenced by many factors other than the relative saturation, complicating the interpretation of the experimental data. There is no consensus in the literature about the stability of pure water foam films even in the absence of evaporation (Peng and Chang, 2014) – while some authors state that they rupture instantly and even use this as a criterion for the purity of their experimental setup (Karakashev et al., 2008; Nguyen and Nguyen, 2010), others report stable films of this kind (Exerowa, 1969; Exerowa and

Kruglyakov, 1998; Yaminsky et al., 2010a). The reported lifetime of such films varies by orders of magnitude depending on the method used for their preparation. Karakashev and Firouzi (Karakashev and Firouzi, 2014) observed stable water films; however, they became unstable following a 200-fold flushing of the entire cell with water. In a saturated environment, after the flushing, pure water films were found to have a lifetime of ~5 s, reaching a thickness of ~30 nm before rupture. In an undersaturated environment, such films ruptured instantly.

Several studies report that the stability of pure water films is also dependent upon the approach velocity of the two water|air interfaces (Del Castillo et al., 2011; Firouzi and Nguyen, 2014; Wang and Qu, 2012; Yaminsky, 2006; Yaminsky et al., 2010a, 2010b). In a saturated environment, if the velocity is above a certain critical value (35 μm/s (Firouzi and Nguyen, 2014), 200 μm/s (Yaminsky et al., 2010b) or less than 11 μm/s (Wang and Qu, 2012)), the two surfaces coalesce instantly. Firouzi and Nguyen (Firouzi and Nguyen, 2014) found that films live for several seconds at an approach velocity of under 35 μm/s. Yaminsky et al. reported a similar finding at both saturated (Yaminsky et al., 2010b) and undersaturated (Yaminsky et al., 2010a) conditions: for approach velocities between ~1 and ~100 μm/s, the average lifetime of their films was about a minute, while below 1 μm/s, it was of the order of hours. Numerous studies devoted to the coalescence of gas bubbles with the water|air interface show a similar dependence on the approach velocity (Del Castillo et al., 2011; Katsir and Marmur, 2014a, 2014b). The stability at low approach rates is attributed to electrostatic repulsion between the two interfaces (Katsir and Marmur, 2014b; Yaminsky et al., 2010b). It is not entirely clear what the cause for this electrostatic repulsion is or by what mechanism it is overcome at high approach rates. Finally, a persistent reason for contradicting reports is the presence of surface-active impurities. Such impurities generally stabilize films under saturated conditions; however, evaporating films made of pure liquid can in fact be destabilized by trace quantities of surfactants (Yaminsky et al., 2010a).

The short review above demonstrates that, though it may not be entirely consistent, there is a body of evidence indicating that *films formed from single-component liquids may be stabilized by evaporation*. Our aim in this study is to clarify the question by **(i)** considering the possible mechanism of stabilization theoretically and **(ii)** investigating evaporating films experimentally under controlled saturation of the ambient air. The basic hypothesis we will test is that evaporation gives rise to a thermal Marangoni effect – an idea formulated by Yaminski et al.

(Yaminsky et al., 2010a). The model we will present in Section II generalizes the classical Maxwell-Langmuir-Fuchs theory (Fuchs, 1959) of the evaporation of a *spherical* droplet to an approximate geometry mimicking the biconcave droplet in the Scheludko cell (Sheludko, 1967); it can also be viewed as a thermal-Marangoni-effect-analogue of Marrucci's theory of the stabilization of films by the Gibbs-Marangoni effect (Marrucci, 1969). For the purpose of testing the qualitative predictions of this model, we performed experiments with evaporating films made of pure water and alkanes under controlled saturation of the ambient air. The results are discussed in Section III.

II.A model for the stability of an evaporating film

The model we develop considers a disc-shaped *foam film* in contact with a ring-like *meniscus*. This mimics the common experimental setup for studying foam films – the Scheludko cell (Sheludko, 1967), Figure 1A, where the film is formed by withdrawing liquid from a biconcave drop situated in a glass capillary (film holder). The typical dimensions in this setup are $R_c \sim 2$ mm for the radius of the capillary, $R_f \sim 150$ μm for the film radius and $h \sim 100$ nm for the film thickness (for the reader's convenience, all symbols and parameter values are tabulated in the supplement S1). The capillary is at a fixed position inside a container filled with air of controlled saturation, Figure 1B; the container is a cylinder of radius $R_{cont} \sim 1$ cm and height $L_{cont} \sim 9$ cm. For all experiments, it is fulfilled that $h << R_f << R_c < R_{cont}$. In most cases, the observed films are approximately plane-parallel – the thickness of the film zone is homogeneous, resulting in homogeneous colour, Figure 1C.

The evaporation gives rise to several conjugated processes in this system:

(i) as evaporation is endothermic, it causes a local temperature drop to develop within the thin film. The temperature of the meniscus is affected to a lesser degree because both the relatively large amount of liquid in it and the glass wall that is in contact with it exert a thermostating effect. This produces a radial temperature gradient, ∇T, in the film.

(ii) The temperature gradient ∇T, in turn, leads to a surface tension gradient, $\nabla \sigma$, which is the driving force for an influx of liquid from the meniscus towards the film, i.e., for a stabilizing Marangoni flow.

(iii) The stabilizing force $\nabla\sigma$ acts against three destabilizing factors: the evaporative mass flux, the capillary pressure and the attractive disjoining pressure, all of which take away liquid from the film. The thermal Marangoni effect slows down the thinning of the film and may eventually lead to the establishment of a stationary film thickness similar to the one caused by the Gibbs-Marangoni effect in Marrucci's theory of coalescence (Marrucci, 1969).

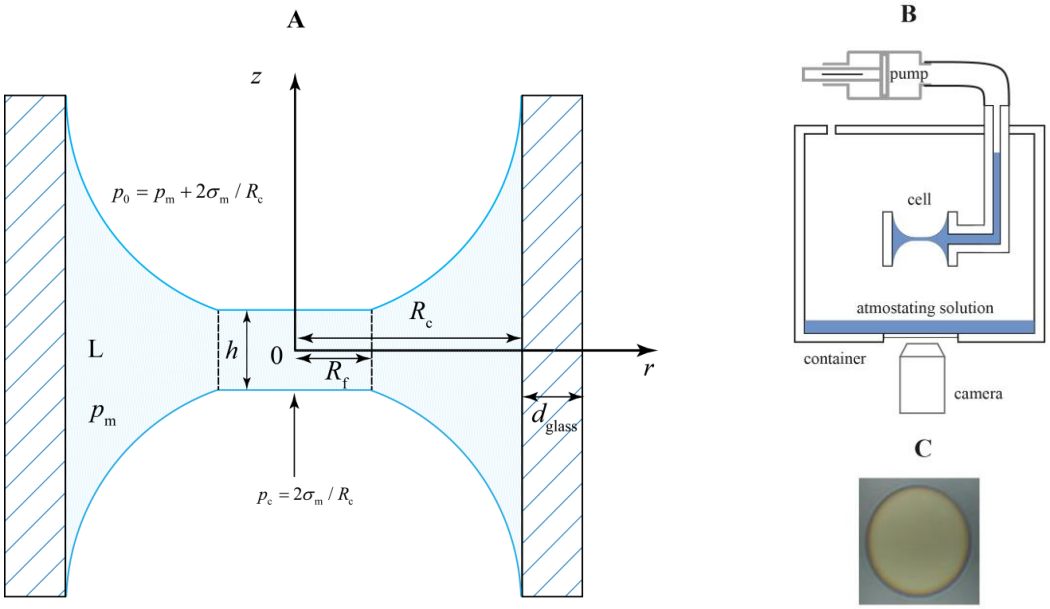

Figure 1. Scheme of a foam film formed in a Scheludko cell. **A**. A disc-shaped film is in contact with a biconcave meniscus that sticks to the wall of a capillary of inner radius R_c ~ 2 mm. The pressure p_m in the meniscus is lower than the atmospheric p_0 by the capillary pressure $2\sigma_m/R_c$, eq. (2), which causes drainage of the film. **B**. The capillary is fixed via a glass tube at height of ~1 cm inside a container (cylinder of radius R_{cont} ~ 1 cm and height L_{cont} ~ 9 cm), the bottom of which is covered by a layer of 'atmostating liquid' maintaining constant humidity. The container was normally sealed, but in some cases it was opened to expose the film to the humidity of the laboratory. **C**. Image of a typical aqueous film and its periphery (focussed on the film zone). The colour corresponds to homogeneous thickness of about h = 110 nm; the film radius is R_f = 200 μm.

A water droplet in dry air is, from Fuchs's *eq. 6.6* (Fuchs, 1959), cooler than its environment by ~20 K once a steady state is reached. A similar temperature difference must occur between the fluid in the meniscus and the ambient gas. The difference between the meniscus and the centre of the film is much smaller (~0.1 K, as will be shown below), yet it is large enough to cause a considerable Marangoni flow, since the surfactant-free liquid surface is highly mobile.

1. Hydrodynamics

A disc-shaped plane-parallel film in contact with a biconcave droplet (Figure 1) drains under the action of the capillary pressure and – for sufficiently thin films – surface forces. As $h << R_f$, the *lubrication approximation* is applicable to the flow within the film (Reynolds, 1886). In addition, the *capillary flow approximation* can be used as $Re \sim 10^{-9}$.

Most practically observed foam films contain at least trace quantities of surfactants, which lead to nearly complete tangential immobilization of the liquid surface ($v_r|_{z=h/2} = 0$) and film drainage according to the Reynolds law (Radoëv et al., 1974; Sheludko, 1967). In contrast, the films we study consist of a single-component liquid and have free mobile surfaces. Therefore, both the normal and tangential velocities can be non-zero at the surfaces of the film,

$$v_r|_{z=\pm h/2} = V_r(r) \quad \text{and} \quad v_z|_{z=\pm h/2} = V_z, \tag{1}$$

where V_z is independent of r. The pressure p_m in the meniscus is lower than p_0 in the gas phase:

$$p_m = p_0 - 2\sigma_m / R_c\,, \tag{2}$$

where σ_m is the tension of the surface of the meniscus. Since $R_f << R_c$, the meniscus (which has the shape of a nodoid) is almost spherical and the capillary pressure is $p_c = 2\sigma_m/R_c$ to a good approximation (Sheludko, 1967). The capillary pressure drives the drainage of the film, which is counteracted by the Marangoni effect dictated by the evaporation-induced surface tension gradient $d\sigma/dr$. The latter exerts a tangential force at the film surface, which is balanced by the rz-component of the viscous stress tensor (Levich, 1962; Radoëv et al., 1974):

$$\frac{d\sigma}{dr} = \eta \left.\frac{\partial v_r}{\partial z}\right|_{z=h/2}, \tag{3}$$

where η is the viscosity of the liquid. The gradient $d\sigma/dr$ originates from the difference between the heat capacities of the meniscus and the film, which results into different cooling rates of the two regions and, therefore, a temperature gradient ∇T^L in the film. For a liquid far from its critical temperature, the dependence of σ on T^L is linear (Palit, 1956):

$$\sigma(r) = \sigma_m - s^S \left(T^L(r) - T_m\right), \tag{4}$$

where $T^L(r)$ is the temperature profile in the film, $s^S = -\partial\sigma/\partial T$ is the surface entropy of the liquid, T_m is the temperature of the meniscus.

Using the above relations as boundary conditions for the Navier-Stokes equations, the tangential and normal velocities v_r and v_z, the pressure distribution $p(r)$ and the radial surface velocity V_r of the film can be expressed with $T^{\mathrm{L}}(r)$ and V_z:

$$v_r = -\frac{h^2 - 4z^2}{8\eta}\frac{\mathrm{d}p}{\mathrm{d}r} + V_r(r)\ , \tag{5}$$

$$v_z = \frac{3h^2 z - 4z^3}{24\eta}\frac{1}{r}\frac{\mathrm{d}}{\mathrm{d}r}\left(r\frac{\mathrm{d}p}{\mathrm{d}r}\right) - \frac{z}{r}\frac{\mathrm{d}rV_r(r)}{\mathrm{d}r}\ , \tag{6}$$

$$p(r) = p_{\mathrm{m}} - \frac{2}{h}s^{\mathrm{S}}\left(T^{\mathrm{L}}(r) - T_{\mathrm{m}}\right), \tag{7}$$

$$V_r(r) = -\frac{hs^{\mathrm{S}}}{6\eta}\frac{\partial T^{\mathrm{L}}}{\partial r} - \frac{r}{h}V_z\ . \tag{8}$$

these expressions are derived in S2; the derivation is similar to that for other film drainage problems, see e.g. (Radoëv et al., 1974).

2. Heat and mass transfer

The evaporation of the biconcave droplet causes cooling of the liquid in the film and the meniscus. However, the meniscus remains warmer due to the thermostating effect of both the large quantity of liquid there and the glass holder. The resulting temperature gradient is controlled by the balance between the heat lost due to evaporation and the heat flux Q through the gas phase (we show in S3.5 that the heat flux through the liquid is negligible).

We assume that the temperature T_{m} of the meniscus is homogeneous, whereas the temperature of the film is a quadratic function of r. Thus, the difference between the temperature of the surface and the ambient air, $\Delta T(r) = T^{\mathrm{L}} - T_\infty$, obeys

$$\Delta T = \begin{cases} \Delta T_{\mathrm{m}} + \dfrac{T_{rr}}{2}\left(r^2 - R_{\mathrm{f}}^2\right), & \text{film surface;} \\ \Delta T_{\mathrm{m}}, & \text{meniscus surface.} \end{cases} \tag{9}$$

Here, $\Delta T_{\mathrm{m}} = T_{\mathrm{m}} - T_\infty$ is the difference in temperature between the meniscus and the surrounding gas, and T_{rr} is a coefficient which we will determine later on. The assumption that $T(r)$ is analogous to the parabolic approximation for the profile of the temperature inside an evaporating spherical droplet (e.g., (Dombrovsky and Sazhin, 2003; Snegirev, 2013)) and is implicitly or explicitly used for many problems for thin film drainage problems that involve Gibbs- and

electro-Marangoni effects – e.g., the integration with respect to r of *eqs. 25a-b* in (Valkovska and Danov, 2001) leads to parabolic profiles of the adsorption and the electrical potential in the film. It can be expected that a better approximation of the T profile (a 4th-order polynomial) will lead to corrections of $O(h^2/R_f^2)$ in the results for the fluxes that follow.

We assume that the vapour concentration at the surface of the liquid follows the temperature profile (9) via the Clausius-Clapeyron equation,

$$C^S = \frac{p^o}{RT^L}\exp\left[-\frac{h_e}{R}\left(\frac{1}{T^L}-\frac{1}{T_e^o}\right)\right], \tag{10}$$

where p° = 101325 Pa is the standard pressure; T_e° is the temperature of boiling of the liquid at p°; h_e is its heat of evaporation, and R is the gas constant. We now substitute T^L with $T_m + \delta T(r)$, where $\delta T = \frac{1}{2}T_{rr}(r^2 - R_f^2)$ is the temperature difference between the film and the meniscus, see eq. (9). Since $\delta T << T_m$, we can expand eq. (10) in a series, which yields:

$$\Delta C^S = \begin{cases} \Delta C_m + \dfrac{C_{rr}}{2}\left(r^2 - R_f^2\right) + O(\delta T^2), & \text{film surface;} \\ \Delta C_m, & \text{meniscus surface.} \end{cases} \tag{11}$$

Here, we used the symbols

$$\Delta C^S = C^S - C_\infty; \quad \Delta C_m = C_{eq} - C_\infty; \tag{12}$$

$$C_{eq} = \frac{p^o}{RT_m}\exp\left[-\frac{h_e}{R}\left(\frac{1}{T_m}-\frac{1}{T_e^o}\right)\right], \tag{13}$$

$$C_{rr} = \left(\frac{h_e}{RT_m} - 1\right)C_{eq}\frac{T_{rr}}{T_m}. \tag{14}$$

where C_{eq} is the Clausius-Clapeyron vapour concentration for the temperature of the meniscus, and C_{rr} is a quantity analogous to T_{rr} – the coefficient of the second-degree term of the concentration profile $C^S(r)$ at the surface of the film. C_∞ is the ambient vapour concentration far from the biconcave droplet, which is related to the relative saturation x as:

$$x = C_\infty / C_{eq}(T_m = T_\infty) = C_\infty / C_{eq0}. \tag{15}$$

Note that x is defined with respect to C_{eq0}, the equilibrium vapour concentration at the ambient temperature.

The evaporating meniscus acts as a vapour source and a heat sink perturbing the concentration and temperature profile from the homogeneous distribution, i.e., it leads to the

formation of diffusion and thermal boundary layers. The characteristic length of these layers is of the order of the size of the biconcave droplet, $R_c \sim 2$ mm, as in the problem for an evaporating spherical drop (Fuchs, 1959). This complicates the model because one must consider the concentration and temperature profiles *outside* the glass capillary and explains why Manev (Manev, 2013) found that the position of the holder within the container influences the process of evaporation. An exact model would require a detailed consideration of the geometry of the holder and the container; such a model would yield a result specific to the construction of the cell and to the shape of the meniscus and will be of little value in terms of generality. Instead of adopting such a treatment, we will use dimensional analysis to obtain a general dependence of the mass flux from the film to the environment (J) and the heat flux from the air towards the film (Q) on all relevant parameters. In S3&4, we formulate a crude model of the geometry of the system, which allows the missing numerical factors in this dependence to be estimated. Naturally, this approach restricts the validity of the final results for the fluxes to only a correct order of magnitude.

Let us first apply dimensional analysis in order to derive the total diffusion flux J through the film surfaces. According to eq. (11), the vapour concentration near the film region is perturbed by two additive effects: ΔC_m due to the cooling of the biconcave droplet as a whole and $\frac{1}{2}C_{rr}(r^2 - R_f^2)$, due to the additional cooling of the film region. The concentration gradient due to the cooling of the biconcave droplet drives a diffusive flux of density j_c proportional to the concentration difference between the meniscus and the surrounding air (ΔC_m, see eq. (12)) divided by the characteristic length (the size of the droplet, $\sim R_c$) of the respective diffusion layer:

$$j_c \sim D\Delta C_m/R_c, \tag{16}$$

where D is the diffusion coefficient of the vapours. As for the second perturbation in the film region, it generates a flux j_f proportional to the concentration difference between the vapours above the colder film and those above the warmer meniscus divided by the characteristic length of the perturbation, the film radius R_f, i.e., $j_f \sim D(C^S|_{r=0} - C^S|_{r=Rf})/R_f$, From eq. (11) it follows that $C^S|_{r=0} - C^S|_{r=Rf} \sim -C_{rr}R_f^2$, which leads to

$$j_f \sim -DR_fC_{rr}. \tag{17}$$

Combining eqs. (17) and (16), we arrive at an expression for the total mass outflux through the surface of the film:

$$J \sim R_{\mathrm{f}}^2 \left(j_{\mathrm{f}} + j_{\mathrm{c}} \right) = D R_{\mathrm{f}}^2 \left(-K_1 R_{\mathrm{f}} C_{rr} + K_2 \frac{\Delta C_{\mathrm{m}}}{R_{\mathrm{c}}} \right). \tag{18}$$

Here, K_1 and K_2 are dimensionless coefficients of value specific to the precise geometry of the system. In S3&4 we estimate those coefficients based on an approximate model of the system. The final result for J reads

$$J = D R_{\mathrm{f}}^2 \left[-\frac{8}{3} R_{\mathrm{f}} C_{rr} + \left(2 - \sqrt{2} \right) \frac{\pi}{R_{\mathrm{c}}} \Delta C_{\mathrm{m}} \right]; \tag{19}$$

J is defined as the total positive diffusive flux through *both* surfaces of the film. Note that our solution to the considered problem neglects the presence of a Knudsen layer and the convective diffusion – we analyse the limitations of these approximations in S5 and 6, respectively; in particular, we show that the convective diffusion is significant for highly volatile liquids, e.g. hexane.

The respective heat flux Q from the air through the surfaces of the film is, by analogy with eq. (19) is

$$Q = \kappa R_{\mathrm{f}}^2 \left[\frac{8}{3} R_{\mathrm{f}} T_{rr} - \left(2 - \sqrt{2} \right) \frac{\pi}{R_{\mathrm{c}}} \Delta T_{\mathrm{m}} \right], \tag{20}$$

where κ is the thermal conductivity of the air. As with the mass transfer problem, we neglect the Fuchs layer and the convective terms in the heat transfer equation, cf. S5 and 6. The heat transfer via radiation is also neglected − by analogy with the case of an evaporating droplet (Fuchs, 1959), this assumption should hold true for the film radii that we consider in this paper (~100 μm). We have also neglected the term $\partial T/\partial t$ in the heat equation; in S3, we show that this is justified for films of $h < 1$ μm.

3. Heat balance

The approximate nature of our solution to the heat and mass transfer problems does not permit a *local* form of the heat balance to be used for our problem. Consequently, in order to determine the unknown coefficient T_{rr} in the temperature profile (9), we will employ an *integral* heat balance for the film. This approach is widely used in the literature for the *force* balance in thin films – e.g., the Reynolds law for thin film drainage is obtained through an integral mechanical balance that substitutes the local Young-Laplace equation as the latter cannot be fulfilled if the

film is assumed to be plane-parallel (Ivanov and Dimitrov, 1974). The integral *heat* balance states that the total heat consumption rate due to evaporation, $h_e J$, is compensated by the integral heat influx Q through the air:

$$h_e J = Q, \tag{21}$$

Substituting here the relations (19) and (20), together with eq. (14) for C_{rr}, we obtain an equation for T_{rr}. Solving it gives the result

$$T_{rr} = 0.69 \frac{T_m}{R_f R_c C_{eq}} \frac{\Delta C_m + \dfrac{\kappa \Delta T_m}{h_e D}}{\dfrac{h_e}{R T_m} - 1 + \dfrac{\kappa T_m}{h_e D C_{eq}}}. \tag{22}$$

The term proportional to ΔT_m in the numerator can in principle nullify T_{rr} – that is, there exists a temperature difference between the meniscus and the ambient air, $\Delta T_m = -h_e D \Delta C_m / \kappa$, such that the temperature drop in the film and the associated Marangoni effect vanish. Thus, once the meniscus becomes cold enough, the thin films can no longer be stabilized by the evaporation.

4. The cooling of the meniscus

The time dependence of the temperature of the meniscus T_m follows from the heat balance for the glass capillary and the liquid in the meniscus. This balance involves the heat flux Q_m coming from the air through both surfaces of the meniscus and the respective evaporative flux J_m. Applying dimensional analysis as done for J above, one can show that $Q_m \propto -\kappa R_c \Delta T_m$. The numerical coefficient in this relation is estimated in S5:

$$Q_m = -4.57 \kappa R_c \Delta T_m . \tag{23}$$

The mass transfer problem leads to a similar expression for the diffusive flux J_m through the surfaces of the meniscus:

$$J_m = 4.57 D R_c \Delta C_m . \tag{24}$$

We make the additional assumption that at all times, there is thermal equilibrium between the meniscus and the glass of the capillary. In this approximation, the rate of change of T_m is determined by the rate of heat loss due to evaporation ($h_e J_m$), and the rate at which heat is gained from the gas phase (Q_m):

$$C_p \frac{dT_m}{dt} = Q_m - h_e J_m = -4.57 R_c \left(\kappa \Delta T_m + h_e D \Delta C_m \right), \tag{25}$$

where C_p is the sum of the heat capacities of the liquid and the part of the glass holder in direct contact with the fluid. Its value is estimated in S8 – for water and a borosilicate capillary of diameter R_c = 2 mm and wall thickness d_{glass} = 1 mm, $C_p \approx 0.18$ J/K.

The right-hand side of eq. (25) can become zero, which means that a stationary temperature difference between the meniscus and the air ($\Delta T_{m,st}$) will be reached eventually, as in the case of a spherical droplet (Fuchs, 1959). This stationary temperature decreases with the decrease of the ambient relative saturation x. To analyse the dependence of $\Delta T_{m,st}$ on x, we set the right-hand side of eq. (25) to zero and rearrange it using eqs. (12)-(13):

$$C_\infty = xC_{eq0} = C_{eq} + \frac{\kappa \Delta T_{m,st}}{h_e D} = \frac{p^0}{R\left(\Delta T_{m,st} + T_\infty\right)} \exp\left[-\frac{h_e}{R}\left(\frac{1}{\Delta T_{m,st} + T_\infty} - \frac{1}{T_e^o} \right) \right] + \frac{\kappa \Delta T_{m,st}}{h_e D}, \quad (26)$$

where we used that, by definition, $x = C_\infty / C_{eq0}$. Instead of the dependence $\Delta T_{m,st}(x)$, this result determines the inverse function, $x(\Delta T_{m,st})$; it is plotted in Fig S8. According to eq. (26), for the experimentally relevant undersaturations, a water meniscus is colder than the ambient air by 5-10 K at the stationary state. The stationary temperature difference predicted by the equation above is precisely the value at which the numerator in eq. (22) for T_{rr} becomes zero – that is, when the temperature drop in the meniscus reaches $\Delta T_{m,st}$, the Marangoni effect disappears. However, as we will show next, the films become unstable even before T_{rr} reaches zero.

The dependence of ΔT_m on time at a given saturation x follows from the heat balance (25):

$$t = -\frac{C_p}{4.57 R_c} \int_0^{\Delta T_m} \frac{\mathrm{d}\Delta T_m}{\kappa \Delta T_m + h_e D \Delta C_m}, \quad (27)$$

where as an initial condition we have used that at $t = 0$, the temperature of the meniscus is equal to that of the surrounding air. The integral (27) is not analytical due to the complicated dependence of ΔC_m on ΔT_m, see eqs. (12)-(13). In S8, we use a series expansion to obtain an analytical expression valid for small ΔT_m and for x close to 1.

5. Drainage and stability of an evaporating film.

Having derived the expression (22) for T_{rr}, we can now explicitly determine the drainage velocity of the film. In order to do so, we will formulate an integral balance of the forces acting in the normal direction, by analogy with the derivation of the Reynolds law for drainage of films of tangentially immobile surfaces (Reynolds, 1886). The integral approach is necessary because

our model states in advance that the studied film is plane-parallel (based on the experiment, Figure 1C), thereby making the local form of the normal force balance inapplicable (Ivanov and Dimitrov, 1974). Employing a local boundary condition would be tantamount to solving the Young-Laplace equation for the film shape (Manev et al., 1997; Tsekov and Ruckenstein, 1994), and goes beyond the aims of our study. The integral normal force balance states that the total force acting on the film in normal direction is zero,

$$2\pi\int_0^{R_f}\left(p_0 - p(r) - \Pi + 2\eta\frac{\partial v_z}{\partial z}\right)\Bigg|_{z=h/2} r\mathrm{d}r = 0\,. \qquad (28)$$

The balance includes the pressure p_0 in the gas, the hydrodynamic pressure $p(r)$, the viscous force in the liquid, $-2\eta\partial v_z/\partial z$, and the disjoining pressure Π (the surface forces) in the film. Vapour recoil force can be neglected for the low to moderate evaporation rates we consider (Oron et al., 1997).

The precise nature of the surface forces acting in films formed from pure liquids is unclear. We assume that the main contribution to Π is the van der Waals h^{-3} attraction,

$$\Pi = \Pi_{\mathrm{vdW}} = -A_{\mathrm{H}}/6\pi h^3, \qquad (29)$$

while the surface charge of the pure liquid and the respective electrostatic disjoining pressure Π_{el} (Sheludko, 1967) are neglected. However, there is evidence that Π_{el} is a significant factor for the stability of pure water films (Exerowa and Kruglyakov, 1998; Yaminsky et al., 2010b) , and the surface of pure water is, in fact, charged (Kolarov et al., 1993; Stubenrauch and Klitzing, 2003). We have two reasons for leaving the question of Π_{el} aside. First, the experimentally observed evaporating saline films in (Karakashev et al., 2008) exhibit considerable stability at electrolyte concentrations of over 1 M, where electrostatic forces are completely screened – this means that even if Π_{el} contributes to the stabilization, there must be another, *dynamic* stabilizing factor. Our second reason is that, for pure water films, the precise dependence of Π_{el} on the film thickness h is unknown. In particular, it is unlikely that Π_{el} follows the DLVO theory, the least reason being that the ionic strength of pure water (10^{-7} M) corresponds to a Debye length and an average distance between two ions that are greater than the experimentally observed h, which violates the assumptions under which the DLVO formula is derived, see Derjaguin (Derjaguin, 1986). In addition, there is no satisfactory explanation of the origin of the surface charge that produces the repulsion – for example, it seems rather far-fetched that hydroxide ions could adsorb at the

air|water interface with an adsorption energy of the order of $20\times k_B T$ (reported in (Marinova et al., 1996)), i.e., comparable to that of sodium dodecyl sulfate (Slavchov et al., 2014). Nevertheless, we performed the whole analysis with the inclusion of the DLVO expression for Π_{el} in S7. However, in view of the arguments stated above, we are sceptical towards its reliability and in the following sections we only consider the van der Waals term (29) in the disjoining pressure. In the worst case, the neglect of Π_{el} makes our model applicable for non-aqueous films only, as there is little evidence of surface charge at the oil surface. It should be pointed out however, that eq. (29) itself is approximate for it neglects the retardation effect – the latter is known to be important for oil films (Israelachvili, 2011; Scheludko et al., 1965).

Substituting the expressions (7),(2),(9),(6),(8) and (29) for $p(r)$, p_m, $T(r)$, v_z, V_r and Π in the force balance (28), we obtain an explicit equation for V_z. Its solution reads:

$$V_z = \frac{R_f^2 s^S T_{rr}}{8\eta}\left(1-\frac{4}{3}\frac{h^2}{R_f^2}\right)-\frac{h}{4\eta}\left(p_c-\Pi_{vdW}\right)\approx \frac{R_f^2 s^S T_{rr}}{8\eta}-\frac{h}{\eta}\frac{\sigma_m}{2R_c}-\frac{1}{\eta}\frac{A_H}{24\pi h^2}, \qquad (30)$$

where we used that $h/R_f << 1$. With knowledge of the drainage velocity V_z, we can proceed with the analysis of the film drainage velocity $\mathrm{d}h/\mathrm{d}t$, which follows from the mass balance of the liquid in the film:

$$\frac{\mathrm{d}h}{\mathrm{d}t} = -\frac{v^L J}{\pi R_f^2}+2V_z \approx \frac{R_f^2 s^S T_{rr}}{4\eta}-\frac{h}{\eta}\frac{\sigma_m}{R_c}-\frac{A_H}{12\pi\eta h^2}, \qquad (31)$$

where v^L is the molar volume of the liquid. The first term in eq. (31) reflects the loss of fluid caused by evaporation and the term $2V_z$ quantifies the normal volume flux density towards the two surfaces of the film. According to eq. (30), there are three factors that influence V_z – the first term ($\propto T_{rr}$) is due to the Marangoni effect, which causes liquid to flow from the meniscus to the film, while the second ($\propto \sigma_m/R_c$) and the third ($\propto A_H$) describe the flow of liquid outward of the film due to the capillary pressure and the disjoining pressure, respectively. For water films of R_f = 150 μm in contact with a thermostated meniscus with the parameters specified in S1, we obtain the following estimates: $v^L J/\pi R_f^2 \sim 10^{-8}$ m/s for the diffusive term (using eq. (19)), $R_f^2 s^S T_{rr}/4\eta \sim 10^{-2}$ m/s for the term due to the Marangoni flux, $h\sigma_m/\eta R_c \sim 10^{-2}$ m/s for the capillary pressure term and $A_H/12\pi\eta h^2 \sim 10^{-5}$ m/s for the one caused by the van der Waals attraction. Thus, somewhat contrary to what one might intuitively expect, the mass loss due to evaporation has a minor impact on the rate of thinning $\mathrm{d}h/\mathrm{d}t$. A similar result has been obtained for an evaporating

sessile droplet (Tsoumpas et al., 2015). The evolution of the film is thus predominantly controlled by the Marangoni flux, the disjoining and the capillary pressure.

One can use eq. (31) to derive the dependence of h on t – the result is discussed in S6. The characteristic time for reaching the stationary thickness of the film is predicted to be of the order of 10^{-6} s. Here, we analyse only the stationary state itself. Setting the right-hand side of eq. (31) to zero and rearranging, we arrive at the following equation for the stationary thickness:

$$\frac{h}{h_{\mathrm{cr}}}+\frac{h_{\mathrm{cr}}^2}{2h^2}=\frac{k}{2}, \tag{32}$$

where the symbols k and h_{cr} stand for

$$k=\frac{1}{2}\frac{R_{\mathrm{f}}^2}{h_{\mathrm{cr}}}\frac{R_{\mathrm{c}}s^{\mathrm{S}}T_{rr}}{\sigma_{\mathrm{m}}}=0.92\frac{R_{\mathrm{f}}}{R_{\mathrm{c}}^{1/3}}\frac{s^{\mathrm{S}}T_{\mathrm{m}}}{A_{\mathrm{H}}^{1/3}\sigma_{\mathrm{m}}^{2/3}}\frac{1-x\dfrac{C_{\mathrm{eq0}}}{C_{\mathrm{eq}}}+\dfrac{\kappa\Delta T_{\mathrm{m}}}{h_{\mathrm{e}}DC_{\mathrm{eq}}}}{\dfrac{h_{\mathrm{e}}}{RT_{\mathrm{m}}}-1+\dfrac{\kappa T_{\mathrm{m}}}{h_{\mathrm{e}}DC_{\mathrm{eq}}}} \quad \text{and} \tag{33}$$

$$h_{\mathrm{cr}}=\left(\frac{A_{\mathrm{H}}R_{\mathrm{c}}}{6\pi\sigma_{\mathrm{m}}}\right)^{1/3}. \tag{34}$$

There are two physically meaningful solutions to eq. (32) for the stationary thickness,

$$h_{\mathrm{st1}}=\frac{h_{\mathrm{cr}}}{6}\left(a^{1/3}+\frac{k^2}{a^{1/3}}+k\right) \quad \text{and} \quad h_{\mathrm{st2}}=-\frac{h_{\mathrm{cr}}}{12a^{1/3}}\left[\left(a^{1/3}-k\right)^2+\mathrm{i}\sqrt{3}\left(a^{2/3}-k^2\right)\right], \tag{35}$$

where i is the imaginary unit and the coefficient a is defined as

$$a=-54+k^3+6\sqrt{81-3k^3}\ . \tag{36}$$

Note that a can be complex and h_{st2} can have real values. Note also that the solutions (35) are *quasistationary*, as they depend on the coefficient T_{rr}, which depends on the temperature of the meniscus (see eq. (22)), and it is therefore a function of time.

6. The limiting case of a thermostated meniscus.

Let us first consider the limiting case in which the temperature of the meniscus is equal to the ambient one ($\Delta T_{\mathrm{m}} = 0$). Under this assumption, the thicknesses h_{st1} and h_{st2} (35) correspond to a true *stationary* state, rather than a *quasistationary* one. The solutions (35) are plotted in Figure 2 – this is the *stability diagram* of pure water films in contact with thermostated meniscus. The first stationary solution h_{st1} gives the stable branch of the diagram, i.e., for any initial thickness h_0

of the film for which $h_0 > h_{st2}$, it is expected that $h(t\to\infty) = h_{st1}$. Once the film reaches the stable thickness h_{st1}, it remains stationary as long as the meniscus does not cool down. The branch h_{st2} of eq. (35) corresponds to an unstable stationary state. A film of initial thickness $h_0 = h_{st2} + \delta$, where δ is a positive perturbation, will thicken until the stable branch is reached ($h = h_{st1}$), while if h_0 is smaller than h_{st2}, the film is expected to drain until rupture (S6, Figure S.2). Our eq. (32) and Figure 2 are analogous to Marrucci's *eq. 16* and *fig. 2* (Marrucci, 1969) that represent a similar balance between the concentration-driven Marangoni effect, the capillary pressure and the van der Waals force.

The mass balance (32) only permits a stationary state if the relative saturation x is below a certain critical value, x_{cr0}, i.e., if the evaporation is intense enough. This critical value corresponds to the maximum of x as a function of h_{st}. There, the film thickness is precisely equal to the critical value h_{cr} from eq. (34), see Figure 2; this must be the smallest observable thickness of the film (for water, it is h_{cr} = 40.1 nm, see S1 for the parameter values). Substituting $h = h_{cr}$ in eq. (32), we obtain that the respective critical value of k is 3. Eq. (33) then leads to the critical value of T_{rr} for a thermostated meniscus:

$$T_{rr0,\mathrm{cr}} = \frac{6^{2/3} A_{\mathrm{H}}^{1/3} \sigma_{\mathrm{m}}^{2/3}}{\pi^{1/3} s^{\mathrm{S}} R_{\mathrm{f}}^2 R_{\mathrm{c}}^{2/3}}\,. \tag{37}$$

Equating the right-hand side of eq. (37) with that of (22), using the definitions (12) and (15) and solving for x, we obtain the sought value of the critical saturation for a thermostated meniscus:

$$x_{\mathrm{cr0}} = 1 - 3.27 \frac{R_{\mathrm{c}}^{1/3}}{R_{\mathrm{f}}} \frac{A_{\mathrm{H}}^{1/3} \sigma_{\mathrm{m}}^{2/3}}{s^{\mathrm{S}} T_\infty} \left(\frac{h_{\mathrm{e}}}{R T_\infty} - 1 + \frac{\kappa T_\infty}{h_{\mathrm{e}} D C_{\mathrm{eq0}}} \right). \tag{38}$$

At relative saturations x greater than x_{cr0} (91% for pure water films of R_f = 150 μm), no stationary thickness exists because the evaporation-driven Marangoni flow is too weak to maintain the stationary state. At $x < x_{cr0}$, the stable stationary film thickness h_{st1} is given by eq. (35). Our critical relative saturation is analogous to the critical concentration occurring in Marrucci's coalescence model (Marrucci, 1969).

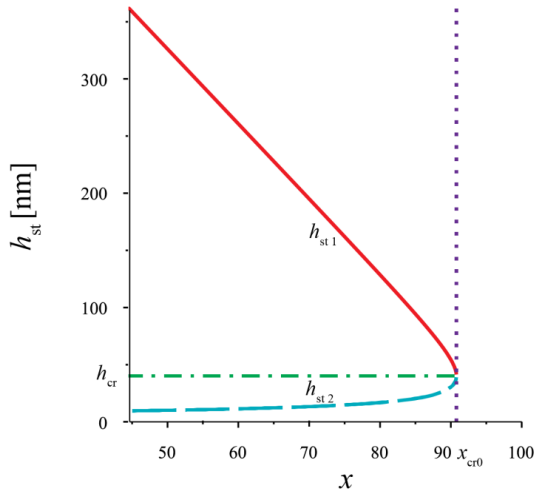

Figure 2. Stationary thickness h_{st} of a wate film as a function of the relative saturation: a stability diagram for a thermostated meniscus, eqs. (35). A stable stationary thickness h_{st1} (solid line), exists for humidities lower than the critical value x_{cr0}. The branch h_{st2} (dashed line) is unstable, i.e., a film of initial thickness $h_0 > h_{st2}$ thickens to h_{st1}, while if $h_0 < h_{st2}$, the film drains until rupture. All films are unstable at $x > x_{cr0}$. At $x = x_{cr0}$ (dotted vertical line), the quasistationary film thickness is equal to h_{cr} (dashdot line).

7. Evaporating thin film in contact with a cold meniscus

The assumption that the meniscus is thermostated leads to the conclusion that evaporating thin water films have an infinite lifetime at $x < x_{cr0}$, which contradicts the experimental data we have gathered (see Section III). This contradiction is resolved when the cooling of the meniscus is accounted for. Let us therefore consider the time dependence of the thickness of a film in contact with a meniscus that cools down following eq. (27). The quasi-stationary film thickness depends on time through ΔT_m. We plot parametrically the stable branch of eq. (35), $h_{st1}(\Delta T_m)$, against $t(\Delta T_m)$ from eq. (27) at several values of the relative saturation; the resulting curves are shown in Figure 3. As the meniscus gradually cools down (Fig. S7), the film remains in a quasistationary state, but its thickness decreases according to eq. (35) in unison with the drop in T_m. The thinning process continues until the film reaches the critical thickness (34), whereupon rupture occurs. It is evident from Figure 3 that the expected lifetime of pure water films strongly depends on the relative humidity of the gas in the Scheludko cell – at $x > x_{cr0}$, no stationary state is possible; for $x < x_{cr0}$, the quasistationary thickness decreases from an initial value of the order of ~100-250 nm to h_{cr} over a time period of $\tau \sim 100$ s.

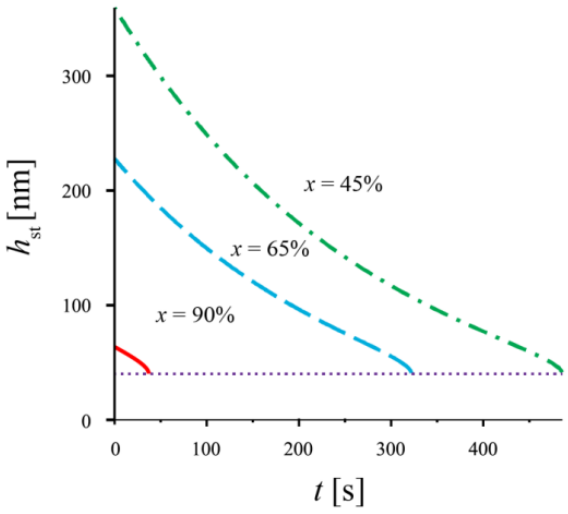

Figure 3. Quaststationary film thickness h_{st} of an evaporating water film in contact with a non-thermostated meniscus as a function of time t for various values of the relative saturation x, at a film radius R_f = 150 μm. The plot is parametric, using $h_{st1}(\Delta T_m)$ from eq. (35) and $t(\Delta T_m)$ from eq. (27). The films thin down to the critical thickness h_{cr} = 40.1 nm (eq. (34), dotted line), whereupon they are predicted to rupture. See S1 for the values of the parameters.

We now turn to the dependence of the lifetime τ of the film on the saturation x, which can be obtained via another parametric plot. The critical value of k corresponding to $h_{st1} = h_{cr}$ following from eq. (32) is $k_{cr} = 3$; we substitute this value in eq. (33) and solve it for x:

$$x_{cr} = \frac{C_{eq}}{C_{eq0}} + \frac{\kappa \Delta T_m}{h_e D C_{eq0}} - 3.27 \frac{R_c^{1/3}}{R_f} \frac{A_H^{1/3} \sigma_m^{2/3}}{s^S T_m} \frac{C_{eq}}{C_{eq0}} \left(\frac{h_e}{R T_m} - 1 + \frac{\kappa T_m}{h_e D C_{eq}} \right). \quad (39)$$

This equation generalizes eq. (38); above the critical humidity x_{cr}, films in contact with a cold meniscus of temperature T_m are predicted to be unstable. To find the film lifetime τ, we substitute eqs. (12)-(13) in eq. (27) for $t(\Delta T_m)$ (using $C_\infty = x C_{eq0}$); then, we substitute x with its critical value (39). The result is τ as function of ΔT_m. Plotting it parametrically against $x_{cr}(\Delta T_m)$ from eq. (39) gives us the sought dependence $\tau(x)$, Figure 4A.

One can infer from eq. (39) that x_{cr} grows with R_f, i.e., the stability of the evaporating film is dependent on its radius. We can rewrite eq. (39) as:

$$R_f = 3.27 \frac{R_c^{1/3} A_H^{1/3} \sigma_m^{2/3}}{s^S T_m} \frac{\frac{h_e}{R T_m} - 1 + \frac{\kappa T_m}{h_e D C_{eq}}}{1 - x \frac{C_{eq0}}{C_{eq}} + \frac{\kappa \Delta T_m}{h_e D C_{eq}}}. \quad (40)$$

According to this formula, films of different radii break at a different value of the temperature T_m of the meniscus, and therefore, have different lifetimes. This is illustrated in Figure 4B, where $R_f(\Delta T_m)$ is plotted parametrically against $t(\Delta T_m)$, eqs. (40) and (27), for x = 45%. At this saturation, quasistationary films are expected only for R_f above a critical value $R_{f,cr}$ = $R_f(\Delta T_m=0)$. For a water film formed in a capillary with R_c = 2 mm, $R_{f,cr}$ is equal to 25 μm, see S1 for details on the parameters of the system.

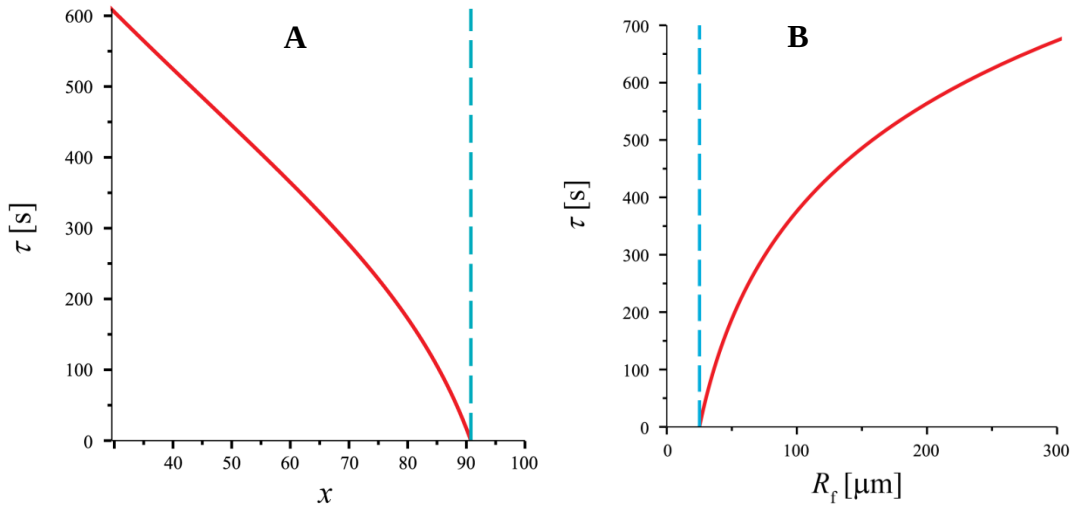

Figure 4. **A**. Expected lifetime τ of quaststationary water films of radius R_f = 150 μm as a function of the relative saturation x of the ambient gas – parametric plot of $t(T_m)$ vs. $x_{cr}(T_m)$, eqs. (27) and (39). No stationary state is possible at $x > x_{cr0}$ = 91% (eq. (38)). For $x < x_{cr0}$ (dashed line), the film lifetime coincides with the time τ required for the temperature T_m of the meniscus to decrease to the critical value that follows from eq. (39). **B**. Lifetime of water films as a function of the film radius R_f at x = 45% – parametric plot of $R_f(\Delta T_m)$ against $t(\Delta T_m)$, eqs. (40) and (27). Stationary films are predicted to exist only for $R_f > R_{f,cr} \approx 25$ μm. See S1 for the parameter values.

The quasistationary approach we use in this section, in which the thickness is a function of time, but dh/dt is still equal to 0, is applicable because of the different timescales of the two processes taking place in the system. The cooling of the meniscus is slow and lasts for minutes, see Fig. S7; in contrast, the drainage of the film from its initial thickness to the quasistationary one occurs over timescales of $\eta R_c/\sigma_0 \sim 10^{-5}$ s (S6). A similar situation was discussed by Marrucci (Marrucci, 1969) for his bubble coalescence problem, where the quasistationary foam film thickness is controlled by a slow diffusion process.

III.Experimental observations of evaporating foam films

The existing data on evaporating films from pure liquids (outlined in the Introduction) are scarce and contradictory, and do not allow the confirmation or rejection of the mechanism of stabilization proposed above. Therefore, we performed our own experimental tests of the predicted trends. For this purpose, we chose to investigate pure aqueous films under controlled moderate humidity *x*, as well as films formed from various pure alkanes. The evaporating alkane films are of practical relevance as a model for fuel and lubricant films occurring in the cylinders of internal combustion engines (Baumgarten, 2006). In addition, alkane films have certain advantages over aqueous from an experimental point of view, outlined below.

1. Materials and methods

We used a version of the Scheludko cell identical to the one described in (Kosior et al., 2014). For the convenience of the reader, its basic components are presented in Figure 1. Two capillaries of different radii (R_c = 2 and 2.3 mm) and wall thicknesses (d_{glass} ~ 1 and 0.5 mm, respectively) were used in order to test the reproducibility of the results. The capillaries were fixed inside a container of radius ~1 cm and height ~9 cm, which was enclosed by a thermostat (HAAKE K10). The films were formed from a biconcave drop situated in the capillary (Figure 1A) by withdrawing liquid with a micropump (Hamilton). Observations of the films were made with an inverted optical microscope (Carl Zeiss Axiovert 200 MAT) connected to a camera (Hitachi HV-D20); the film thickness was determined interferometrically (Sheludko, 1967). Several dozens of films were formed for each loading of the apparatus; each run like this lasted for several hours. Runs were repeated up to three times to test the reproducibility.

Aqueous films were formed from triply distilled water. For comparison, we tested also HPLC water, but the results were less reproducible. Following Manev (Manev, 1975), the humidity in the container was maintained (*atmostated*) by placing on the bottom of the sealed container a certain amount (~400 μL) of *atmostating solution* – concentrated $MgCl_2$ in triply distilled water (Figure 1B). The solutions used were of concentration 1.60 and 4.93 mol/kg, corresponding to 90 and 45% relative humidity, respectively (Robinson and Stokes, 1959). Experiments under saturated conditions, with ~400 μL of pure water as the atmostating liquid, were also performed.

Hydrocarbon films were formed from hexane, nonane and hexadecane (Fluka), either with the container open to the ambient air (corresponding to zero vapour concentration, $x = 0$), or with the container sealed and 600-800 μL of the hydrocarbon placed on its bottom (maintaining saturated conditions, $x = 1$).

The observed films were normally circular and plane-parallel (Figure 1C), but with exceptions. We investigated films of different sizes – the experimental setup provides the opportunity to monitor the film radius with accuracy of ±5 μm and to control it manually with good precision. Once the film was formed, its radius remained constant during the whole drainage process until rupture, with the exception of the first several films in a run. The latter often expanded or shrunk significantly, perhaps in relation to highly undersaturated conditions – the atmostating liquid and the gas only equilibrate after several minutes. For each film, the rupture thickness h_{cr} and the film radius R_f were measured; for several of them, the whole $h(t)$ curve was recorded. Within a single run, the film stability exhibited a dependence on the time t_{load} between the loading of the cell (the moment of the hermetic sealing of the container after the cell is loaded with fluid and the bottom of the container is loaded with atmostating liquid) and the formation of the film, so this parameter was also monitored.

Most atmostated film experiments were performed with the container sealed. Measurements were also performed with an open container and films exposed to the ambient humidity in the laboratory. This option was used as a qualitative test of the effect of abrupt changes in the humidity on the stability of the films.

A number of experimental factors complicate the interpretation of the results obtained with the setup described above. One is the long time scale for reaching the stationary vapour pressure inside the container – it is of the order of $\sim L_{cont}^2/D \sim 5$ min (L_{cont} – height of the container, ~ 9 cm; D – diffusion coefficient of water molecules in air, 2.6×10^{-5} m^2/s). Due to that, the first 1-3 films of each run drain under saturation between that in the laboratory (humidity 45-65%) and the one set by the atmostating liquid. A related issue is that each film was formed in the cloud of vapours left after the previous one ruptured.

A second problem is the possible presence of surface-active contaminations, which can drastically affect the behaviour of the films we study. Even a very low concentration of surface-active impurities will cause a solutal Marangoni effect strong enough to counteract the thermal Marangoni effect discussed here. Hu and Larson (Hu and Larson, 2005) have demonstrated that

for an evaporating sessile drop, an adsorption as low as one molecule per 3000 nm^2 can effectively suppress the Marangoni flow. In another paper (Hu and Larson, 2006), Hu and Larson observed that the Marangoni flow pattern in an evaporating sessile droplet is accurately predicted by their theory for octane droplets, but for water, the experimental Marangoni flow is much weaker than expected, due to contaminants at the water surface (Hu and Larson, 2006). The impurities present in the alkane, on the other hand, are unlikely to have a significant affinity to the oil|air interface. To avoid contaminants, we used triply distilled water, and after each set of experiments, we lavishly washed the measuring cell and cleaned it in an oven at high temperature.

A third factor that introduces uncertainty into the interpretation of our experimental data on water films is the presence of CO_2, whose dissolution in water introduces hydrogen carbonate and carbonate ions that allegedly charge the surface (Katsir and Marmur, 2014b) – this problem is also eliminated with the hydrocarbon films.

The validity of our model is restricted not only by these experimental complications, but also by our approximate treatment of the studied system, particularly the simplified model for the surface forces (29) and the approximate values of the numerical coefficients and C_p in eqs. (19)-(20)&(23)-(25) (estimated for geometry of the system that only roughly matches the real one). Moreover, at high evaporation rates, non-linear effects related to convective transport and inertia are likely to be present. Therefore, we do not expect quantitative agreement between theory and experiment – we seek only qualitative correspondence, in terms of similar trends in response to variation of the experimental conditions and similar orders of magnitude of the relevant quantities (h_{cr}, τ, $R_{f,cr}$ etc.).

2. Aqueous films

In an undersaturated environment, the observed film lifetimes varied considerably with the time after cell loading (t_{load}). Typically, each successive film would live shorter than the preceding one, provided that their radii were similar – this behaviour is illustrated in Figure 5a. In contrast, no significant changes with t_{load} were observed under saturated conditions. The decrease of the lifetime between two consecutive films was more pronounced when the period between the formations of the two films was shorter, and when the films are formed at higher undersaturation. The films were also morphologically different depending on t_{load}: at low loading

times, films were not plane-parallel upon formation; at large t_{load}, the films had approximately homogeneous thickness at their formation (Figure 6A&B). The observed trend with t_{load} can be explained with the fact that the formation of several consecutive evaporating films leads to a significant cooling of the glass holder. The meniscus, the glass capillary and probably the supporting glass tube are progressively colder at the formation of each next film and the time between the formations of two films is insufficient for them to relax to the ambient temperature T_∞. If the initial temperature of the meniscus is lower than T_∞, then the lifetime of the film will be decreased (see S8).

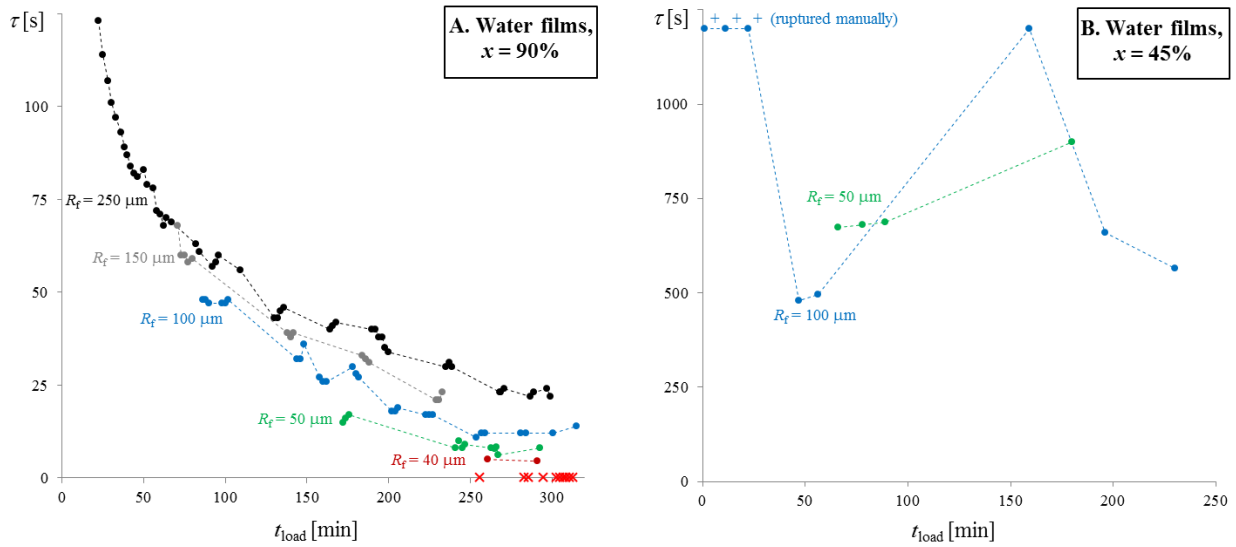

Figure 5. Dependence of the lifetime τ of water films during one run on the time t_{load} after loading the cell. **A.** 90% humidity. Diagonal crosses indicate films that rupture instantly. **B.** 45% humidity. The first 3 films indicated with "+" were ruptured manually ten minutes after formation.

100% humidity. Stable, thick films were formed in saturated atmosphere (Figure 1C), in agreement with many previous reports (Exerowa, 1969; Yaminsky et al., 2010a) and contrary to what our model predicts. The films drained until reaching a plateau thickness of $h(t\rightarrow\infty)$ = 60-110 nm and did not rupture on the timescale of the experiment. Even though the experiments lasted for several hours, there was no change of film stability with the passing of time after cell loading. By a small manual change of the pump pressure, the films could be forced to drain – a black spot formed and grew until at a certain point the film ruptured (Figure 6C). This behaviour is indicative of the existence of a weak barrier for the drainage.

The first two films formed right after the cell loading, while the air in the container was still not completely saturated, had a finite lifetime (50 and 90 s), and their radii shrunk significantly (from 100 to 50 μm).

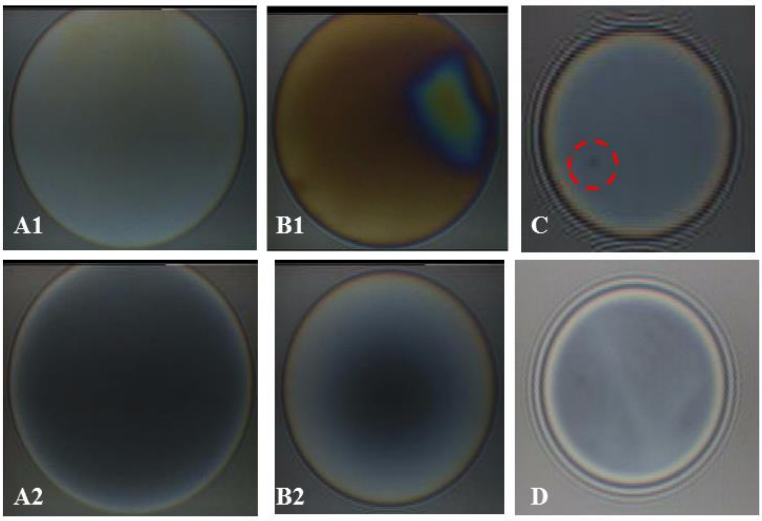

Figure 6. Representative images of the observed films. **A.** Water film, x = 90%, high loading time, R_f = 250 μm; A1 – initial state, A2 – seconds before rupture. **B.** Water film, x = 90%, low loading time, R_f = 250 μm; B1 – initial state, B2 – seconds before rupture. **C.** Water film, x = 100%, black dot observed immediately before breakage. **D.** Nonane film, x = 100%, R_f ~ 100 μm, lived for 50 s.

90% humidity. Using eq. (40) with $\Delta T_m = 0$, we can calculate that the model predicts no stable films at R_f below 125 μm. However, we observed films of R_f = 50-100 μm exhibiting lifetimes of 10-50 s, depending on R_f and t_{load} (Figure 5a). For the films of radius R_f = 150 and 250 μm, the model predicts lifetimes of 37 and 145 s, respectively. These values agree in order of magnitude with the experimentally measured range of 20-70 s for R_f = 150 μm and 20-300 s for R_f = 250 μm (the lifetimes still depend on t_{load}). The expected increase of the lifetime with the size of the films is confirmed – it is clearly seen in Figure 5A (22.3±0.3°C, R_c = 2 mm). Large films lived longer at all loading times – for example, at t_{load} ~ 180 min, films of radius 40-200 μm drained for 5-35 s, respectively.

The films ruptured at a critical value of the thickness that varied in the range h_{cr} = 26-48 nm, in qualitative agreement with the value 40 nm predicted by our model, eq. (34). The observed h_{cr}, however, depended on t_{load} – the first few films ruptured at 26-30 nm, while those at t_{load} = 250 min ruptured at 40-48 nm.

The very first film was extremely stable and lived for 5 min before we ruptured it manually – the most probable reason for its stability is that the container was not yet atmostated at the time when the film was formed (t_{load} = 17 min), i.e., x was less than 90% and evaporation was more intense than it was for the following films.

Unstable films that ruptured immediately after formation were observed after t_{load} = 250 min, and the frequency of their occurrence increased with t_{load}. At t_{load} > 300 min, we could no longer observe films smaller than R_f = 50 μm, which suggests that conditions at which $R_{f,cr}$ is above 50 μm had been reached by that point.

45% humidity. All films (formed at 22.0±0.3°C, R_c = 2.3 mm) were very stable and lived much longer than the films at x = 90% – lifetimes were of the order of 10 min, as illustrated in Figure 5B. This confirms qualitatively our theoretical prediction that lifetime increases with undersaturation, see Figure 4. The theoretical values of τ (~140 s for R_f = 50 μm, ~300 s for R_f = 100 μm) agree in order of magnitude with the experimental ones (τ ~ 500–1000 s). Let us remark that under such low humidities one of the approximations we used in our model fails: eq. (27) predicts that at t ~ 500 s, the meniscus temperature drops by 7 K, and at such large temperature differences, the series expansion of the boundary condition (10) is inaccurate. In addition, these films were not plane parallel.

3. Hydrocarbon films

n-Hexane films. Both for saturated conditions (x = 1) and for zero ambient concentration (x = 0), all films ruptured instantly. In contrast, at x = 0, our theory predicts the existence of quasistationary hexane films with a lifetime of τ ~ 700 s for R_f = 200 μm. The discrepancy is likely due to hexane's high volatility (vapour pressure 19.9 kPa), which could lead to failure of the approximations of our theoretical model. Our calculations, which the reader can find in S6, show that convective mass transport, disregarded in our model, is not negligible for C_6H_{14} – the mass transfer Péclet number, which measures the relative importance of convective diffusion, reaches values of ~0.1 for hexane and just 10^{-3}-10^{-2} for all other studied liquids.

n-Nonane. *Saturated atmosphere, x* = 1. It can be expected that such films would break immediately in the absence of a repulsive disjoining pressure, but instead, they were stable for tens of seconds – an experimental run is illustrated in Figure 4. For more details on the behaviour of non-evaporating nonane films, see S9.

We employed different methods of perturbing the nonane films formed in a saturated environment. We first tried to perturb the liquid-vapour equilibrium by raising the temperature of the thermostat from 21 to 30°C ("*cell heated*" region in Figure 7). This was expected to result in a temporary undersaturation in the container which, according to the theoretical results in Section II, should in turn result in an increased stability of the film. Indeed, the first film formed after the temperature increase was very stable and lived for 210 s. In the following minutes, the film lifetime decreased back to the values we observed for all non-evaporating nonane films (50-60 s), which suggests that by that time, the air in the container was already saturated with respect to the new temperature. We then changed the saturation more drastically by opening the container towards the air in the laboratory ("*cell opened*" region in Figure 7A). For this case, we expect a gradient of the vapour pressure to arise inside the container, starting from complete saturation near the surface of the atmostating solution and reaching zero saturation at the container entrance. Assuming that the gradient is constant (C is a linear function of z) and that the meniscus is located at height of approximately 15% from the height L_{cont} of the container, one can estimate that after the cell is opened, the relative saturation in the vicinity of the film is ~85%. Therefore, the opening of the container should increase the film lifetime. This was indeed observed – all films formed after the cell was opened lived for ~140 s, significantly more than those formed in a saturated environment.

Open cell, $x \approx 0$. Fifteen films of various sizes were formed in an open cell in the absence of atmostating liquid. Their behaviour was dependent on t_{load} (Figure S9) – the first five films expanded considerably after formation from R_f = 50 μm initially to 80-180 μm just before rupture. The radius of all films formed 40 min after loading was stable, and R_f was either ~50, 100 or 150 μm. Their respective lifetimes were τ ~ 20, 35 and 45 s – thus, in qualitative agreement with our theory (see Figure 4B), lifetime increased with R_f. However, the experimental increase is relatively small compared to the theoretical: the model predicts that films with R_f = 50 μm do not reach a quasistationary state, and for R_f = 100 and 150 μm, the theoretical τ is 14 and 230 s, respectively.

Interestingly, the films formed at x = 0 were less stable than those formed at intermediate saturations ($x \approx 85\%$ for films formed in the presence of atmostating liquid but in an open cell, see above), suggesting a non-monotonous dependence of the stability on x, in contrast with the predictions of our theory.

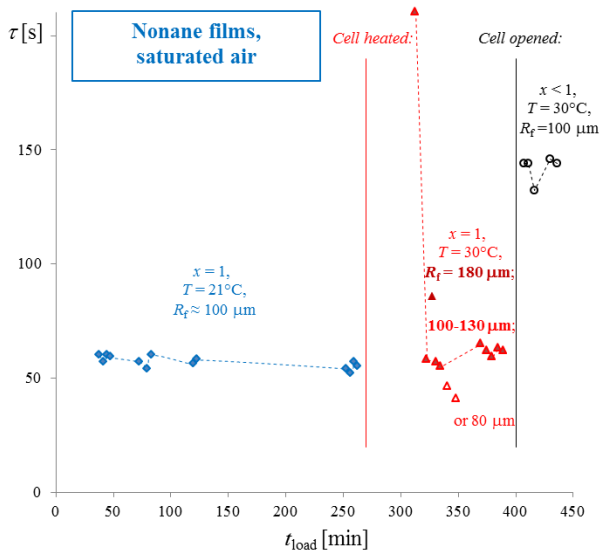

Figure 7. Lifetime τ of nonane films formed during one experimental run vs. time after loading the cell, t_{load} (21°C, R_c = 2 mm, non-evaporating films in saturated environment). After 270 min, the system was heated to 30°C – this resulted in a temporary decrease of the relative saturation and an increased stability of the film formed immediately afterwards. After 400 min, the container was opened towards the air in the laboratory, which also decreased the saturation and increased τ of all films formed thereafter.

The evolution of the film thickness $h(t)$ is compared to the theoretical one for a film of R_f ~ 125 μm at 21ºC in Fig. S10. The film drained from ~260 to 40 nm, whereupon it ruptured. The theoretical $h(t)$ was calculated as explained in Section II. Qualitative agreement between theory and experiment was observed, although the quantitative differences are significant. The critical thickness at which the films ruptured was ~42.9 nm This is 30% less than the theoretical value following from eq. (34), 60.3 nm. The observed drainage rate is faster than the theoretical by a factor of about 5, which is reasonably good agreement in view of the major approximations employed in the calculation of the numerical coefficients in eqs. (19)-(20), (23)-(24) and (27).

n-Hexadecane. Experiments were performed under unsaturated conditions only (x ~ 0). Instant rupture was observed in all cases. This is in agreement with the predictions of our theory – from eq. (38) it follows that the non-volatile hexadecane films are unstable over the whole experimental range of R_f.

IV.Conclusions

We have proposed **a mechanism for the stabilization of evaporating foam films made of pure liquid**, and gathered experimental evidence of its validity. Our theory explains the observed stability with the existence of a quasi-stationary state sustained by the evaporation-driven thermal Marangoni flow. The evaporation of fluid causes a local temperature drop in the film region and therefore an increase in the surface tension σ, which brings about a Marangoni flux from the meniscus towards the film. The predicted spatial variation of σ across the film is relatively small ($\Delta\sigma \sim T_{rr}s^{S}R_f^2/2 \sim 10^{-3}$-$10^{-2}$ mN/m difference between the centre and the meniscus), but it is sufficient to stabilize a film formed from a pure liquid because its surfaces are tangentially mobile.

The experimentally observed decrease of the film thickness h with time is explained with the evolution of the quasi-stationary state that follows the slow cooling down of the meniscus due to the evaporation (similar to Marrucci's theory (Marrucci, 1969) where the slow diffusion plays the same role). Once the meniscus reaches a certain critical temperature $T_{m,cr}$, the Marangoni effect can no longer counteract the attractive van der Waals force and the capillary pressure, leading to film rupture at the critical thickness h_{cr}. The lifetime of the film is the time needed for the meniscus to cool down to $T_{m,cr}$.

We were able to confirm experimentally several qualitative predictions of our theory, as follows.

(i) According to our model, films formed under lower ambient saturation, i.e., more intense evaporation, have an enhanced stability (Figure 4). This assertion is supported by a number of observations:

- the comparison between water films at x = 45% and 90% shows that lowering the humidity in the container indeed stabilizes the films – the lifetime is an order of magnitude longer at x = 45%, in agreement with the theoretical estimate;

- the comparison of the volatile nonane films vs. the non-volatile hexadecane films (both at x = 0) shows that the evaporating nonane films are quite stable, while the non-evaporating hexadecane films rupture upon formation;

- perturbing the liquid-vapour equilibrium by raising the temperature or by opening the container leads to faster evaporation and more stable nonane films, Figure 7;

- the increased stability of the first film formed during each run in the case of water films at x = 90% can be explained with the air in the container still being undersaturated (the complete saturation requires several minutes);

- the expected trend of τ vs. x. has been observed by other authors – according to Karakashev and Firouzi (Karakashev and Firouzi, 2014), pure water films break upon formation at 97% humidity and live for several seconds at x = 78-88%.

(ii) The model predicts that films of greater radii have longer lifetimes, see Figure 4B, which is confirmed for most evaporating water and nonane films, Figure 5 and Figure S9. The experimental and the theoretical trends of the dependence τ vs. R_f are in adequate agreement. The theory predicts that films of size smaller than a certain critical value $R_{f,cr}$ must be unstable. With water films at 90%, we found some evidence for the existence of $R_{f,cr}$ – under these conditions we observed many unstable films that rupture immediately upon formation and no films with a radius of less than 100 μm were stable after t_{load} = 300 min, see Figure 5A.

(iii) The model predicts the existence of a critical thickness h_{cr} of film rupture, at which the thermal Marangoni mechanism of stabilization ceases to act, eq. (34). The experimentally measured h_{cr} of water and nonane compare adequately with the theoretical value. The model also gives an approximate expression for the evolution of the film thickness with time which is in qualitative agreement with the experimental one (although the observed rate of thinning is faster than the theoretical, Fig. S10).

Some of these observations can be explained with other hypothetical stabilizing mechanisms, but not the combination of them. For example, the assumption for the existence of electrostatic repulsion can lead to a critical thickness of rupture similar to that in the Scheludko-Vrij (Radoev et al., 1983; Vrij, 1966) mechanism of film rupture through the occurrence of capillary waves; it, however, cannot explain the effect of the abrupt changes of the saturation on the film stability, nor the trend of the dependence of the lifetime τ on the film radius R_f. The presence of impurities (Yaminsky et al., 2010a) and dissolved and dissociated CO_2 (Katsir and Marmur, 2014b) may in part explain the behaviour of water films, but not that of alkane films. We can therefore say that the phenomena summarized in **(i-iii)** above have their simplest possible explanation in the evaporation-driven thermal Marangoni effect.

Yet, it must not be overlooked that several of our observations do not align with the theoretical predictions. Nearly all of these points of disagreement could be traced to the

unanswered question of **why pure *non-evaporating* films are stable**. We obtained the following experimental results that give useful hints about the nature of this stabilization:

(i) We consistently obtained aqueous films that were *stable* in a saturated atmosphere, thus confirming the results of Exerowa (Exerowa, 1969) and Yaminsky et al. (Yaminsky et al., 2010a). These films drained until they reached a stable thickness ~100 nm and had a lifetime longer than 30 min. This stability is indicative of the presence of an additional force, probably of electrostatic nature (Yaminsky et al., 2010b).

(ii) We consistently obtained non-evaporating nonane films of relatively high stability (of the order of tens of seconds). In contrast, our hexane films and Yaminsky's (Yaminsky, 2006) n-pentane films were unstable in a saturated atmosphere. It is puzzling that films from short- and long-chained alkanes behave differently in saturated atmosphere; it is also puzzling that water films are stable for hours while nonane films break after a minute. With nonane films, there is a clear dependence of film lifetime on film radius – larger films live longer.

(iii) We observed that non-evaporating films are typically more stable than slowly evaporating films. Water films formed after the complete saturation of the container (x = 100%, t_{load} > 9 min) had indefinitely long lifetimes, while the first films formed before saturation lived for 40-50 s, and films at x = 90% humidity lived for about a minute. Introducing a low rate of evaporation also noticeably destabilized the nonane films. These experimental findings contradict our theory. Another prediction that is at odds with the data is that we expect no stable films at low evaporation rates and humidities above a certain critical value x_{cr0} (eq. (38) and Figure 4).

These discrepancies are not surprising in view of the fact that our model neglects the electrostatic repulsion under all circumstances and therefore incorrectly predicts that pure non-evaporating films should rupture immediately. However, devising an accurate model of the electrostatic disjoining pressure in a pure liquid is a challenging task that goes well beyond the aims of our current study. The double layer in our water films is of a very sparse structure – the concentration of ions in pure water corresponds to one ion per 300×300 nm^2 for a film of thickness 100 nm. The characteristic distances of the electrostatic interaction are the Debye length and the average distance between two ions – for pure water, both are of the order of hundreds of nanometres, more than the film thickness. Electric double layers of such sparse structure have not, to our knowledge, been investigated, and may give rise to various peculiar

effects – for example, the time required for the formation of the sparse double layer is of the order of $L_D^2/D_{ion} \sim 0.1$ ms for water, and much more for alkanes. A fast dynamic phenomenon such as a capillary wave or the formation of a foam film will be able to perturb this structure – and perhaps decrease the repulsion. In view of these comments, our tentative hypothesis about the observed discrepancies between theory and experiment is that low evaporation rates decrease film stability due to an unclear mechanism of perturbation of the structure of the sparse electric double layer in the film, leading to suppression of the electrostatic repulsion that stabilizes the non-evaporating films. Further increase of the evaporation leads to stabilization, in accordance with our theory.

The study presented here is a first step towards the explanation of a family of similar phenomena, such as: the stability of evaporating films formed from concentrated electrolyte solutions (Karakashev et al., 2008); the destabilization of evaporating films by small amounts of non-volatile surfactants (Yaminsky et al., 2010a); the stability of evaporating films containing volatile surface-active agents (e.g., the dynamic stabilization of evaporating films formed from aqueous butanol solutions indicated by an unpublished experimental study of ours). Naturally, additional complications are expected in these systems because all of them involve conjugated thermal and solutal Marangoni effects. Phenomena of practical importance such as the occurrence of reflux in the injector nozzle after the injection event (Wang, 2012) are probably driven by a combination of such effects.

Acknowledgements. R.S. acknowledges support from BP through the BP International Centre for Advanced Materials (BP-ICAM). J.N. thanks Trinity College and the Clarendon Fund of the University of Oxford for a Clarendon-Titley Scholarship. Numerous discussions with Stoyan Karakashev, Emil Manev, Boryan Radoev, Roumen Tsekov, Krassimir Danov, Sorin Filip and Colin Bain helped us with the formulation of the problem.

Supplementary information:

S1. List of symbols from the main text and values of the parameters

S2. Hydrodynamics

S3. Heat currents through the liquid and the air

S4. Mass current through the air

S5. Knudsen and Fuchs transition layers

S6. Properties of the system at the stationary state for a thermostated meniscus

S7. Effect of the electrostatic disjoining pressure

S8. The cooling of the meniscus

S9. Additional experimental data

References

Baumgarten, C., 2006. Mixture Formation in Internal Combustion Engine, Heat, Mass Transfer. Springer Berlin Heidelberg, Berlin. doi:10.1007/3-540-30836-9

Chandramohan, A., Dash, S., Weibel, J.A., Chen, X., Garimella, S. V, 2016. Marangoni Convection in Evaporating Organic Liquid Droplets on a Nonwetting Substrate. Langmuir 32, 4729–4735. doi:10.1021/acs.langmuir.6b00307

Danov, K.D., Alleborn, N., Raszillier, H., Durst, F., 1998. The stability of evaporating thin liquid films in the presence of surfactant. I. Lubrication approximation and linear analysis. Phys. Fluids 10, 131–143. doi:10.1063/1.869555

Del Castillo, L.A., Ohnishi, S., Horn, R.G., 2011. Inhibition of bubble coalescence: Effects of salt concentration and speed of approach. J. Colloid Interface Sci. 356, 316–324. doi:10.1016/j.jcis.2010.12.057

Derjaguin, B.V., 1986. Theory of the Stability of Colloids and Thin Films (in Russian). Nauka, Moscow.

Dombrovsky, L.A., Sazhin, S.S., 2003. A simplified non-isothermal model for droplet heating and evaporation. Int. Commun. Heat Mass Transf. 30, 787–796. doi:10.1016/S0735-1933(03)00126-X

Du, L., Folliard, K.J., 2005. Mechanisms of air entrainment in concrete. Cem. Concr. Res. 35, 1463–1471. doi:10.1016/j.cemconres.2004.07.026

Exerowa, D., 1969. Effect of adsorption, ionic strength and pH on the potential of the diffuse electric layer. Kolloid-Zeitschrift und Zeitschrift für Polym. 232, 703–710. doi:10.1007/BF01500168

Exerowa, D., Kruglyakov, P.M., 1998. Foam and Foam Films. Theory, Experiment, Application. Elsevier, Amsterdam.

Firouzi, M., Nguyen, A. V., 2014. Effects of monovalent anions and cations on drainage and

lifetime of foam films at different interface approach speeds. Adv. Powder Technol. 25, 1212–1219. doi:10.1016/j.apt.2014.06.004

Fuchs, N.A., 1959. Evaporation and Droplet Growth in Gaseous Media. Pergamon Press, London.

Hu, H., Larson, R.G., 2006. Marangoni Effect Reverses Coffee-Ring Depositions. J. Phys. Chem. B 110, 7090–7094. doi:10.1021/jp0609232

Hu, H., Larson, R.G., 2005. Analysis of the Effects of Marangoni Stresses on the Microflow in an Evaporating Sessile Droplet. Langmuir 21, 3972–3980. doi:10.1021/la0475270

Israelachvili, J.N., 2011. Intermolecular and Surface Forces, 3rd ed. Academic Press, London.

Ivanov, I.B., Dimitrov, D.S., 1974. Hydrodynamics of thin liquid films. Colloid Polym. Sci. 252, 982–990. doi:10.1007/BF01566619

Karakashev, S.I., Firouzi, M., 2014. Personal Communication.

Karakashev, S.I., Nguyen, P.T., Tsekov, R., Hampton, M.A., Nguyen, A. V., 2008. Anomalous Ion Effects on Rupture and Lifetime of Aqueous Foam Films Formed from Monovalent Salt Solutions up to Saturation Concentration. Langmuir 24, 11587–11591. doi:10.1021/la801456j

Katsir, Y., Marmur, A., 2014a. Rate of Bubble Coalescence Following Dynamic Approach: Collectivity-Induced Specificity of Ionic Effect. Langmuir 30, 13823–13830. doi:10.1021/la503373d

Katsir, Y., Marmur, A., 2014b. Rate of Bubble Coalescence following Quasi-Static Approach: Screening and Neutralization of the Electric Double Layer. Sci. Rep. 4, 4266. doi:10.1038/srep04266

Kolarov, T., Yankov, R., Esipova, N.E., Exerowa, D., Zorin, Z.M., 1993. Charge reversal at the air/water interface as inferred from the thickness of foam films. Colloid Polym. Sci. 271, 519–520. doi:10.1007/BF00657398

Kosior, D., Zawala, J., Todorov, R., Exerowa, D., Malysa, K., 2014. Bubble bouncing and stability of liquid films formed under dynamic and static conditions from n-octanol solutions. Colloids Surf., A. 460, 391–400. doi:10.1016/j.colsurfa.2013.11.022

Levich, V.G., 1962. Physicochemical Hydrodynamics. Prentice-Hall, Inc., Englewood Cliffs, N.J.

Li, X., Karakashev, S.I., Evans, G.M., Stevenson, P., 2012. Effect of Environmental Humidity on

Static Foam Stability. Langmuir 28, 4060–4068. doi:10.1021/la205101d

Manev, E., Tsekov, R., Radoev, B., 1997. EFFECT OF THICKNESS NON-HOMOGENEITY ON THE KINETIC BEHAVIOUR OF MICROSCOPIC FOAM FILM. J. Dispers. Sci. Technol. 18, 769–788. doi:10.1080/01932699708943771

Manev, E.D., 2013. Personal Communication.

Manev, E.D., 1975. Effect of the disjoining pressure and surfactant diffusion on the thinning rate of aniline foam films. Ann. Univ. Sofia Fac. Chem. 70, 97–109.

Manev, E.D., Nguyen, A. V., 2005. Effects of surfactant adsorption and surface forces on thinning and rupture of foam liquid films. Int. J. Miner. Process. 77, 1–45. doi:10.1016/j.minpro.2005.01.003

Marinova, K.G., Alargova, R.G., Denkov, N.D., Velev, O.D., Petsev, D.N., Ivanov, I.B., Borwankar, R.P., 1996. Charging of Oil−Water Interfaces Due to Spontaneous Adsorption of Hydroxyl Ions. Langmuir 12, 2045–2051. doi:10.1021/la950928i

Marrucci, G., 1969. A theory of coalescence. Chem. Eng. Sci. 24, 975–985. doi:10.1016/0009-2509(69)87006-5

Nguyen, P.T., Nguyen, A. V, 2010. Drainage, Rupture, and Lifetime of Deionized Water Films: Effect of Dissolved Gases? Langmuir 26, 3356–3363. doi:10.1021/la9031333

Oron, A., Davis, S.H., Bankoff, S.G., 1997. Long-scale evolution of thin liquid films. Rev. Mod. Phys. 69, 931–980. doi:10.1103/RevModPhys.69.931

Palit, S.R., 1956. Thermodynamic Interpretation of the Eötvös Constant. Nature 177, 1180–1180. doi:10.1038/1771180a0

Peng, T., Chang, T.-M., 2014. Molecular processes of ion effects on aqueous nanofilm rupture. J. Mol. Liq. 193, 139–151. doi:10.1016/j.molliq.2013.12.031

Radoëv, B.P., Dimitrov, D.S., Ivanov, I.B., 1974. Hydrodynamics of thin liquid films effect of the surfactant on the rate of thinning. Colloid Polym. Sci. 252, 50–55. doi:10.1007/BF01381695

Radoev, B.P., Scheludko, A.D., Manev, E.D., 1983. Critical thickness of thin liquid films: Theory and experiment. J. Colloid Interface Sci. 95, 254–265. doi:10.1016/0021-9797(83)90094-2

Reynolds, O., 1886. On the Theory of Lubrication and Its Application to Mr. Beauchamp Tower's Experiments, Including an Experimental Determination of the Viscosity of Olive

Oil. Proc. R. Soc. London 40, 191–203. doi:10.1098/rspl.1886.0021

Robinson, R.A., Stokes, R.H., 1959. Electrolyte Solutions, 2nd ed. Butterworths Scientific Publications, London.

Scheludko, A., Platikanov, D., Manev, E., 1965. Disjoining pressure in thin liquid films and the electro-magnetic retardation effect of the molecule dispersion interactions. Discuss. Faraday Soc. 40, 253. doi:10.1039/df9654000253

Sheludko, A., 1967. Thin liquid films. Adv. Colloid Interface Sci. 1, 391–464. doi:10.1016/0001-8686(67)85001-2

Slavchov, R.I., Karakashev, S.I., Ivanov, I.B., 2014. Ionic Surfactants and Ion-Specific Effects: Adsorption, Micellization, and Thin Liquid Films, in: Romsted, L.S. (Ed.), Surfactant Science and Technology: Retrospects and Prospects. CRC Press, Boca Raton, FL, pp. 53–117.

Slavchov, R.I., Novev, J.K., 2012. Surface tension of concentrated electrolyte solutions. J. Colloid Interface Sci. 387, 234–243. doi:10.1016/j.jcis.2012.07.020

Snegirev, A.Y., 2013. Transient temperature gradient in a single-component vaporizing droplet. Int. J. Heat Mass Transf. 65, 80–94. doi:10.1016/j.ijheatmasstransfer.2013.05.064

Stubenrauch, C., Klitzing, R. von, 2003. Disjoining pressure in thin liquid foam and emulsion films—new concepts and perspectives. J. Phys. Condens. Matter 15, R1197–R1232. doi:10.1088/0953-8984/15/27/201

Sullivan, A.P., Kilpatrick, P.K., 2002. The Effects of Inorganic Solid Particles on Water and Crude Oil Emulsion Stability. Ind. Eng. Chem. Res. 41, 3389–3404. doi:10.1021/ie010927n

Sultan, E., Boudaoud, A., Amar, M. Ben, 2005. Evaporation of a thin film: diffusion of the vapour and Marangoni instabilities. J. Fluid Mech. 543, 183. doi:10.1017/S0022112005006348

Tsekov, R., Ruckenstein, E., 1994. Dimple formation and its effect on the rate of drainage in thin liquid films. Colloids Surf., A. 82, 255–261. doi:10.1016/0927-7757(93)02633-P

Tsoumpas, Y., Dehaeck, S., Rednikov, A., Colinet, P., 2015. Effect of Marangoni Flows on the Shape of Thin Sessile Droplets Evaporating into Air. Langmuir 31, 13334–13340. doi:10.1021/acs.langmuir.5b02673

Valkovska, D.S., Danov, K.D., 2001. Influence of Ionic Surfactants on the Drainage Velocity of Thin Liquid Films. J. Colloid Interface Sci. 241, 400–412. doi:10.1006/jcis.2001.7757

Vrij, A., 1966. Possible mechanism for the spontaneous rupture of thin, free liquid films. Discuss. Faraday Soc. 42, 23. doi:10.1039/df9664200023

Wang, L., Qu, X., 2012. Impact of interface approach velocity on bubble coalescence. Miner. Eng. 26, 50–56. doi:10.1016/j.mineng.2011.10.016

Wang, Y.C., 2012. Study of Deposit Formation Inside Diesel Injectors Nozzles. PhD Thesis. Massachusetts Institute of Technology.

Yaminsky, V.V., 2006. Bubble vortex at surfaces of evaporating liquids. J. Colloid Interface Sci. 297, 251–260. doi:10.1016/j.jcis.2005.10.004

Yaminsky, V. V., Ohnishi, S., Vogler, E.A., Horn, R.G., 2010a. Stability of Aqueous Films between Bubbles. Part 2. Effects of Trace Impurities and Evaporation. Langmuir 26, 8075–8080. doi:10.1021/la904482n

Yaminsky, V. V., Ohnishi, S., Vogler, E.A., Horn, R.G., 2010b. Stability of Aqueous Films between Bubbles. Part 1. The Effect of Speed on Bubble Coalescence in Purified Water and Simple Electrolyte Solutions. Langmuir 26, 8061–8074. doi:10.1021/la904481d

Yiantsios, S.G., Higgins, B.G., 2006. Marangoni flows during drying of colloidal films. Phys. Fluids 18, 82103. doi:10.1063/1.2336262

Zuiderweg, F.J., Harmens, A., 1958. The influence of surface phenomena on the performance of distillation columns. Chem. Eng. Sci. 9, 89–103. doi:10.1016/0009-2509(58)80001-9

Evaporating Foam Films of Pure Liquid Stabilized via the Thermal Marangoni Effect

Supplementary Information

Javor K. Novev[1], Nikolay Panchev[2], Radomir I. Slavchov[3]*

[1]*Department of Chemistry, Physical and Theoretical Chemistry Laboratory,*
University of Oxford, South Parks Road, Oxford OX1 3QZ, U.K.

[2]*Institute of Physical Chemistry,*
Bulgarian Academy of Sciences, Acad. G. Bonchev Str., Block 11, Sofia 1113, Bulgaria

[3]*Department of Chemical Engineering and Biotechnology,*
University of Cambridge, Philippa Fawcett Drive, Cambridge CB0 3SA, U.K.

1. List of symbols from the main text and values of the parameters

a — coefficient appearing in the solutions for h_{st} for a cold meniscus,

$$a = -54 + k^3 + 6\sqrt{81 - 3k^3}$$

A_H — Hamaker constant [J]

C — vapour concentration [mol/m^3]

C_∞ — vapour concentration in the ambient air [mol/m^3]

C_{eq0} — equilibrium vapour concentration at temperature T_∞ of the ambient air,

$$C_{eq0} = \frac{p^o}{RT_\infty}\exp\left[-\frac{h_e}{R}\left(\frac{1}{T_\infty} - \frac{1}{T_e^o}\right)\right] \text{[mol/m}^3\text{]}$$

C_{eq} — equilibrium vapour concentration in the meniscus region for a cold meniscus

$$C_{eq} = \frac{p^0}{RT_m}\exp\left[-\frac{h_e}{R}\left(\frac{1}{T_m} - \frac{1}{T_e^o}\right)\right] \text{[mol/m}^3\text{]}$$

C^S — vapour concentration at the surface of the liquid,

$$C^S = \frac{p^o}{RT^L}\exp\left[-\frac{h_e}{R}\left(\frac{1}{T^L} - \frac{1}{T_e^o}\right)\right] \text{[mol/m}^3\text{]}$$

ΔC — deviation of the local vapour concentration from C_∞, $\Delta C = C - C_\infty$ [mol/m^3]

ΔC_m — value of ΔC at $R_f < r < R_c$ for the case of a cold meniscus [mol/m^3]

ΔC^S — deviation of the vapour concentration at the surface from C_∞, $\Delta C^S = C^S - C_\infty$ [mol/m^3]

C_{rr} — second derivative of the model concentration profile for the liquid with respect to r [mol/m^5]

C_p — total heat capacity of the system meniscus-capillary [J/K]

D — diffusion coefficient [m^2/s]

d_{glass} — thickness of the glass capillary of the Sheludko cell [m]

h — film thickness [m]

h_{cr} — critical film thickness [m]

h_{st} — stationary/quasistationary film thickness [m]

h_e — enthalpy of evaporation of the liquid [J/mol]

J	diffusive flux through both surfaces of the film [mol/s]
j_c	density of the mass flux caused by the concentration difference between the region in contact with the meniscus and the surrounding air [mol·s^{-1}·m^{-2}]
j_f	density of the mass flux caused by the concentration difference between the region in contact with the film and that in contact with the meniscus [mol·s^{-1}·m^{-2}]
J_m	diffusive flux through both surfaces of the meniscus [mol/s]
k	constant appearing in the form (33) of the mass balance, $k = R_f^2 R_c s^S T_{rr}/2h_{cr}\sigma_m$
p	pressure profile in the fluid [Pa]
p_0	pressure of the ambient gas [Pa]
p^o	standard pressure, $p^o = 101325$ [Pa]
p_c	capillary pressure, $p_c = 2\sigma_m/R_c$ [Pa]
p_m	pressure of the fluid in the meniscus, $p\big\|_{r=R_f} = p_m = p_0 - 2\sigma_m / R_c$ [Pa]
Q	heat flux from the air through both surfaces of the film [J/s]
Q_m	heat flux from the air through both surfaces of the meniscus [J/s]
r	radial cylindrical coordinate [m]
R	gas constant [J·mol^{-1}·K^{-1}]
R_f	film radius [m]
R_c	cell radius [m]
s^S	surface entropy of the liquid [J·K^{-1}·m^{-2}]
t	time [s]
T	temperature profile for the gas phase [K]
T_∞	temperature of the ambient gas [K]
ΔT	profile of the temperature difference in the air, $\Delta T = T - T_\infty$ [K]
T_e^o	boiling temperature of the liquid at p^o [K]
T^L	temperature profile for the liquid phase [K]
δT	temperature difference between film and meniscus, $\delta T = T^L(0 < r < R_f) - T_m$ [K]
T_m	temperature of the liquid in the meniscus, $T_m = T^L(R_f)$ [K]

ΔT_m	difference between the temperature of the meniscus and the ambient gas, $\Delta T_m = T_m - T_\infty$ [K]
$\Delta T_{m,cr}$	critical temperature difference between the temperature of the meniscus and the ambient gas at which the film breaks [K]
T_{rr}	second derivative of the model temperature profile for the liquid with respect to r [K/m^2]
$T_{rr0,cr}$	critical value of T_{rr} for a thermostated meniscus [K/m^2]
$\boldsymbol{v}$	velocity vector field [m/s]
v_r	radial component of the velocity [m/s]
V_r	radial component of the velocity at the surface of the film $V_z = v_z(z=h/2)$ [m/s]
v_z	vertical component of the velocity [m/s]
V_z	vertical component of the velocity at the surface of the film, $V_r = v_r(z=h/2)$ [m/s]
x	relative saturation of the ambient gas, $x = C_\infty/C_{eq}$
x_{cr0}	critical value of the relative saturation for thermostated meniscus
x_{cr}	critical value of the relative saturation for a cold meniscus
z	vertical coordinate [m]
η	viscosity of the liquid [Pa·s]
κ^L	heat conductivity of the liquid phase [W·m^{-1}·K^{-1}]
κ	heat conductivity of the gas phase [W·m^{-1}·K^{-1}]
Π_{vdW}	van der Waals disjoining pressure [Pa]
$\sigma(r)$	surface tension profile of the liquid [N/m]
σ_m	surface tension of the liquid in the meniscus [N/m]
χ^L	thermal diffusivity of the liquid phase [m^2/s]
χ	thermal diffusivity of the gas phase [m^2/s]
ρ	density of the liquid [kg/m^3]

Table 1 lists the typical values of the parameters that we have used in our calculations; it also gives the numerical values of the most important quantities for the studied systems in the case of a thermostated meniscus. These quantities are given only for the single most commonly encountered value of R_f, R_c and x.

Table 1. Values of the parameters used for the calculations cited throughout the text. The choice of relative saturation for water films (x = 45%) coincides with the lowest value in our experiments, see Section 3.2 of the main text; all calculations are for a thermostated meniscus ($\Delta T_m = 0$). For more details on the entries marked with an asterisk, consult S6.

	Water	**Hexane**	**Nonane**	**Hexadecane**
R_f [m]	1.5×10^{-4}			
R_c [m]	2×10^{-3}			
d_{glass} [m]	1×10^{-3}			
h (stable stationary value) [m]	3.47×10^{-7}	2.63×10^{-6}	1.32×10^{-7}	none
T_∞ [K]	298.15			
p^o [Pa]	101325			
T_e^o [K]	373.15 (Lide, 2005)	341.88 (Lide, 2005)	423.97 (Lide, 2005)	560.01 (Lide, 2005)
A_H [J]	4.38×10^{-20} (Visser, 1972)	2.76×10^{-20} (Butt and Kappl, 2010)	4.66×10^{-20} (Drummond and Chan, 1997)	5.2×10^{-20} (Israelachvili, 2011)
c_p [J·kg^{-1}·K^{-1}]	4.181×10^3 (Sabbah et al., 1999)	2.270×10^3 (Lide, 2005)	2.217×10^3 (Lide, 2005)	2.215×10^3 (Růžička et al., 1991)
C_p [J/K]	0.185	0.140	0.141	0.143
D [m^2/s]	2.6×10^{-5} (Lee and Wilke, 1954)	7.32×10^{-6} (Lugg, 1968)	5.07×10^{-6} (Zhu et al., 2007)	4.05×10^{-6} (Wilke and Lee, 1955)
h_e [J/mol]	43.990×10^3 (Lide, 2005)	31.56×10^3 (Lide, 2005)	46.55×10^3 (Lide, 2005)	81.35×10^3 (Lide, 2005)
s^S [J·K^{-1}·m^{-2}]	1.38×10^{-4}	1.022×10^{-4} (Jasper and Kring, 1955)	9.347×10^{-5} (Jasper and Kring, 1955)	8.54×10^{-5} (Jasper and Kring, 1955)
v^L [m^3/mol]	1.81×10^{-5} (Lide, 2005)	1.30×10^{-4} (Lide, 2005)	1.78×10^{-4} (Lide, 2005)	2.94×10^{-4} (Lide, 2005)
x	45 %	0 %	0 %	0 %
η [Pa·s]	8.903×10^{-4} (Kestin et al., 1978)	3.00×10^{-4} (Lide, 2005)	6.65×10^{-4} (Lide, 2005)	3.032×10^{-3} (Lide, 2005)
κ^L [W·m^{-1}·K^{-1}]	0.6067 (Nieto de Castro et al., 1986)	0.1167 (Lide, 2005)	0.1269 (Lide, 2005)	0.140 (Lide, 2005)
κ [W·m^{-1}·K^{-1}]	2.62×10^{-2} (Lide, 2005)			
ρ [kg/m^3]	997 (Lide, 2005)	660.6 (Lide, 2005)	719.2 (Lide, 2005)	770.1 (Lide, 2005)

σ_0 [N/m]	71.99×10^{-3} (Vargaftik et al., 1983)	17.89×10^{-3} (Lide, 2005)	22.38×10^{-3} (Lide, 2005)	27.05×10^{-3} (Lide, 2005)
χ^L [m^2/s]	1.45×10^{-7}	7.78×10^{-8} (Lide, 2005)	7.96×10^{-8} (Lide, 2005)	8.21×10^{-8} (Lide, 2005)
χ [m^2/s]	2×10^{-5}			
h_{cr} [m], eq. (34)*	40.1×10^{-9}	54.7×10^{-9}	60.4×10^{-9}	-
V_z [m/s], exact form of eq. (30)*	1.2×10^{-8}	3.3×10^{-7}	1.9×10^{-8}	-
$V_r(R_f)$ [m/s], eq. (S.109)*	-2.7×10^{-5}	-9.4×10^{-4}	-2.3×10^{-5}	-
$Re = \rho h V_z/\eta$*	4.8×10^{-9}	1.9×10^{-6}	2.7×10^{-9}	-
$Pe^L_{heat} \sim R_f^2 V_z/\chi^L h$, eq. (S.113)*	2.8×10^{-3}	1.8×10^{-2}	2.0×10^{-2}	-
$Pe^A_{heat,\,r} \sim R_f V_r/\chi$, eq. (S.114)*	1.0×10^{-4}	3.5×10^{-3}	8.6×10^{-5}	-
$Pe^A_{heat,\,z}$, eq. (S.116)*	1.3×10^{-4}	4.7×10^{-4}	2.0×10^{-5}	-
$Pe_{mass,\,r}$, eq. (S.119)*	7.4×10^{-3}	5.1×10^{-1}	2.2×10^{-2}	-
$Pe_{mass,\,z}$, eq. (S.121)*	1.4×10^{-2}	1.0×10^{-1}	7.5×10^{-3}	-

2. Hydrodynamics

This section provides more context on the hydrodynamic problem and derives eqs. (5)-(8) from the main text. We consider a plain parallel circular of thickness h and radius R_f, for which $h/R_f \sim 10^{-3}$, see S1, and therefore, the *lubrication approximation* is applicable to the flow within it (Reynolds, 1886). In addition, the inertial terms of the Navier-Stokes equations can be disregarded due to their proportionality to the small Reynolds number (*capillary flow approximation*). For a thin liquid film of pure water of density $\rho \sim 10^3$ kg/m^3, viscosity $\eta \sim 10^{-3}$ Pa.s, $h \sim 10^{-7}$ m, normal velocity at the surface $v_z|_{z=h/2} \equiv V_z \sim 10^{-8}$ m/s (see S1&6), the Reynolds number is of the order of $Re = \rho h V_z/\eta \sim 10^{-9}$. Using both approximations, we arrive at the following form of the radial and the normal components of the Navier-Stokes equation in cylindrical coordinates (Reynolds, 1886):

$$\frac{\partial p}{\partial r} = \eta \frac{\partial^2 v_r}{\partial z^2}; \tag{S.41}$$

$$\frac{\partial p}{\partial z} = 0, \tag{S.42}$$

where p is the hydrodynamic pressure. The coordinate system is defined so that its origin is in the centre of the film and the film surfaces coincide with the planes $z = \pm h/2$. The radial (v_r) and normal (v_z) components of the velocity vector field $\boldsymbol{v}$ are related via the continuity equation,

$$\frac{1}{r}\frac{\partial r v_r}{\partial r} + \frac{\partial v_z}{\partial z} = 0. \tag{S.43}$$

We solve eq. (S.41) for v_r subject to the boundary condition (1) at the film surface, giving

$$v_r = -\frac{h^2 - 4z^2}{8\eta}\frac{\mathrm{d}p}{\mathrm{d}r} + V_r(r). \tag{S.44}$$

By substitution of this result in the continuity equation (S.3) and subsequent integration over z from 0 to $h/2$ with $v_z|_{z=0}$ set to 0 (following from the symmetry of the problem), we obtain for v_z

$$v_z = \frac{3zh^2 - 4z^3}{24\eta}\frac{1}{r}\frac{\mathrm{d}}{\mathrm{d}r}\left(r\frac{\mathrm{d}p}{\mathrm{d}r}\right) - \frac{z}{r}\frac{\mathrm{d}rV_r(r)}{\mathrm{d}r}. \tag{S.45}$$

The tangential (V_r) and normal (V_z) surface velocities can be related by using eq. (S.45) in conjunction with the boundary condition at the film surface, eq. (1):

$$V_r(r) = \frac{h^2}{12\eta}\frac{\mathrm{d}p}{\mathrm{d}r} - \frac{r}{h}V_z. \tag{S.46}$$

The pressure gradient in the film, $\mathrm{d}p/\mathrm{d}r$, which appears in (S.44)-(S.46), is caused by the evaporation-induced surface tension gradient $\mathrm{d}\sigma/\mathrm{d}r$. The two are connected through the tangential force balance at the film surface, which relates $\mathrm{d}\sigma/\mathrm{d}r$ with the rz-component of the viscous stress tensor (Levich, 1962; Radoëv et al., 1974),

$$\frac{\mathrm{d}\sigma}{\mathrm{d}r} = \eta\left.\frac{\partial v_r}{\partial z}\right|_{z=h/2} = \frac{h}{2}\frac{\mathrm{d}p}{\mathrm{d}r}, \tag{S.47}$$

where we used eq. (S.44). For simplicity, we neglect the surface viscous tensor here although its contribution may be important for similar systems (Scriven and Sternling, 1960).

We now substitute the surface tension profile (4), together with the explicit expression (6) for v_r, in the tangential force balance at the surface (3), which we then solve for p:

$$p(r) = p_{\mathrm{m}} - \frac{2}{h} s^{\mathrm{S}} \left(T^{\mathrm{L}}(r) - T_{\infty} \right). \tag{S.48}$$

Next, we substitute eq. (S.48) back into eq. (S.46) in order to obtain the following relation between the radial surface velocity V_r and the temperature profile:

$$V_r(r) = -\frac{h s^{\mathrm{S}}}{6\eta} \frac{\partial T^{\mathrm{L}}}{\partial r} - \frac{r}{h} V_z \ . \tag{S.49}$$

3. Heat currents through the liquid and the air

In this supplement, we will estimate the numerical coefficients in eqs. (19)-(20) and (23)-(24) for Q, J, Q_{m} and J_{m}, based on a simplified model of the geometry of the film. In our model of the heat and mass transfer in the system we will neglect the curvature of the surface of the meniscus, considering it planar (as depicted in Figure S.1) – that is, we approximate the shape of the meniscus with a cylinder of height h and radius R_{c} with a hole of radius R_{f} in the centre. As all characteristic lengths in the real and the model system are similar, the obtained numerical coefficients must be accurate enough for our purposes: in view of the many uncertainties in the experiment, a more accurate model would be superfluous.

3.1. Heat transfer through the air

In our treatment, the temperature profile in the gas phase (T) is controlled by the stationary heat equation,

$$\frac{1}{r} \frac{\partial}{\partial r} r \frac{\partial \Delta T}{\partial r} + \frac{\partial^2 \Delta T}{\partial z^2} = 0 , \tag{S.50}$$

where ΔT is defined with respect to the ambient temperature, $\Delta T = T - T_{\infty}$. For the heat transfer in the air, it is convenient to use a coordinate system in which the surface of the film coincides with the plane $z = 0$ (Figure S.1). Since the Péclet number that compares the relative contribution of radial convective and conductive heat transport ($Pe^{\mathrm{A}}_{\mathrm{heat},r}$) is low - $Pe^{\mathrm{A}}_{\mathrm{heat},r} \sim 10^{-4}$ for a water film (see S1&6), we do not need to consider convective terms in eq. (S.50). When the evaporation is

very fast, the normal velocity and the respective convective flux in the gas phase can in principle become significant, possibly restricting the validity of eq. (S.50). However, for all films studied here, the Péclet number that compares the contribution of convective heat transfer in the z-direction with the conductive heat transfer, $Pe^{\mathrm{A}}_{\mathrm{heat},z}$ is also much smaller than unity, typically $Pe^{\mathrm{A}}_{\mathrm{heat},z} \sim 10^{-4}$ (S1&6).

The first boundary condition of eq. (S.50) is that far from the fluid surface the temperature difference ΔT tends to zero,

$$\Delta T\big|_{z\to\infty} = 0 \ . \tag{S.51}$$

The boundary condition at the plane $z = 0$, which coincides with the film surface, is more complicated and contains contributions from the three different regions of the system. To formulate this boundary condition, we now introduce a number of additional approximations, which should lead to a reasonably simple estimate of the numerical coefficients in the dependence of the heat flux Q on the parameters of the system without affecting the functional dependence itself

(i) film ($0 < r < R_{\mathrm{f}}$). As discussed in the main text, we assume that the evaporation causes a difference between the temperature of the film and the meniscus that can be described with a second-order polynomial in r:

$$z = 0,\ r < R_{\mathrm{f}}: \qquad \Delta T(r)\big|_{z=0} = \Delta T_{\mathrm{m}} + \frac{T_{rr}}{2}\left(r^2 - R_{\mathrm{f}}^2\right). \tag{S.52}$$

(ii) Meniscus ($R_{\mathrm{f}} < r < R_{\mathrm{c}}$). We assume that the temperature of the liquid in the meniscus region is homogeneous but lower than the ambient by ΔT_{m},

$$z = 0,\ R_{\mathrm{f}} < r < R_{\mathrm{c}}: \quad \Delta T(r)\big|_{z=0} = \Delta T_{\mathrm{m}}. \tag{S.53}$$

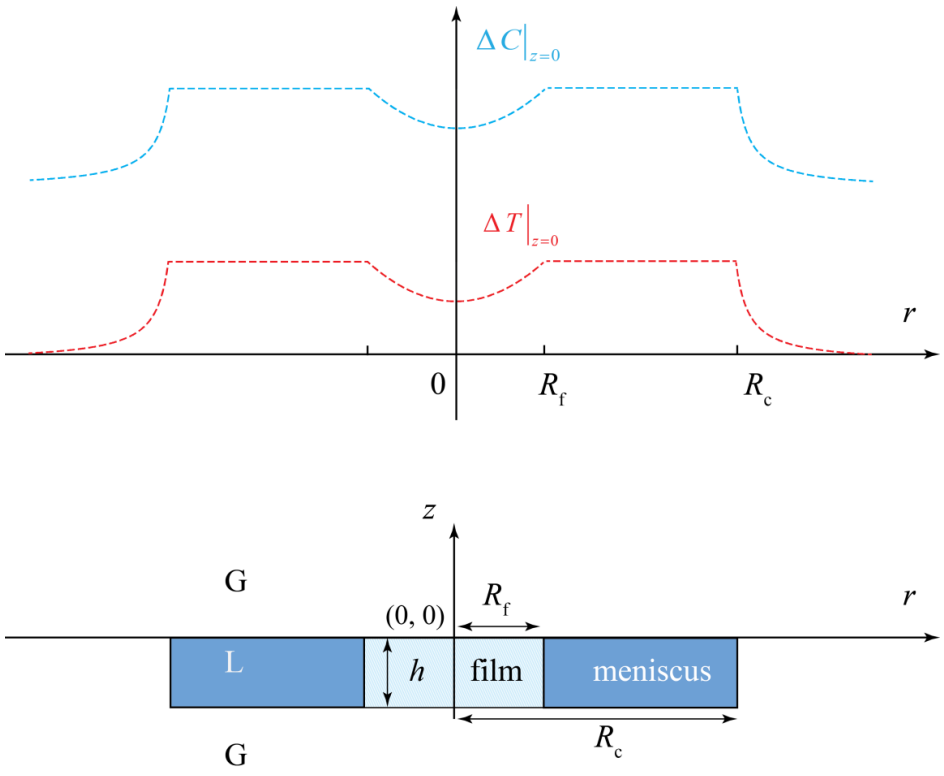

Figure S.1. Scheme of the models for the temperature distribution $\Delta T = T - T_\infty$(solid line) and the concentration profile $\Delta C = C - C_\infty$ (dashed line) in the gas phase at $z = 0$, as given by eqs. (S.56) and (S.100), respectively. These models are used for the estimation of the numerical coefficients in eqs. (S.57) -(S.58) and (S.101)-(S.102) for the heat and mass fluxes through the film and the meniscus.

(iii) Surrounding gas ($r > R_c$). The disturbance in the temperature profile of the air propagates of the order of the radius of the Scheludko cell R_c at the stationary state; for that reason, we need to include the region outside the cell in our models for the heat and mass transfer. For the boundary condition of ΔT at $z = 0$ and $r > R_c$, we assume that the temperature difference in this region is inversely proportional to the radial coordinate, in accordance with the expected asymptotic behaviour at large r, compare to the temperature profile in the vicinity of a spherical drop (Fuchs, 1959):

$$z = 0,\ r > R_c: \qquad \Delta T(r)\big|_{z=0} = \Delta T_m \frac{A}{r}. \tag{S.54}$$

We checked the validity of the approximation (S.54) by adding a higher-order term (B/r^2) in the expression for $\Delta T|_{z=0}$. This led to the same final result for the heat flux Q which justifies the

assumption. In order to determine the coefficient A, we assume continuity of $\Delta T|_{z=0}$ at $r = R_c$, which yields

$$A = R_c. \tag{S.55}$$

The stricter approach for the determination of A is to use a condition that sets the normal integral heat flux in the region outside the Scheludko cell to zero. In S3.2 we demonstrate that this stricter condition leads to the exact same result (S.55).

Thus, combining (S.52)-(S.54), we arrive at the boundary condition

$$\Delta T^{L}(r) = \Delta T(r)\big|_{z=0} = \frac{T_{rr}}{2}\left(r^2 - R_f^2\right)\theta(R_f - r) + \Delta T_m\left(\theta(R_c - r) + \frac{R_c}{r}\theta(r - R_c)\right), \tag{S.56}$$

where θ is the Heaviside step function.

In our model, we make the assumption that the temperatures of the liquid and the adjacent air are equal, and therefore eq. (S.56) also serves as the boundary condition for the problem for the temperature distribution $\Delta T(r,z) = T(r,z) - T_\infty$ in the liquid phase. The assumption that the temperature is continuous at the interface breaks down when the Hertz-Knudsen heat current and the total heat current through the surface are of the same order of magnitude. In the latter case, one needs to account for the existence of a temperature jump inside a transition region (the *Knudsen layer*) with thickness of the order of the mean free path of the gas molecules (Badam et al., 2007; Langmuir, 1915), see also S 5.

Now that we have the necessary boundary conditions for the heat equation in the gas phase, we can proceed with the determination of the heat flux Q from the air through the surfaces of the film. As the derivation of Q is rather lengthy, instead of giving it here, we will describe it in S3.3. The approximate end result valid provided that $R_f << R_c$ is eq. (20) from the main text,

$$Q = \kappa R_f^2\left[\frac{8}{3}R_f T_{rr} - \left(2 - \sqrt{2}\right)\frac{\pi}{R_c}\Delta T_m\right]. \tag{S.57}$$

The heat flux through the surfaces of the meniscus is

$$Q_m = -4.57\kappa R_c \Delta T_m\,. \tag{S.58}$$

In deriving eq. (S.58), we have used a series expansion valid for $R_f << R_c$; the interested reader may find the full derivation in S 3.4.

3.2. Determination of the constant *A*

Here, we will disclose the stricter approach to the determination of the constant A appearing in eq. (S.54). Instead of assuming continuity of the temperature profile T at $z = 0$ as in S3.1, we will use the more physically grounded condition that the integral heat flux from the region outside the Scheludko cell is zero.

We solve the heat equation for the gas phase (S.50) with the boundary conditions (S.51) and (S.56) by applying a Fourier-Bessel transform defined with the identities $\tilde{F}\left(\xi\right)=\int_0^\infty rF(r)\mathrm{J}_0(r\xi)\mathrm{d}r$ for the forward Fourier-Bessel transformation of F to its image $\tilde{F}$ and $F(r)=\int_0^\infty \xi\tilde{F}\left(\xi\right)\mathrm{J}_0(r\xi)\mathrm{d}\xi$ for the inverse transform of $\tilde{F}$, where $\mathrm{J_n}(r)$ denotes the Bessel function of the first kind and the n-th order and ξ is the Fourier-Bessel variable.

The Fourier-Bessel transform of eq. (S.50) reads

$$\frac{\partial^2\Delta\tilde{T}}{\partial z^2}=\xi^2\Delta\tilde{T}\,. \tag{S.59}$$

The solution to eq. (S.59) that satisfies the boundary condition (S.51) can be written as

$$\Delta\tilde{T}=\Delta\tilde{T}^{\mathrm{S}}(\xi)\exp(-\xi z)\,. \tag{S.60}$$

The unknown function $\Delta\tilde{T}^{\mathrm{S}}(\xi)$ is determined via direct application of the boundary condition at $z = 0$, in which rather than using (S.56) we have left the constant A undetermined. Each of the three distinct regions of the studied system has an additive contribution to $\Delta\tilde{T}^{\mathrm{S}}(\xi)$:

$$\Delta\tilde{T}^{\mathrm{S}}(\xi)=\Delta\tilde{T}^{\mathrm{S}}_{\mathrm{film}}(\xi)+\Delta\tilde{T}^{\mathrm{S}}_{\mathrm{meniscus}}(\xi)+\Delta\tilde{T}^{\mathrm{S}}_{\mathrm{air}}(\xi)\,. \tag{S.61}$$

The functions $\Delta\tilde{T}^{\mathrm{S}}_{\mathrm{i}}(\xi)$ in eq. (S.61), which are simply the Fourier-Bessel images of the corresponding terms in the boundary condition (S.56), are defined as follows:

$$\Delta\tilde{T}^{\mathrm{S}}_{\mathrm{film}}(\xi)=\frac{T_{rr}R_{\mathrm{f}}}{\xi^3}\left(\xi R_{\mathrm{f}}\,\mathrm{J}_0(\xi R_{\mathrm{f}})-2\mathrm{J}_1(\xi R_{\mathrm{f}})\right),\ \Delta\tilde{T}^{\mathrm{S}}_{\mathrm{meniscus}}(\xi)=\frac{R_{\mathrm{c}}\Delta T_{\mathrm{m}}}{\xi}\mathrm{J}_1(\xi R_{\mathrm{c}}),$$

$$\Delta\tilde{T}^{\mathrm{S}}_{\mathrm{air}}(\xi)=\frac{A\Delta T_{\mathrm{m}}}{\xi}+\frac{A\Delta T_{\mathrm{m}}R_{\mathrm{c}}}{2}\left[\pi\mathrm{J}_0(\xi R_{\mathrm{c}})\mathrm{H}_1(\xi R_{\mathrm{c}})-\pi\mathrm{J}_1(\xi R_{\mathrm{c}})\mathrm{H}_0(\xi R_{\mathrm{c}})-2\mathrm{J}_0(\xi R_{\mathrm{c}})\right]. \tag{S.62}$$

In the equations above, $\mathrm{H_n}$ signifies the n-th order Struve function.

The normal heat flux through the region outside the capillary or, equivalently, the derivative $\partial\Delta T/\partial z$ must equal zero at $z = 0$,

$$\left.\frac{\partial \Delta T}{\partial z}\right|_{z=0} = \int_0^\infty \xi \left.\frac{\partial \Delta \tilde{T}}{\partial z}\right|_{z=0} \mathrm{J}_0(\xi r)\mathrm{d}\xi = 0,\ r > R_\mathrm{c}. \tag{S.63}$$

Because of the approximate character of the solution ΔT (stemming from the approximate boundary condition at $z = 0$), the condition (S.63) can be applied only to the integral heat flux:

$$2\pi \int_{R_\mathrm{c}}^\infty r \int_0^\infty \xi \left.\frac{\partial \Delta \tilde{T}}{\partial z}\right|_{z=0} \mathrm{J}_0(\xi r)\mathrm{d}\xi\mathrm{d}r = 0. \tag{S.64}$$

The double integral in eq. (S.64) is equivalent to a successive application of the reverse and forward Fourier-Bessel transformation to the function $\partial\tilde{T} / \partial z$:

$$\int_{R_\mathrm{c}}^\infty r \int_0^\infty \xi \left.\frac{\partial \Delta \tilde{T}}{\partial z}\right|_{z=0} \mathrm{J}_0(\xi r)\mathrm{d}\xi\mathrm{d}r = \left[\int_{R_\mathrm{c}}^\infty r\mathrm{J}_0(\xi_1 r)\int_0^\infty \xi \left.\frac{\partial \Delta \tilde{T}}{\partial z}\right|_{z=0} \mathrm{J}_0(\xi r)\mathrm{d}\xi\mathrm{d}r\right]\Bigg|_{\xi_1=0} =$$

$$= \left[\int_0^\infty r\mathrm{J}_0(\xi_1 r)\int_0^\infty \xi \left.\frac{\partial \Delta \tilde{T}}{\partial z}\right|_{z=0} \mathrm{J}_0(\xi r)\mathrm{d}\xi\mathrm{d}r - \int_0^{R_\mathrm{c}} r\mathrm{J}_0(\xi_1 r)\int_0^\infty \xi \left.\frac{\partial \Delta \tilde{T}}{\partial z}\right|_{z=0} \mathrm{J}_0(\xi r)\mathrm{d}\xi\mathrm{d}r\right]\Bigg|_{\xi_1=0} =$$

$$= \left.\frac{\partial \Delta \tilde{T}(\xi_1, z)}{\partial z}\right|_{z=0,\xi_1=0} - R_\mathrm{c}\int_0^\infty \mathrm{J}_1(\xi R_\mathrm{c}) \left.\frac{\partial \Delta \tilde{T}}{\partial z}\right|_{z=0} \mathrm{d}\xi = \left.\frac{\partial \Delta \tilde{T}}{\partial z}\right|_{z=0,\xi=0} + R_\mathrm{c}\int_0^\infty \xi\mathrm{J}_1(\xi R_\mathrm{c})\Delta\tilde{T}^\mathrm{S}\mathrm{d}\xi. \tag{S.65}$$

Directly applying the definition of $\Delta\tilde{T}^\mathrm{S}(\xi)$, eqs. (S.61)-(S.62), we obtain the expression $\left.\partial\Delta\tilde{T} / \partial z\right|_{z=0,\xi=0} = -\Delta T_\mathrm{m} A$. Substituting it in (S.65) results in an equation for A,

$$-A\Delta T_\mathrm{m} + R_\mathrm{c}\int_0^\infty \xi\mathrm{J}_1(\xi R_\mathrm{c})\Delta\tilde{T}^\mathrm{S} d\xi = 0. \tag{S.66}$$

In order for eq. (S.66) to be even approximately fulfilled, it is mandatory that the integral $\int_0^\infty \xi\mathrm{J}_1(\xi R_\mathrm{c})\Delta\tilde{T}^\mathrm{S}\mathrm{d}\xi$ is finite-valued, which is only possible if its integrand tends to zero at $\xi\to\infty$.

Taking the series expansion of the integrand with accuracy $\mathrm{O}(1/\xi^2)$, we get the simple equation

$$\frac{2}{\pi\xi}\left(\frac{A\Delta T_\mathrm{m}}{R_\mathrm{c}} - \Delta T_\mathrm{m}\right)\left[\cos\left(R_\mathrm{c}\xi + \frac{\pi}{4}\right)\right]^2 = 0. \tag{S.67}$$

Evidently, it is only fulfilled for all ξ if $A = R_c$. It should be noted that even with $A = R_c$, (S.64) is not exactly fulfilled and the flux from outside the cell is

$$2\pi\kappa\int_{R_c}^{\infty} r\int_{0}^{\infty}\xi\left.\frac{\partial\Delta\tilde{T}}{\partial z}\right|_{z=0} \mathrm{J}_0(\xi r)\mathrm{d}\xi\mathrm{d}r \sim \kappa\Delta T_m R_c\,. \tag{S.68}$$

In a similar fashion, a term of the form B/r^2 could be introduced in eq. (S.54), but this requires more involved calculations, while the end result for the heat flux Q remains unchanged (eq. (S.57)).

3.3. Derivation of the expression for the integral diffusive flux through the surface of the film

The calculation of the integral heat flux through the film surfaces (Q) is presented here as it is too lengthy to be included elsewhere.

By definition, Q is the positive flux from the warmer air towards the colder film surface. Using that and the temperature profile in the form (S.60), we arrive at the following expression for Q:

$$Q = 4\pi\kappa\int_{0}^{R_f} r\left.\frac{\partial\Delta T}{\partial z}\right|_{z=0}\mathrm{d}r = -4\pi\kappa\int_{0}^{\infty}\xi^2\Delta\tilde{T}^{S}(\xi)\int_{0}^{R_f} r\mathrm{J}_0(\xi r)\mathrm{d}r\mathrm{d}\xi. \tag{S.69}$$

Q could be subdivided into three terms which correspond to the addends in the boundary condition (S.56), which in turn describe the three regions of the model system (film, meniscus, surrounding air). To make the exposition more clear, we will discuss them individually.

The heat flux related in this way to the film and meniscus regions can be calculated via direct integration:

$$Q_{\mathrm{film}} = -4\pi\kappa\int_{0}^{\infty}\xi^2\Delta\tilde{T}^{S}_{\mathrm{film}}(\xi)\int_{0}^{R_f} r\mathrm{J}_0(\xi r)\mathrm{d}r\mathrm{d}\xi = \frac{8}{3}\kappa R_f^3 T_{rr}, \tag{S.70}$$

$$Q_{\mathrm{meniscus}} = -4\pi\kappa\int_{0}^{\infty}\xi^2\Delta\tilde{T}^{S}_{\mathrm{meniscus}}(\xi)\int_{0}^{R_f} r\mathrm{J}_0(\xi r)\mathrm{d}r\mathrm{d}\xi = -8\kappa\Delta T_m R_c\left(\mathrm{K}\left(R_f\,/\,R_c\right)-\mathrm{E}\left(R_f\,/\,R_c\right)\right), \tag{S.71}$$

where K(r) is the complete elliptic integral of the first kind and E(r) is the complete elliptic integral of the second kind (Erdelyi, 1954). As we are interested in films of radius R_f much

smaller than that of the capillary (R_c), we can expand the elliptic integrals in eq. (S.71) in a series for R_f/R_c <<1 (Erdelyi, 1953a):

$$Q_{\text{meniscus}} \xrightarrow{R_f/R_c \to 0} -2\pi\kappa \frac{R_f^2}{R_c}\Delta T_m + \mathrm{O}\left(\left(\frac{R_f}{R_c}\right)^4\right). \tag{S.72}$$

In order to calculate the flux Q_{air}, we first perform the integration over r:

$$Q_{\text{air}} = -4\pi\kappa\int_0^\infty \xi^2 \Delta\tilde{T}_{\text{air}}^S(\xi)\int_0^{R_f} r\mathrm{J}_0(\xi r)\mathrm{d}r\mathrm{d}\xi = -4\pi\kappa R_f\int_0^\infty \xi\Delta\tilde{T}_{\text{air}}^S(\xi)\mathrm{J}_1(R_f\xi)\mathrm{d}\xi =$$

$$-4\pi\kappa R_f R_c \Delta T_m \int_0^\infty \mathrm{J}_1(R_f\xi)\left[1+\xi\frac{R_c}{2}\left(\pi\mathrm{J}_0(\xi R_c)\mathrm{H}_1(\xi R_c)-\pi\mathrm{J}_1(\xi R_c)\mathrm{H}_0(\xi R_c)-2\mathrm{J}_0(\xi R_c)\right)\right]\mathrm{d}\xi. \tag{S.73}$$

The evaluation of the integral in eq. (S.73) requires a change of variables,

$$Q_{\text{air}} \xrightarrow{\Xi=\xi R_f,\ \hat{r}=R_c/R_f}$$

$$-2\pi\kappa R_c\Delta T_m\int_0^\infty\left[2+\hat{r}\Xi\left(\pi\mathrm{J}_0(\hat{r}\Xi)\mathrm{H}_1(\hat{r}\Xi)-\pi\mathrm{J}_1(\hat{r}\Xi)\mathrm{H}_0(\hat{r}\Xi)-2\mathrm{J}_0(\hat{r}\Xi)\right)\right]\mathrm{J}_1(\Xi)\mathrm{d}\Xi =$$

$$= -2\pi\kappa R_c\Delta T_m I. \tag{S.74}$$

The integrand in eq. (S.74) could be expanded for $\hat{r}\to\infty$:

$$\left[2+\hat{r}\Xi\left(\pi\mathrm{J}_0(\hat{r}\Xi)\mathrm{H}_1(\hat{r}\Xi)-\pi\mathrm{J}_1(\hat{r}\Xi)\mathrm{H}_0(\hat{r}\Xi)-2\mathrm{J}_0(\hat{r}\Xi)\right)\right]\mathrm{J}_1(\Xi)\xrightarrow{\hat{r}\to\infty}$$

$$\xrightarrow{\hat{r}\to\infty}\frac{2}{\sqrt{\pi}}\left(\mathrm{J}_1(\Xi)\frac{\cos(\hat{r}\Xi)}{\sqrt{\hat{r}\Xi}}-\mathrm{J}_1(\Xi)\frac{\sin(\hat{r}\Xi)}{\sqrt{\hat{r}\Xi}}\right)+\mathrm{O}\left(\frac{1}{\hat{r}}\right). \tag{S.75}$$

Integrating the first and second terms in eq. (S.75) over Ξ from 0 to ∞ is equivalent to applying respectively a Fourier cosine and Fourier sine transform on the function $2\mathrm{J}_1(\Xi)/\sqrt{\pi\hat{r}\Xi}$. The integral evaluates in this way to (Erdelyi, 1954)

$$I \approx -\frac{1}{2}\sqrt{2}\,\frac{{}_2\mathrm{F}_1\left(3/4,5/4;\,2,\hat{r}^{-2}\right)}{\hat{r}^2}. \tag{S.76}$$

In eq. (S.76), ${}_2\mathrm{F}_1(a, b; c, x)$ denotes the Gaussian hypergeometric series (Erdelyi, 1954).

Expanding (S.76) in a series for $\hat{r}\to\infty$, we get the following asymptotic result for the integral I (Erdelyi, 1953a, 1953b) , which should be sufficiently accurate for the purposes of our study:

$$I = -\frac{1}{\sqrt{2}}\frac{1}{\hat{r}^2} + \mathrm{O}\left(\frac{1}{\hat{r}^4}\right). \tag{S.77}$$

Substituting in eq. (S.74), we obtain the flux determined by the concentration profile outside the capillary,

$$Q_{\mathrm{air}} = \sqrt{2}\pi\kappa\Delta T_{\mathrm{m}}\frac{R_{\mathrm{f}}^2}{R_{\mathrm{c}}}. \tag{S.78}$$

The total diffusive flux through both surfaces of the film is the sum of (S.70), (S.72) and (S.78), eq. (S.57). Due to the complete analogy between heat and mass transport in our model, the expressions (S.70), (S.72) and (S.78) set the explicit value of the mass transfer coefficients K_1 and K_2 in eq. (18) from the main text for the considered geometry, compare to, e.g., those in (Tsoumpas et al., 2015; Yiantsios and Higgins, 2006).

3.4. Derivation of the expression for the integral heat flux through the surface of the meniscus

Here, we present the derivation of eq. (23) for the heat flux through a cold meniscus. By definition, the heat flux from the air through both surfaces of the meniscus is

$$Q_{\mathrm{m}} = 4\pi\kappa\int_{R_{\mathrm{f}}}^{R_{\mathrm{c}}} r\left.\frac{\partial\Delta T}{\partial z}\right|_{z=0}\mathrm{d}r. \tag{S.79}$$

Using eq. (S.60) for the Fourier-Bessel image of ΔT and the definition of the Fourier-Bessel transform, we can express Q_{m} as

$$Q_{\mathrm{m}} = -4\pi\kappa\int_0^{\infty}\xi^2\Delta\tilde{T}^{\mathrm{S}}(\xi)\int_{R_{\mathrm{f}}}^{R_{\mathrm{c}}} r\mathrm{J}_0(\xi r)\mathrm{d}r\mathrm{d}\xi. \tag{S.80}$$

The function $\Delta\tilde{T}^{\mathrm{S}}(\xi)$ is the Fourier-Bessel image of eq. (S.56), the boundary condition at $z = 0$, which contains contributions from the different regions of the system, see eqs. (S.61)-(S.62):

$$\Delta\tilde{T}(\xi, z=0) = \Delta\tilde{T}^{\mathrm{S}}(\xi) = \Delta\tilde{T}^{\mathrm{S}}_{\mathrm{film}}(\xi) + \Delta\tilde{T}^{\mathrm{S}}_{\mathrm{meniscus+air}}(\xi),$$

where $\Delta\tilde{T}^{\mathrm{S}}_{\mathrm{film}}(\xi) = \frac{T_{rr}R_{\mathrm{f}}}{\xi^3}\left(\xi R_{\mathrm{f}}\mathrm{J}_0(\xi R_{\mathrm{f}}) - 2\mathrm{J}_1(\xi R_{\mathrm{f}})\right)$, and

$$\Delta\tilde{T}^{\mathrm{S}}_{\mathrm{meniscus+air}}(\xi)=\frac{R_{\mathrm{c}}\Delta T_{\mathrm{m}}}{\xi}\mathrm{J}_1(\xi R_{\mathrm{c}})+\frac{R_{\mathrm{c}}\Delta T_{\mathrm{m}}}{\xi}+\frac{R_{\mathrm{c}}^2\Delta T_{\mathrm{m}}}{2}\Big(\pi\mathrm{J}_0(\xi R_{\mathrm{c}})\mathrm{H}_1(\xi R_{\mathrm{c}})-$$

$$-\pi\mathrm{J}_1(\xi R_{\mathrm{c}})\mathrm{H}_0(\xi R_{\mathrm{c}})-2\mathrm{J}_0(\xi R_{\mathrm{c}})\Big). \qquad \text{(S.81)}$$

The heat flux may be subdivided into two contributions stemming from the respective region of the system. The flux related to the perturbation of the temperature profile at the film is

$$Q_{\mathrm{m\,film}}=-4\pi\kappa\int_0^\infty\xi^2\Delta\tilde{T}^{\mathrm{S}}_{\mathrm{film}}(\xi)\int_{R_{\mathrm{f}}}^{R_{\mathrm{c}}}r\mathrm{J}_0(\xi r)\mathrm{d}r\mathrm{d}\xi=4\pi\kappa\int_0^\infty\xi\Delta\tilde{T}^{\mathrm{S}}_{\mathrm{film}}(\xi)\Big(R_{\mathrm{f}}\mathrm{J}_1(R_{\mathrm{f}}\xi)-R_{\mathrm{c}}\mathrm{J}_1(R_{\mathrm{c}}\xi)\Big)\mathrm{d}\xi=$$

$$=4\pi\kappa T_{rr}R_{\mathrm{f}}\int_0^\infty\frac{1}{\xi^2}\Big(\xi R_{\mathrm{f}}\mathrm{J}_0(\xi R_{\mathrm{f}})-2\mathrm{J}_1(\xi R_{\mathrm{f}})\Big)\Big(R_{\mathrm{f}}\mathrm{J}_1(R_{\mathrm{f}}\xi)-R_{\mathrm{c}}\mathrm{J}_1(R_{\mathrm{c}}\xi)\Big)\mathrm{d}\xi=$$

$$=-\frac{8}{3}R_{\mathrm{f}}^2R_{\mathrm{c}}\kappa T_{rr}\left[\frac{R_{\mathrm{f}}}{R_{\mathrm{c}}}+\left(1-2\frac{R_{\mathrm{c}}^2}{R_{\mathrm{f}}^2}\right)\mathrm{E}(R_{\mathrm{f}}/R_{\mathrm{c}})-2\left(1-\frac{R_{\mathrm{c}}^2}{R_{\mathrm{f}}^2}\right)\mathrm{K}(R_{\mathrm{f}}/R_{c})\right]. \qquad \text{(S.82)}$$

As $R_{\mathrm{f}} << R_{\mathrm{c}}$, we can expand this result about $R_{\mathrm{f}} = 0$:

$$Q_{\mathrm{m\,film}}=-\frac{8}{3}R_{\mathrm{f}}^3\kappa T_{rr}+\mathrm{O}(R_{\mathrm{f}}^4). \qquad \text{(S.83)}$$

The heat flux associated with the meniscus region and the air outside the cell is

$$Q_{\mathrm{m\,meniscus+air}}=-4\pi\kappa\int_0^\infty\xi^2\Delta\tilde{T}^{\mathrm{S}}_{\mathrm{meniscus+air}}(\xi)\int_{R_{\mathrm{f}}}^{R_{\mathrm{c}}}r\mathrm{J}_0(\xi r)\mathrm{d}r\mathrm{d}\xi$$

$$=4\pi\kappa\int_0^\infty\xi\Delta\tilde{T}^{\mathrm{S}}_{\mathrm{meniscus+air}}(\xi)\Big(R_{\mathrm{f}}\mathrm{J}_1(R_{\mathrm{f}}\xi)-R_{\mathrm{c}}\mathrm{J}_1(R_{\mathrm{c}}\xi)\Big)\mathrm{d}\xi. \qquad \text{(S.84)}$$

Using again that $R_{\mathrm{f}} << R_{\mathrm{c}}$, we can neglect the first term in brackets, which greatly simplifies the calculation of the integral. After a change of variables, we obtain

$$Q_{\mathrm{m\,meniscus+air}}\approx-4\pi\kappa R_{\mathrm{c}}^2\Delta T_{\mathrm{m}}\int_0^\infty\left[\frac{R_{\mathrm{c}}\xi}{2}\Big(\pi\mathrm{J}_0(\xi R_{\mathrm{c}})\mathrm{H}_1(\xi R_{\mathrm{c}})-\pi\mathrm{J}_1(\xi R_{\mathrm{c}})\mathrm{H}_0(\xi R_{\mathrm{c}})-2\mathrm{J}_0(\xi R_{\mathrm{c}})\Big)+\right.$$

$$\left.\mathrm{J}_1(\xi R_{\mathrm{c}})+1\right]\mathrm{J}_1(R_{\mathrm{c}}\xi)\mathrm{d}\xi\xrightarrow{R_{\mathrm{c}}\xi=\Xi}$$

$$\longrightarrow-4\pi\kappa R_{\mathrm{c}}\Delta T_{\mathrm{m}}\int_0^\infty\left[\mathrm{J}_1(\Xi)+1+\frac{\Xi}{2}\Big(\pi\mathrm{J}_0(\Xi)\mathrm{H}_1(\Xi)-\pi\mathrm{J}_1(\Xi)\mathrm{H}_0(\Xi)-2\mathrm{J}_0(\Xi)\Big)\right]\mathrm{J}_1(\Xi)\mathrm{d}\Xi=$$

$$=-4\pi\kappa R_{\mathrm{c}}\Delta T_{\mathrm{m}}\int_0^\infty f(\Xi)\mathrm{d}\Xi\ . \qquad \text{(S.85)}$$

To calculate the definite integral in (S.85), we expand the integrand $f(\Xi)$ in a series about $\Xi \to \infty$,

$$f_\infty(\Xi) = -\frac{1}{\pi}\frac{\cos(2\Xi)}{\Xi^2} + \mathrm{O}\left(\Xi^{-5/2}\right). \tag{S.86}$$

Using the expansion (S.86), we can evaluate the numerical value of the integral using the exact integrand for small Ξ and the approximate function for $\Xi \to \infty$:

$$Q_{\mathrm{m\ meniscus\ +\ air}} \approx -4\pi\kappa R_\mathrm{c}\Delta T_\mathrm{m}\left(\int_0^{100} f(\Xi)\mathrm{d}\Xi + \int_{100}^{\infty} f_\infty(\Xi)\mathrm{d}\Xi\right) = -4.57\kappa R_\mathrm{c}\Delta T_\mathrm{m}. \tag{S.87}$$

Combining (S.83) and (S.87), we attain the following for the heat flux through the surface of the meniscus:

$$Q_\mathrm{m} = Q_{\mathrm{m\ film}} + Q_{\mathrm{m\ meniscus\ +\ air}} \approx -\kappa\left(\frac{8}{3}R_\mathrm{f}^3 T_{rr} + 4.57 R_\mathrm{c}\Delta T_\mathrm{m}\right). \tag{S.88}$$

For the typical parameters of a thin water film and the expected order of magnitude of ΔT_m (~ –2 K), the first term is small ($8T_{rr}R_\mathrm{f}^3/3$ ~ $10^{-2}\Delta T_\mathrm{m}R_\mathrm{c}$) in comparison with the second and can be neglected, which yields eq. (23) from the main text.

3.5. Heat current through the liquid phase

The heat equation for the liquid film reads

$$\frac{1}{r}\frac{\partial}{\partial r}r\frac{\partial T^\mathrm{L}}{\partial r} + \frac{\partial^2 T^\mathrm{L}}{\partial z^2} = 0\,. \tag{S.89}$$

Here, we only consider the conductive heat transport through the liquid, since the Péclet number, which compares the relative importance of conduction and convection in transferring heat (Bergman et al., 2011), is much smaller than unity ($Pe^\mathrm{L}_\mathrm{heat} \approx 10^{-3}$ for a typical water film, see S6). We have also neglected the dependence of T^L on time though in principle, even after a quasi-stationary state is reached, the temperature distribution T^L still depends on t through the film thickness $h(t)$. Below, we will demonstrate that this dependence is not significant and, therefore, $\partial T^\mathrm{L}/\partial t$ need not be considered in the heat equation above.

Let the centre of the film be at $z = 0$ and its surfaces be at $z = \pm h/2$. A dimensional analysis of the two terms in eq. (S.89) shows that $\partial^2 T^\mathrm{L}/\partial z^2$ is greater in absolute value, which allows us to write in first approximation that $\partial^2 T^\mathrm{L}/\partial z^2 = 0$. As due to the symmetry of the problem $\partial T^\mathrm{L}/\partial z|_{z=0} =$

0, in first approximation, T^{L} is independent of z, i.e., $T^{\mathrm{L}} \approx T^{\mathrm{L}}(r)$. This complicates the analysis of the normal heat flux through the liquid: as its density is $q^{\mathrm{L}} \sim \partial T^{\mathrm{L}}/\partial z$, the first approximation leads to the unphysical result that the flux is zero and the film that does not cool down. In point of fact, the result $T^{\mathrm{L}} \approx T^{\mathrm{L}}(r)$ only means that the order of magnitude of q^{L} is lower than the one predicted via dimensional analysis, which is $q^{\mathrm{L}} \sim \kappa^{\mathrm{L}} \Delta T/h$, where $\kappa^{\mathrm{L}} = \chi^{\mathrm{L}}\rho c_p$ is the thermal conductivity of the liquid phase, c_p [J·kg^{-1}·K^{-1}] is its specific heat capacity at constant pressure, χ^{L} its thermal diffusivity. The correct order of magnitude of q^{L} is actually lower by a factor of $(h/R_{\mathrm{f}})^2$. This result is obtained via integration of eq. (S.89) with respect to z from 0 to $h/2$ (using that $\partial T^{\mathrm{L}}/\partial z|_{z=0} = 0$):

$$q^{\mathrm{L}}\Big|_{z=h/2} = -\kappa^{\mathrm{L}} \left.\frac{\partial T^{\mathrm{L}}}{\partial z}\right|_{z=h/2} = \kappa^{\mathrm{L}} \int_0^{h/2} \frac{1}{r}\frac{\partial}{\partial r} r \frac{\partial T^{\mathrm{L}}(r)}{\partial r} \mathrm{d}z = \frac{\kappa^{\mathrm{L}} h}{2r}\frac{\partial}{\partial r} r \frac{\partial T^{\mathrm{L}}}{\partial r}, \tag{S.90}$$

i.e., indeed $q^{\mathrm{L}} \sim \kappa^{\mathrm{L}}\Delta T h/R_{\mathrm{f}}^2$. Eq. (S.90) is essentially an iteration, as we neglect the dependence on z of the "small" term under the integral, as it follows from the first approximation. The quantity q^{L} given by eq. (S.90) is the density of the positive heat flux from the warmer core of the film towards its surface.

At the surface of the film, the temperatures of the liquid and the adjacent air are assumed to be equal, therefore, eq. (S.56) also serves as the boundary condition for the problem for the temperature distribution $\Delta T(r,z) = T(r,z) - T_\infty$ in the air. This assumption fails when the Hertz-Knudsen heat current and the total heat current through the surface are of the same order of magnitude (Badam et al., 2007; Langmuir, 1915), see also S5.

The heat flux through the upper surface of the film, $z = h/2$, is equal to that through the lower one, $z = -h/2$. Hence, the total heat flux from the liquid phase to the air through *both* surfaces (Q^{L}) is given by the following surface integral:

$$Q^{\mathrm{L}} = 4\pi \int_0^{R_{\mathrm{f}}} r q^{\mathrm{L}}\Big|_{z=h/2} \mathrm{d}r\,. \tag{S.91}$$

By substituting eqs. (S.90) and (S.56) in the integrand, we arrive at an explicit relation between Q^{L} and the temperature coefficient T_{rr}:

$$Q^{\mathrm{L}} = 2\pi\kappa^{\mathrm{L}} h R_{\mathrm{f}}^2 T_{rr}. \tag{S.92}$$

A more precise form of the heat balance for the film, eq. (21) in the main text, would include the heat flux through the liquid,

$$h_e J = Q + Q^L. \tag{S.93}$$

Substituting eqs. (19), (20) and (S.92) for J, Q and Q^L in the equation above and solving for T_{rr} results in the following expression:

$$T_{rr} = 0.69 \frac{T_m}{R_c R_f C_{eq}} \frac{\Delta C_m + \dfrac{\kappa \Delta T_m}{h_e D}}{\dfrac{h_e}{RT_\infty} - 1 + \dfrac{\kappa T_m}{h_e D C_{eq}} + \dfrac{3\pi}{4} \dfrac{h}{R_f} \dfrac{\kappa^L T_m}{h_e D C_{eq}}} \tag{S.94}$$

Substituting the values of the parameters corresponding to a thin water film of R_f = 150 μm at a humidity of x = 0.45 (h = 3.47×10^{-7} m, consult S1 for a full list of parameters) in contact with a thermostated meniscus, we can evaluate the order of magnitude of the dimensionless quantities in parenthesis in eq. (S.94): $(h_e/RT_m - 1) \sim 17$; $\kappa^A T_m/(h_e D C_{eq}) \sim 6$; $3\pi\kappa T_m \cdot h/(4R_f h_e D C_{eq}) \sim 2\times10^6 \cdot h/[\mathrm{m}]$. The comparison between them shows that, for sufficiently thin films (h < 1 μm), one can neglect the last term to obtain eq. (22) for T_{rr}. Thus, the coefficient T_{rr} is independent of the film thickness h, which justifies the assumption that the time derivative $\partial T^L/\partial t = (\partial T^L/\partial h)\cdot(\partial h/\partial t)$ in the heat equation (S.89) is negligible. For films thicker than 1 μm, the dependence of T_{rr} on h is significant, but as it is difficult to investigate such films experimentally, we do not consider them here.

4. Mass current through the air

In this supplement, we take advantage of the analogy between heat and mass transport to derive equations for the diffusive fluxes through the film and the meniscus, J and J_m.

We suppose that a quasistationary state is quickly established, as is the case with an evaporating drop (Fuchs, 1959). The distribution of the vapour concentration in the gas phase obeys the stationary diffusion equation,

$$\frac{1}{r}\frac{\partial}{\partial r} r \frac{\partial \Delta C}{\partial r} + \frac{\partial^2 \Delta C}{\partial z^2} = 0\,; \tag{S.95}$$

ΔC is defined as $\Delta C = C - C_\infty$, where $C_\infty = C(z\to\infty)$ is the vapour concentration at an infinite distance from the film. It should be noted that by adopting the form (S.95), of the diffusion equation, we make the implicit assumption that the dependence of the diffusion coefficient on temperature is negligible – this holds for small temperature differences between the film and the

air (Fuchs, 1959). Furthermore, just as the heat transfer in the system is dominated by conduction (see S3.1), the mass transfer is dominated by diffusion, which follows from the values of the appropriate Péclet numbers (Cussler, 2009). $Pe_{\mathrm{mass},r}$ and $Pe_{\mathrm{mass},z}$, which give the ratio between the convective mass flux in the respective direction and the overall diffusive flux through the film surface, are of the order of $Pe_{\mathrm{mass},r} \sim 10^{-3}$-$10^{-2}$ and $Pe_{\mathrm{mass},z} \sim 10^{-2}$ for water films (consult S1&6). Hence, the convective mass fluxes in both the radial and the normal direction are neglected in the diffusion equation (S.95). However, this approximation fails for the very volatile hexane films, for which $Pe_{\mathrm{mass},\,r}$ and $Pe_{\mathrm{mass},\,z}$ are of the order of 0.1 (S1) and convection is important.

The first boundary condition for eq. (S.95) states that

$$\Delta C|_{z\to\infty} = 0. \tag{S.96}$$

As in our derivation of the heat flux, S3.1, we will neglect the curvature of the meniscus and regard the interface as planar (Figure S.1); in addition, we will neglect the presence of the glass holder. Just like in our model for the heat transfer, there are three distinct regions of the plane $z = 0$.

(i) Film ($0 < r < R_\mathrm{f}$). As discussed in the main text, we obtain the concentration profile at $z = 0$ for the film region by noting that the temperature of the film differs from that of the meniscus by $\delta T(r) = T_\mathrm{m} + \tfrac{1}{2}T_{rr}(r^2 - R_\mathrm{f}^2)$. Thus, setting T^L to $T_\mathrm{m} + \delta T(r)$ in the Clausius-Clapeyron equation (10) and expanding in a series about $\delta T(r)$, we obtain

$$z = 0,\ r < R_\mathrm{f}: \qquad \Delta C = \Delta C_\mathrm{m} + \frac{1}{2} C_{rr}\left(r^2 - R_\mathrm{f}^2\right) + \mathrm{O}(\delta T^2), \tag{S.97}$$

where we have also used the definitions of ΔC_m and C_{rr}, eqs. (12) and (14), respectively.

(ii) Meniscus ($R_\mathrm{f} < r < R_\mathrm{c}$). For the meniscus region, the temperature at $z = 0$ is equal to T_m, see eq. (S.56); according to the Clausius-Clapeyron equation, this corresponds to

$$z = 0,\ R_\mathrm{f} < r < R_\mathrm{c}: \quad \Delta C = \Delta C_\mathrm{m}. \tag{S.98}$$

(iii) Surrounding gas ($r > R_\mathrm{c}$). The characteristic diffusion length in the air is of the order of the radius of the Scheludko cell R_c, and the cell is "immersed" into a cloud of vapours of size ~R_c with a stationary concentration profile. By analogy with the heat transfer problem, we assume that the concentration difference at $z = 0$ and $r > R_\mathrm{c}$, in this region is proportional to $1/r$, i.e., it follows the expected asymptotic behaviour at large r:

$$z = 0,\ r > R_c: \qquad \Delta C = \Delta C_m \frac{R_c}{r}. \tag{S.99}$$

Combining **(i)-(iii)**, we can write the approximate boundary condition at $z = 0$ as

$$\Delta C\big|_{z=0} = \frac{C_{rr}}{2}\left(r^2 - R_f^2\right)\theta(R_f - r) + \Delta C_m\left(\theta(R_c - r) + \frac{R_c}{r}\theta(r - R_c)\right). \tag{S.100}$$

Taking advantage of the analogy between our treatment of the heat and mass transport – compare eqs. (S.50), (S.51), (S.56) to eqs. (S.95), (S.96) and (S.100) – we can infer that the integral mass fluxes through the surfaces of the film and the meniscus are respectively

$$J = DR_f^2\left[-\frac{8}{3}R_f C_{rr0} + \left(2-\sqrt{2}\right)\pi\frac{\Delta C_{m0}}{R_c}\right] \text{ and} \tag{S.101}$$

$$J_m = \frac{8}{3}DR_f^3 C_{rr} + 4.57DR_c\Delta C_m \approx 4.57DR_c\Delta C_m, \tag{S.102}$$

corresponding to eqs. (19) and (24) from the main text. In eq. (S.102), we used that the first term is small in comparison with the second one as $8C_{rr}R_f^3/3 \sim 10^{-3}\Delta C_m R_c$.

5. Knudsen and Fuchs transition layers

If the mass flux through the liquid|gas interface is large, the boundary condition we used for the diffusion problem – that the vapour concentration $C_{z=0}$ at $z = 0$ equals the Clausius-Clapeyron concentration C_{eq} (i.e., continuity of the chemical potential) – may fail. This happens when the total flux j approaches the Hertz-Knudsen flux $C_{z=0}(RT/2\pi M)^{1/2}$ from the gas toward the surface. The flux continuity requires that

$$j = C_{eq}\sqrt{\frac{RT}{2\pi M}} - C_{z=0}\sqrt{\frac{RT}{2\pi M}}, \tag{S.103}$$

where we assumed that every hit at the surface is effective – consult Dondlinger et al. (Dondlinger et al., 2005). The order of magnitude of j is $D(C_{z=0} - C_\infty)/R_c$, compare to eq. (37); therefore, the chemical potential becomes discontinuous when

$$D\frac{C_{z=0} - C_\infty}{R_c} \sim \left(C_{eq} - C_{z=0}\right)\sqrt{\frac{RT}{M}}, \tag{S.104}$$

or equivalently,

$$\frac{C_{z=0}}{C_{eq}} \sim \frac{1+\sqrt{\frac{M}{RT}}\frac{D}{R_c}\frac{C_\infty}{C_{eq}}}{1+\sqrt{\frac{M}{RT}}\frac{D}{R_c}} \sim 1-\sqrt{\frac{M}{RT}}\frac{D}{R_c}\left(1-\frac{C_\infty}{C_{eq}}\right).$$

Thus, $C_{z=0}$ differs significantly from C_{eq} only in case that $D(M/RT)^{1/2} << R_c$. The length $D(M/RT)^{1/2}$ is of the order of the mean free path of a molecule in the gas phase, ~100 nm in air, and is indeed small compared to the characteristic length in our problem (R_c ~ 2 mm). Therefore, we can safely assume that $C_{z=0} = C_{eq}$. Similarly, one can show that the continuity of T holds. The discontinuities of T and C can become very important at low pressures in the gas, e.g., for the system considered by Badam et al. (Badam et al., 2007), where the pressure is low and the mean free path is ~10 μm.

6. Properties of the system at the stationary state for a thermostated meniscus

This section provides some additional details on the stationary state of the system for the case in which the temperature of the meniscus is fixed and equal to that of the ambient air, i.e., $T_m = T_\infty$ and $\Delta T_m = 0$.

As we mentioned in Section 2.5 of the main text, the kinetics of film drainage can be described in terms of the dependence $t(h)$,

$$t = \frac{1}{2}\int_{h_0}^{h} V_z^{-1} \mathrm{d}h, \qquad \text{(S.105)}$$

where h_0 denotes the initial film thickness and V_z is given by eq. (30). Depending on the value of h_0, (S.105) predicts three different scenarios: 1) if $h_0 > h_{st1}$ (eq. (35)), the film drains until reaching h_{st1}; 2) if $h_{st2} < h_0 < h_{st1}$, the film thickens until h reaches h_{st1}; 3) if $h_0 < h_{st2}$, the film drains until rupture. All three cases are illustrated in Figure S. 2A-B. As the figure indicates, the drainage occurs over timescales of 10^{-7}-10^{-5} s, much shorter than that of the cooling down of the meniscus (Figure 5). This is why in Section 2.7 we assume that the film thickness instantaneously reaches the quasistationary value determined by the temperature drop in the meniscus (ΔT_m).

It is worthy of note that at the limit of $x \to 100\%$, which corresponds to a saturated environment, the normal velocity profile v_z simplifies to

$$v_{z0} = -\frac{z}{2\eta}\left(p_c - \Pi_{vdW}\right) = -\frac{z}{2\eta}\left(\frac{2\sigma}{R_c} + \frac{A_H}{6\pi h^3}\right). \qquad \text{(S.106)}$$

Equation (S.106) differs notably from the velocity profile for the classic Reynolds problem for a film with van der Waals disjoining pressure, $v_{z,Re}(h/2) = -h^3(p_c - \Pi_{vdW})/(3\eta R_f^2)$. It predicts values of v_z that are orders of magnitude higher, $v_z(h/2) \sim R_f^2/h^2\ v_{z,Re}(h/2)$. This dissimilarity arises from the difference in the boundary conditions for the two problems – the Reynolds formula is derived for films with tangentially immobile surfaces.

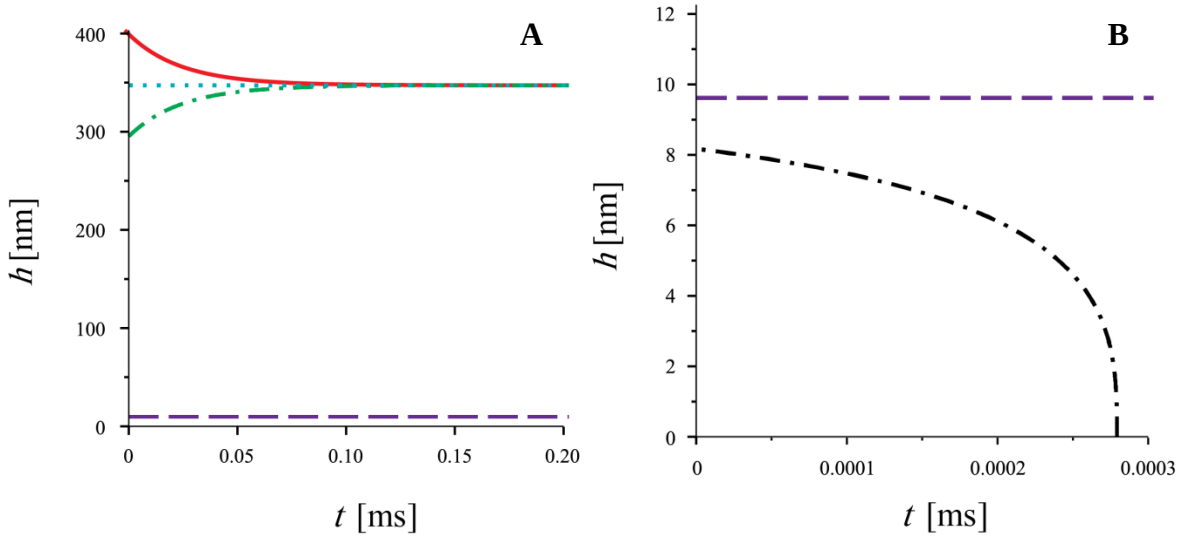

Figure S. 2. Modes of film drainage depending on the initial film thickness. **A**) Films of initial thickess $h_0 > h_{st1}$ drain until reaching $h = h_{st1}$ (solid line, $h_0 = 1.15 \cdot h_{st1}$); for $h_{st2} < h_0 < h_{st1}$, the films are expected to thicken until reaching h_{st1} (dashdot line, $h_0 = 0.85 \cdot h_{st1}$). In both cases, the characteristic time for reaching the stationary value is $\eta \cdot R_c/\sigma_m \sim 2\times10^{-5}$ s. **B**) Films of initial thickness $h_0 < h_{st2}$ (dashdot line, $h_0 = 0.85 \cdot h_{st2}$) are expected to drain until rupture over the even shorter timescale of 10^{-7} s. The predicted characteristic times of drainage indicate that the change in film thickness is instantaneous in comparison with the cooling of the meniscus (Figure 5) and the thickness at any point in time can be set to its quasistationary value determined by the momentary value of the temperature change ΔT_m. In both **A**) and **B**), h_{st1} is represented by a dotted line and h_{st2} – by a dashed line. The results shown in the figure pertain to films of R_f = 150 μm formed at relative humidity x = 45%.

The limit of the radial velocity profile at $x \to 100\%$ is

$$v_{r0} = \frac{r}{4\eta}\left(p_c - \Pi_{vdW}\right) = \frac{r}{4\eta}\left(\frac{2\sigma_m}{R_c} + \frac{A_H}{6\pi h^3}\right) . \quad \text{(S.107)}$$

At $x \rightarrow 100\%$, the lubrication approximation breaks down and v_{r0} and v_{z0} do not adequately describe the velocity profile but are given here for completeness.

Due to a cancellation of leading terms, in order to obtain the correct orders of magnitude of the surface velocities V_z and V_r at the stationary point, one must use the more accurate form of T_{rr} given in S3.5 with eq. (S.94) instead of eq. (22) from the main text. The approximate form, eq. (22), which neglects the weak dependence of T_{rr} on h, leads to a sufficiently accurate $h_{st}(t)$ (differing by less than 10% from the one obtained with $T_{rr0}(h)$), which is the reason why calculations in Section 2.4-7 are carried out with it. However, if we were to use the approximate expressions for T_{rr} and the stable stationary thickness h_{st1}, eqs. (22) and (35), to calculate V_r, we would obtain the unphysical result that it is identically zero. The correct evaluation of V_z and V_r at the stationary state therefore requires the solution to the exact mass balance for h_{st} – eq. (31) in which the exact forms eq. (30) for V_z and eq. (S.94) for T_{rr} have been substituted. The solution is more easily obtained for $x(h_{st})$ than for $h_{st}(x)$:

$$x = 1 - 6.83\frac{h_{st}R_c\left(p_c - \Pi_{vdW}\right)\left[\frac{1}{DC_{eq0}}\left(3\pi h_{st}\kappa^L + 4R_f\kappa\right) - \frac{4R_f h_e}{T_\infty}\left(1 - \frac{h_e}{RT_\infty}\right)\right]}{3\pi R_f^2 h_e s^S\left(1 - \frac{4h_{st}^2}{3R_f^2}\right) - 8\nu^L\eta\left(3\pi\kappa^L h_{st} + 4R_f\kappa\right)} . \quad \text{(S.108)}$$

To evaluate the normal surface velocity, we set the relative humidity x to 45% in eq. (S.108) and R_f to 150 μm, solve the resulting equation numerically for h_{st} and substitute the solution that corresponds to the stable branch of the $h_{st}(x)$ diagram (h_{st} = 347 nm) together with eq. (S.94) for T_{rr} into the exact form of eq. (30) for V_z, reaching the result $V_z \approx 1.2\times10^{-8}$ m.s^{-1} for a water filmSimilarly, to obtain a correct value for V_r, we must substitute the model temperature profile (9) for the film and the exact expression (30) for V_z in eq. (8), leading to the result

$$V_r = \frac{r}{4\eta}\left(-\frac{s^S T_{rr} R_f^2}{2h} + p_c - \Pi_{vdW}\right) = \frac{r}{4\eta}\left(-\frac{s^S T_{rr} R_f^2}{2h} + \frac{2\sigma_m}{R_c} + \frac{A_H}{6\pi h^3}\right) .$$

(S.109)

We proceed to evaluate V_r in the same way as V_z – we set x to 45% in eq. (S.108), then substitute its stable solution for h_{st} and eq. (S.94) for T_{rr} in eq. (S.109). Thus, we reach the result $V_r(R_f) \approx$

-2.7×10^{-5} m.s^{-1}, which has the correct order of magnitude – from dimensional analysis it follows that V_r/V_z must be of the same order of magnitude as R_f/h, and this is indeed the case. It is worth noting that at the stationary state, the radial component of the velocity field is negative for all z, corresponding to a flux from the meniscus to the film that exactly compensates the loss of fluid due to evaporation.

Having determined the surface velocities V_r and V_z, we can proceed with the evaluation of the dimensionless numbers relevant to the problem. We can assess the importance of the convective heat transfer through the liquid by calculating the relevant Péclet number,

$$Pe^{\mathrm{L}}_{\mathrm{heat}} = \left| \frac{q^{\mathrm{L}}_{\mathrm{convective}}}{q^{\mathrm{L}}_{\mathrm{conductive}}} \right|_{z=h/2}, \tag{S.110}$$

where $q^{\mathrm{L}}_{\mathrm{i}}$ are the contributions of conduction and convection to the density of the heat flux through the liquid. If we were to take convection in the liquid into account, the heat equation for that domain would take the form

$$v_r \frac{\partial T^{\mathrm{L}}}{\partial r} + v_z \frac{\partial T^{\mathrm{L}}}{\partial z} = \chi \left(\frac{1}{r} \frac{\partial}{\partial r} r \frac{\partial T^{\mathrm{L}}}{\partial r} + \frac{\partial^2 T^{\mathrm{L}}}{\partial z^2} \right). \tag{S.111}$$

As in S3.5, we can perform an iteration to determine the normal heat flux through the film

$$q^{\mathrm{L}}\Big|_{z=h/2} = -\kappa \frac{\partial T^{\mathrm{L}}}{\partial z}\bigg|_{z=h/2} = \kappa \int_0^{h/2} \left[\frac{1}{r} \frac{\partial}{\partial r} r \frac{\partial T^{\mathrm{L}}}{\partial r} - \frac{1}{\chi} v_r \frac{\partial T^{\mathrm{L}}}{\partial r} \right] \mathrm{d}z, \tag{S.112}$$

where we have used that the dependence of T^{L} on z is weak and the term $\partial T^{\mathrm{L}}/\partial z$ is thus negligible. Having derived the estimate (S.112) for q^{L}, we can proceed to evaluate the ratio between the two terms that contribute to it, i.e., $Pe^{\mathrm{L}}_{\mathrm{heat}}$:

$$Pe^{\mathrm{L}}_{\mathrm{heat}} = \left| \frac{\dfrac{1}{\chi^{\mathrm{L}}} \displaystyle\int_0^{h/2} v_r \frac{\partial T^{\mathrm{L}}}{\partial r} \mathrm{d}z}{\displaystyle\int_0^{h/2} \frac{1}{r} \frac{\partial}{\partial r} r \frac{\partial T^{\mathrm{L}}}{\partial r} \mathrm{d}z} \right| = \left| \frac{\dfrac{1}{\chi^{\mathrm{L}}} \dfrac{\partial T^{\mathrm{L}}}{\partial r} \dfrac{r}{2} V_z}{\dfrac{h}{2} \dfrac{1}{r} \dfrac{\partial}{\partial r} r \dfrac{\partial T^{\mathrm{L}}}{\partial r}} \right| \sim$$

$$\left| \frac{R_{\mathrm{f}}^2 V_z}{2\chi^{\mathrm{L}} h} \right| = \left| \frac{R_{\mathrm{f}}^2}{8\chi^{\mathrm{L}} h \eta} \left[\frac{R_{\mathrm{f}}^2 s^{\mathrm{S}} T_{rr}}{2} \left(1 - \frac{4}{3} \frac{h^2}{R_{\mathrm{f}}^2} \right) - h\left(p_{\mathrm{c}} - \Pi_{\mathrm{vdW}} \right) \right] \right|, \tag{S.113}$$

where we used eq. (9) for the temperature of the film region and eq. (30) for V_z. To evaluate $Pe^{\mathrm{L}}_{\mathrm{heat}}$ at the stationary state, we need to use the explicit expression for T_{rr}, eq. (S.94). T_{rr} contains

the concentration difference ΔC_m, which we express through x using eq. (13); note that for a thermostated meniscus, $\Delta C_m = C_{eq0} - C_\infty$. Using the relationship between the stationary thickness h_{st} and the humidity x (S.108), we express Pe^L_{heat} as a function of h_{st}. Finally, we plot $Pe^L_{heat}(h_{st})$ parametrically versus $x(h_{st})$ with h_{st} as a parameter. In order to plot only the experimentally observable branch of Pe^L_{heat}, we use a range of h_{st} between h_{cr} and the stationary thickness corresponding to $x \to 0\%$ ($h_{st} \sim 10^{-7}$ m). The resulting graph is shown in Figure S. 3 for three typical experimental values of the film radius; the observed values of Pe^L_{heat} (~10^{-3}) justify our neglect of the convective heat transfer through the liquid phase in Section 2.3.

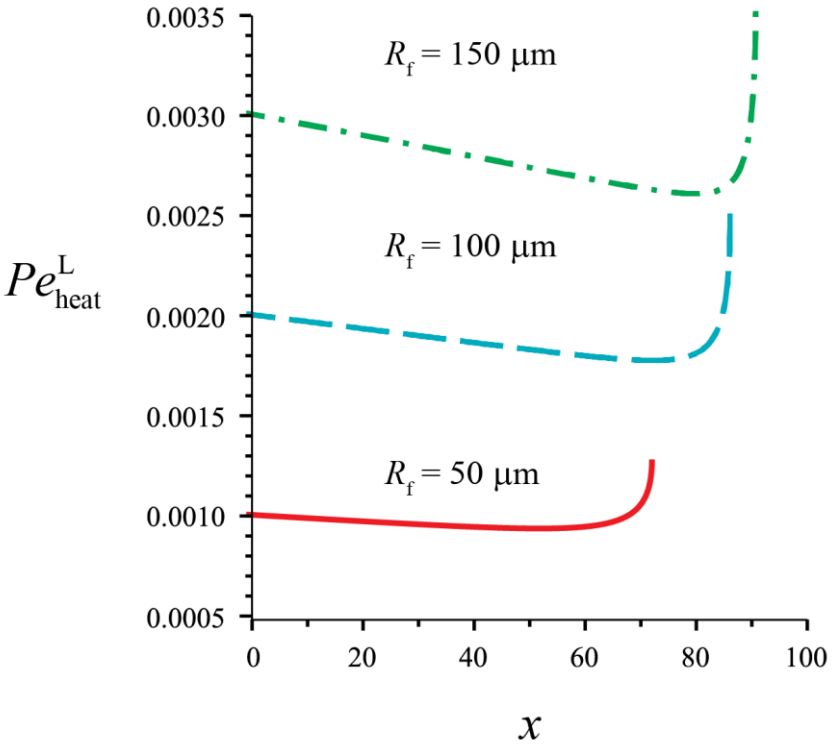

Figure S. 3. Péclet number for the heat transfer in the liquid phase (Pe^L_{heat}) at the stationary state for three different values of the film radius. The observed values ($Pe^L_{heat} << 1$) justify the neglect of the convective term in the heat equation (S.89) for the liquid.

The Péclet numbers for the heat transfer in the gas phase are evaluated in a completely analogous way. We define $Pe^A_{heat,r}$ as the ratio of the convective heat flux in the r-direction to the conductive heat flux,

$$Pe^{\mathrm{A}}_{\mathrm{heat},r} = \left| \frac{q_{\mathrm{convective},r}}{q_{\mathrm{conductive}}} \right|_{z=h/2, r=R_\mathrm{f}} \sim \left| \frac{V_r \dfrac{\partial T}{\partial r}}{\chi \dfrac{1}{r}\dfrac{\partial}{\partial r} r \dfrac{\partial T}{\partial r}} \right|_{z=h/2, r=R_\mathrm{f}} . \tag{S.114}$$

In eq. (S.114), we use that at the surface of the film, the velocities of the liquid and gas phases are equal; χ denotes the thermal diffusivity of the gas phase. Substituting the model expression (9) for T and eq. (S.109) for V_r in eq. (S.114) leads to

$$Pe^{\mathrm{A}}_{\mathrm{heat},r} \sim \left| \frac{R_\mathrm{f} V_r(R_\mathrm{f})}{2\chi} \right| = \frac{R_\mathrm{f}^2}{8\eta\chi} \left| \left(-\frac{s^{\mathrm{S}} T_{rr} R_\mathrm{f}^2}{2h} + p_\mathrm{c} - \Pi_{\mathrm{vdW}} \right) \right| . \tag{S.115}$$

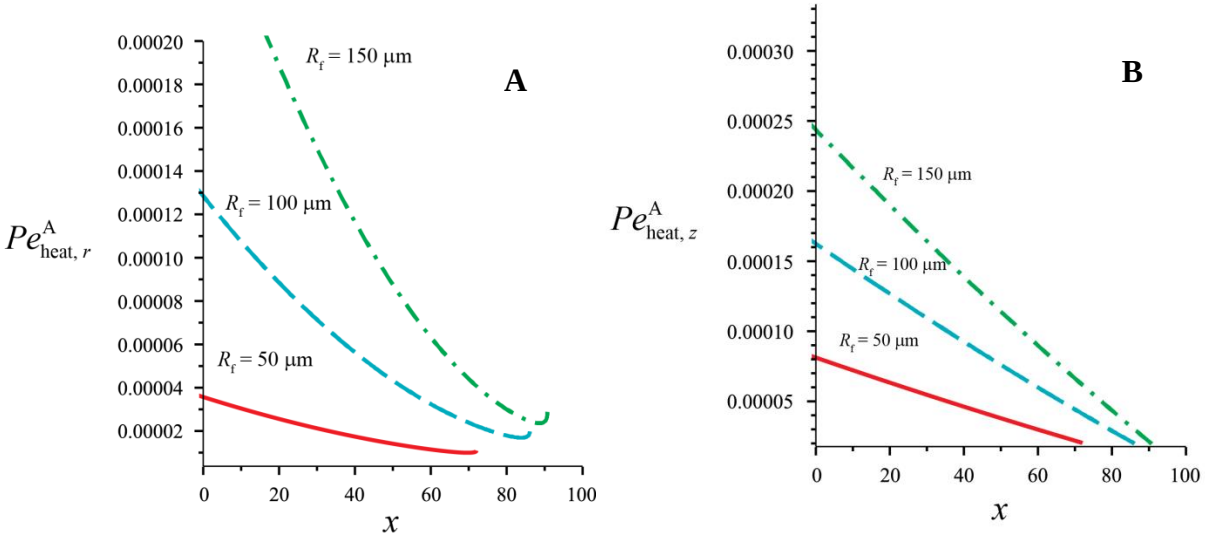

Figure S. 4. Péclet numbers for the heat transfer in the gas phase at the stationary state for three different values of the film radius. $Pe^{\mathrm{A}}_{\mathrm{heat},r}$ (**A**) gives the comparison between the convective heat transfer in the radial direction with the diffusive heat transfer, while $Pe^{\mathrm{A}}_{\mathrm{heat},z}$ (**B**) does the same for the convective heat transport in the z-direction. The fact that $Pe^{\mathrm{A}}_{\mathrm{heat},r} << 1$ and $Pe^{\mathrm{A}}_{\mathrm{heat},z} << 1$ means that the convective contribution to the heat flux through the air is negligible, as assumed in S3.1-3.4 (see eq. (S.50)).

In a similar manner, we can define $Pe^{\mathrm{A}}_{\mathrm{heat},z}$ as the ratio of the convective heat flux in the z-direction to the conductive heat flux,

$$Pe^{\mathrm{A}}_{\mathrm{heat},z} \sim \left| \frac{V_z^{\mathrm{G}} \dfrac{\partial T}{\partial z}}{\chi \dfrac{1}{r}\dfrac{\partial}{\partial r} r \dfrac{\partial T}{\partial r}} \right|_{z=h/2} \sim \left| \frac{V_z^{\mathrm{G}} \displaystyle\int_0^{R_\mathrm{f}} \frac{1}{r}\frac{\partial}{\partial r} r \frac{\partial T}{\partial r} \mathrm{d}z}{\chi \dfrac{1}{r}\dfrac{\partial}{\partial r} r \dfrac{\partial T}{\partial r}} \right|_{z=h/2} \sim \frac{\nu^{\mathrm{G}} J}{2\pi\chi R_\mathrm{f}} , \tag{S.116}$$

where as in eq. (S.90) we have used an iteration to evaluate $\partial T/\partial z|_{z=h/2}$ and we have substituted the model temperature distribution (9), as well as the estimate $V_z^G \sim v^G J/\pi R_f^2$ for the normal velocity in the gas phase at the interface, $v^G = R\cdot T/p_0$ being the molar volume of the gas. Using eq. (S.101) for J in eq. (S.116) yields

$$Pe^{A}_{\text{heat},\,z} \sim \frac{1}{2\pi}\frac{RT_\infty}{p^O}\frac{DR_f}{\chi}\left[-\frac{8}{3}R_f C_{rr} + \left(2-\sqrt{2}\right)\pi\frac{\Delta C_m}{R_c}\right] \tag{S.117}$$

for the convective heat transfer in the normal direction; note that for a thermostated meniscus, C_{rr} (eq. (14)) simplifies to

$$C_{rr}\Big|_{T_m=T_\infty} = \left(\frac{h_e}{RT_\infty}-1\right)C_{eq0}\frac{T_{rr}}{T_\infty}\,. \tag{S.118}$$

Next, we use the exact result for T_{rr} from S3.5, (S.94), in which we express ΔC_m through x using eqs. (12)-(13); then, we use eq. (S.108) to express x as a function of the stationary thickness h_{st}, thus obtaining the explicit expressions $Pe^{A}_{\text{heat},r}(h_{st})$, $Pe^{A}_{\text{heat},z}(h_{st})$. Finally, we plot the two numbers parametrically versus $x(h_{st})$ for values of h_{st} ranging from h_{cr} to ~10^{-7} m at three different film radii (Figure S. 4). The calculated values of the heat transfer Péclet number ($Pe^{A}_{\text{heat},r}$ ~ 10^{-4}, $Pe^{A}_{\text{heat},z}$ ~ 10^{-4}) indicate that the convective heat transfer through the gas is negligible, as asserted in Section 2.2.

We now turn to the evaluation of the Péclet numbers for mass transport. $Pe_{\text{mass},r}$ compares the integral convective mass flux in the r-direction with the integral diffusive mass flux,

$$Pe_{\text{mass},r} = \left|\frac{J_{\text{convective},r}}{J_{\text{diffusive}}}\right| = \left|\frac{\int_0^{R_f} rV_r\,C\,\mathrm{d}r}{D\sqrt{\left(\int_0^{R_f} r\frac{\partial\Delta C}{\partial r}\mathrm{d}r\right)^2+\left(\int_0^{R_f} r\frac{\partial\Delta C}{\partial z}\mathrm{d}r\right)^2}}\right|_{z=0}\,. \tag{S.119}$$

Substituting the model expression (11) for the concentration profile in the film, eq. (S.109) for V_r and eq. (S.101) for the normal diffusive flux in the definition of the $Pe_{\text{mass},r}$, (S.119), we obtain:

$$Pe_{\text{mass},r} \sim \frac{1}{12}\frac{R_f}{\eta D}\frac{\left(-\frac{s^S T_{rr}R_f^2}{2h}+p_c-\Pi_{vdW}\right)\left(C_{eq0}-\frac{1}{5}C_{rr}R_f^2\right)}{\sqrt{R_f^2\frac{C_{rr}^2}{9}+\frac{1}{16\pi^2}\left[-\frac{8}{3}R_f C_{rr}+\left(2-\sqrt{2}\right)\pi\frac{\Delta C_m}{R_c}\right]^2}}\,. \tag{S.120}$$

We can define a second Péclet number for the convective mass transfer in the z-direction, by analogy with eq. (S.116),

$$Pe_{\mathrm{mass},z} = \left| \frac{J_{\mathrm{convective},z}}{J_{\mathrm{diffusive}}} \right| = \left| \frac{\int_0^{R_\mathrm{f}} r V_z^{\mathrm{G}} C \mathrm{d}r}{D\sqrt{\left(\int_0^{R_\mathrm{f}} r \frac{\partial \Delta C}{\partial r} \mathrm{d}r \right)^2 + \left(\int_0^{R_\mathrm{f}} r \frac{\partial \Delta C}{\partial z} \mathrm{d}r \right)^2}} \right|_{z=0}, \qquad \text{(S.121)}$$

where we use the same estimate for V_z^{G} as in $Pe_{\mathrm{heat},z}^{\mathrm{A}}$ above, $V_z^{\mathrm{G}} \sim v^{\mathrm{G}} J/\pi R_\mathrm{f}^2$ and eq. (S.101) for J, thus obtaining an explicit expression for $Pe_{\mathrm{mass},z}$,

$$Pe_{\mathrm{mass},z} \sim \frac{1}{2\pi} \frac{RT_\infty^{\mathrm{A}}}{p^{\mathrm{o}}} \left| \frac{\left[-\frac{8}{3} R_\mathrm{f} C_{rr} + \left(2-\sqrt{2}\right)\pi \frac{\Delta C_\mathrm{m}}{R_\mathrm{c}} \right] \left(C_{\mathrm{eq}0} - \frac{1}{4} C_{rr} R_\mathrm{f}^2 \right)}{\sqrt{R_\mathrm{f}^2 \frac{C_{rr}^2}{9} + \frac{1}{16\pi^2} \left[-\frac{8}{3} R_\mathrm{f} C_{rr} + \left(2-\sqrt{2}\right)\pi \frac{\Delta C_\mathrm{m}}{R_\mathrm{c}} \right]^2}} \right|. \qquad \text{(S.122)}$$

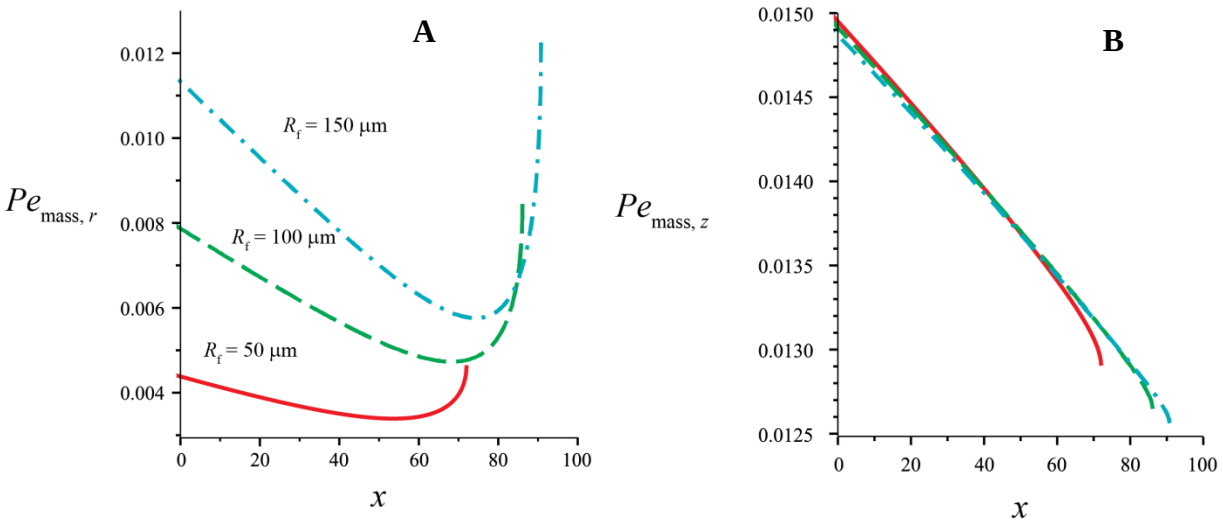

Figure S. 5. Péclet numbers for mass transport at the stationary state for three different values of the film radius (R_f = 50 μm – solid lines, R_f = 100 μm – dashed lines, R_f = 150 μm – dashdot lines). $Pe_{\mathrm{mass},r}$ (**A**) quantifies the ratio of the convective mass flux in the r-direction to the total diffusive mass flux; $Pe_{\mathrm{mass},z}$ (**B**) does the same for the z-direction. The calculated values ($Pe_{\mathrm{mass},r} \sim 10^{-2}$, $Pe_{\mathrm{mass},z} \sim 10^{-2}$) justify our disregard of the convective contribution to the diffusive flux.

As with Pe^{A}_{heat} and Pe^{L}_{heat}, writing eqs. (S.120) and (S.122) explicitly and setting x to $x(h_{st})$, eq. (S.108), we can plot $Pe_{mass,r}$ and $Pe_{mass,z}$ as a function of x using h as a parameter, as seen in Figure S. 5. The low values of the Péclet numbers for mass transport ($Pe_{mass,r} \sim 10^{-3}$-10^{-2}, $Pe_{mass,z} \sim 10^{-2}$) justify our approach of neglecting convective mass transfer for water and nonane films. However, for films formed from the much more volatile hexane, $Pe_{mass,r} \sim 0.1$ and $Pe_{mass,z} \sim 0.1$, which means that convection needs to be included and explains the discrepancy between our model and the experimental data on hexane (see Section 3.3).

As the inclusion of the heat transfer in meniscus introduces no qualitative difference in the properties of the system at the stationary state discussed above, we will not give the analysis for that case here.

7. Effect of the electrostatic disjoining pressure

The experimental data of Yaminsky et al. (Yaminsky et al., 2010a, 2010b) suggest that the electrostatic disjoining pressure (Π_{el}) plays a significant part in the behaviour of evaporating films comprised of pure liquids. According to the simplest possible model for Π_{el}, the DLVO theory, the electrostatic disjoining pressure in a solution of a 1:1 electrolyte is given by the equation (Sheludko, 1 967)

$$\Pi_{el} = \Pi_0 \exp\left(-h / L_D\right), \tag{S.123}$$

with $\Pi_0 = 64 C_{el} RT_\infty \tanh(F\phi^S/RT_\infty)^2$, ϕ^S being the surface potential, C_{el} the electrolyte concentration in the liquid [mol·m^{-3}], F – the Faraday constant and L_D – the Debye length, $L_D = (RT_\infty \varepsilon / 2C_{el}F^2)^{1/2}$, where ε is the absolute dielectric permittivity of the liquid. Yaminsky et al. (Yaminsky et al., 2010a) used eq. (S.123) to fit the measured the disjoining pressure isotherm for pure water films and determined the values $\phi^S = -57$ mV and $C_{el} = 4$ mmol·m^{-3}. However, eq. (S.123) is only valid if $h >> L_D$ (Kralchevsky et al., 2009), which is not fulfilled for films of pure water. DLVO's Π_{el} obeys the general equation (Churaev et al., 1987)

$$\Pi_{el} = RT_\infty C_{el} u(\Phi_m), \tag{S.124}$$

where $u(\Phi) = \Phi + \Phi^{-1} - 2$ is a dimensionless electrostatic energy density, $\Phi = \exp(-F\phi/RT_\infty)$ is the electrostatic Boltzmann factor for a positive monovalent ion and Φ_m is its value at the centre of the film. Φ_m is related to the film thickness through the second integral of the Poisson-Boltzmann equation:

$$h = 2L_D \int_{\Phi_m}^{\Phi^S} \frac{d\Phi}{\Phi\sqrt{u(\Phi) - u(\Phi_m)}}\ , \tag{S.125}$$

with $\Phi^S = \exp(-F\phi^S/RT_\infty)$. Further, for the constant charge regime, we will need the analogue of the Gouy equation for a thin film,

$$\frac{(\rho^S)^2}{2\varepsilon RT_\infty C_{el}} = u(\Phi^S) - u(\Phi_m), \tag{S.126}$$

where ρ^S is the surface charge density due to specifically adsorbed charge.

We will consider two limiting cases for Π_{el}: those of constant surface potential and constant surface charge. The disjoining pressure corresponding to a fixed surface potential of $\phi^S = -57$ mV is determined by eqs. (S.124) and (S.125) (a parametric dependence with parameter Φ_m) and is shown in Figure S. 6.

At constant charge, the adsorption does not depend on the film thickness while ϕ^S does. We determine Π_{el} for this case by simultaneously solving eqs. (S.124), (S.125) and (S.126) for Φ^S, Π_{el} and h at a set of values of Φ_m; the value of the surface charge density is $\rho^S = -250$ μC/m^2 is used (it yields -57 mV at $h \to \infty$ and $\Phi_m \to 1$). The charge regulation regime is, unfortunately, impossible to analyse in the absence of a reasonable hypothesis for the adsorption isotherm of the specifically adsorbed ions.

We will assume that the water we use for forming the films is saturated with CO_2 and we will neglect the presence of divalent carbonate ions in it; using data for the dissociation equilibria of CO_2 from Harned and Davis (Harned and Davis, 1943), we can calculate that under these assumptions, $C_{el} = 2.5$ mmol·m^{-3}. In Figure S. 6, we compare $\Pi(h)$ from eq. (S.123) and the dependences for constant surface potential and charge. In the figure, we see that at constant potential, $\Pi < p_c$ for all h and in the absence of a Marangoni flow, the films are expected to drain under the action of the capillary pressure. However, at constant charge, or when eq. (S.123) is used, for each isotherm there are two thicknesses at which $\Pi_{el} + \Pi_{vdW} = p_c$ of which the one with $\partial\Pi/\partial h < 0$ is stable.

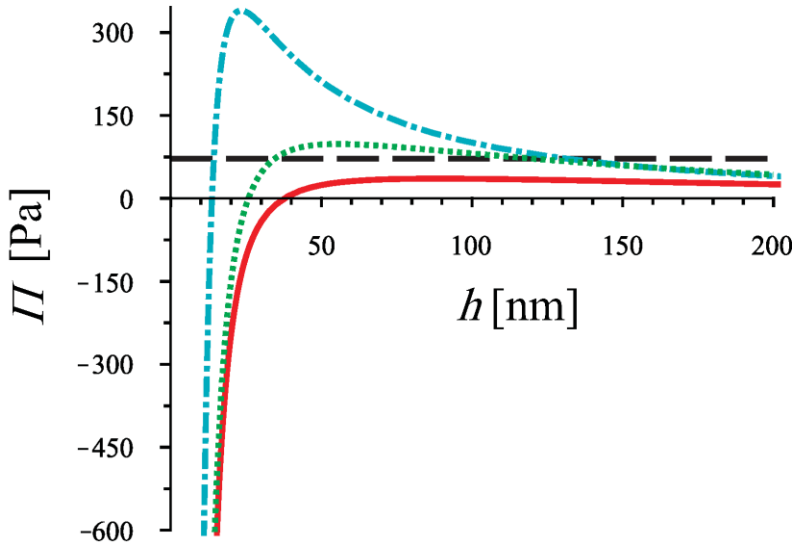

Figure S. 6. Disjoining pressure for the various considered cases for Π_{el}: the limitng formula for thick films, eq. (S.123) – dotted line, $\Pi(h)$ for constant surface potential (ϕ_0 = –57 mV) – solid line, $\Pi(h)$ for constant surface charge – dashdot line, and capillary pressure p_c, eq. (2) from the main text – dashed line. Note that for all considered cases except that of fixed surface potential, there are two points for which $\Pi(h) = p_c$ and equilibrium non-evaporating films are predicted to exist.

We follow the approach from Section 2.7 to derive the stability diagram of evaporating films in with both a van der Waals and an electrostatic disjoining pressure. We determine the normal velocity V_z, from the normal force balance at the surface, which has the form (28), but with $\Pi = \Pi_{el} + \Pi_{vdW}$. The solution for the normal velocity itself, eq. (30), is amended in the same way,

$$V_z \approx \frac{1}{8}\frac{R_f^2 s^S T_{rr}}{\eta} - \frac{h}{4\eta}\left(p_c - \Pi\right). \tag{S.127}$$

As in Section 2.7, the mass balance (31) can be simplified to

$$\frac{dh}{dt} \approx 2V_z \ . \tag{S.128}$$

Substituting eq. (S.127), the explicit expression (22) for T_{rr} and the definition of the relative humidity, x, into eq. (S.128) with the right-hand side set to zero, we obtain an equation for the quasistationary film thickness as a function x. It is, however, more convenient to work with the inverse function, $x(h_{st})$:

$$x = \frac{C_{eq}}{C_{eq0}}\left[1 + \frac{\Delta T_m \kappa}{C_{eq} D h_e} + \frac{16}{3\pi\left(2-\sqrt{2}\right)} h_{st} \frac{R_c}{R_f} \frac{\left(p_c - \Pi\right)}{T_m s^S}\left(1 - \frac{h_e}{RT_m} - \frac{\kappa T_m}{C_{eq} D h_e}\right)\right]. \quad \text{(S.129)}$$

Just as in Section 2.6, the quasistationary film thickness h_{st} depends on time implicitly through T_m – as the meniscus cools down, the Marangoni flow weakens and h_{st} diminishes. To analyse the evolution of h_{st} with time, we first calculate the temperature difference between meniscus and air, ΔT_m, at a number of points in time using eq. (27). Then, we substitute the calculated ΔT_m into eq. (S.129) for $x(h_{st})$. Setting the humidity to a particular value, x_{exp} we calculate h_{st} at each moment from the equation $x(h_{st}) = x_{exp}$. We do that using three different forms of $\Pi_{el}(h)$ – eq. (S.123), and polynomial expressions fit to the dependences for constant charge and constant potential illustrated in Figure S. 6.

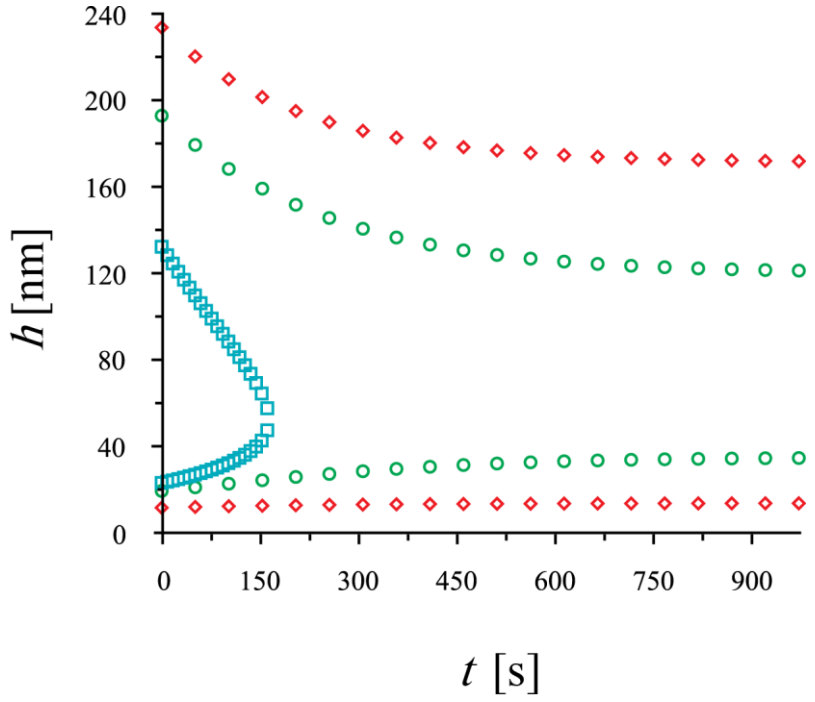

Figure S. 7. Quasistationary thickness as a function of time, $h_{st}(t)$, for a water film of R_f = 150 μm with both electrostatic and van der Waals contributions to the disjoining pressure (x = 89%). The curves are calculated with Π_{el} according to eq. (S.123) (circles), as well as in the constant surface potential (squares) and constant surface charge (diamonds) regimes.

The $h(t)$ obtained in this way are plotted in Figure S. 7 for x_{exp} = 0.9; predictably, in all cases, the addition of Π_{el} leads to an increase in film lifetime with respect to the case with no

electrostatic repulsion (Figure 3). In the constant surface potential regime, Figure S. 7 predicts a lifetime approximately three times longer than that in Figure 3. Furthermore, using Π_{el} for the constant surface charge regime or the asymptotic eq. (S.123) leads to the prediction that the films become stable at $t \to \infty$. As seen in the graph, for the latter cases, when ΔT_m reaches its stationary value (see Section 2.6) and the Marangoni effect vanishes, the film is stabilized by electrostatic repulsion and reaches its equilibrium thickness, h_{eq}. For thin water films, its value is h_{eq} = 170 nm in the limit of constant charge (or h_{eq} = 120 nm according to the asymptotic formula eq. (S.123)). However, as we pointed out in Section 2.5, the electrostatic repulsion is likely in the charge regulation regime rather than any of the limiting cases considered here.

8. The cooling of the meniscus

We need to clarify how the total heat capacity, which appears in the heat balance for the case of a cold meniscus (58), is calculated. C_p is the sum of the total heat capacities of the liquid (C_p^L) and the part of the glass capillary in direct contact with the fluid ($C_{p\,glass}$).

$$C_p = C_p^L + C_{p\,glass}. \tag{S.130}$$

The heat capacity of the spherical meniscus is determined by its volume:

$$C_p^L = \frac{2}{3}\pi R_c^3 \rho c_p. \tag{S.131}$$

The part of the glass capillary in contact with the fluid is a cylindrical shell of inner radius R_c, outer radius $R_c + d_{glass}$ and height $2R_c$. The corresponding heat capacity is:

$$C_{p\,glass} = \rho_{glass} V_{glass} c_{p\,glass} = 2R_c \pi \left(2R_c d_{glass} + d_{glass}^2\right) \rho_{glass} c_{p\,glass}, \tag{S.132}$$

where V_{glass} [m^3], ρ_{glass} [kg/m^3] and $c_{p\,glass}$ [$J \cdot kg^{-1} \cdot K^{-1}$] are respectively the volume, the density and the specific heat capacity of the glass. For borosilicate glass, typically used for laboratory equipment, ρ_{glass} = 2200 kg/m^3 and $c_{p\,glass}$ = 830 $J \cdot kg^{-1} \cdot K^{-1}$. We used two Sheludko cells, one with R_c = 2 mm and d_{glass} ~ 1 mm and the other with R_c = 2.3 mm and d_{glass} ~ 0.5 mm. For water films in the former case, $C_{p\,glass} \approx 0.11$ $J \cdot K^{-1}$ and $C_p^L = 0.07$ $J \cdot K^{-1}$, while for the latter, $C_{p\,glass} \approx 0.07$ $J \cdot K^{-1}$ and $C_p^L = 0.11$ $J \cdot K^{-1}$.

Let us also note that for small temperature differences, the divisor of the integrand in eq. (27) from the main text, which controls the dependence of the meniscus temperature on time, can be expanded in a series with respect to ΔT_m up to the linear term, leading to

$$t \approx -\frac{C_p}{4.57 R_\mathrm{c}} \frac{T_\infty}{h_\mathrm{e} D C_{\mathrm{eq}0}} \frac{\ln\left[1+\left(\frac{h_\mathrm{e}}{R T_\infty}-1+\frac{\kappa T_\infty}{h_\mathrm{e} D C_{\mathrm{eq}0}}\right)\frac{\Delta T_\mathrm{m}}{T_\infty}\frac{1}{1-x}\right]}{\frac{h_\mathrm{e}}{R T_\infty}-1+\frac{\kappa T_\infty}{h_\mathrm{e} D C_{\mathrm{eq}0}}}, \tag{S.133}$$

which gives the correct temporal evolution of temperature if x close to 1; otherwise, it is only adequate for the initial time period – consult Figure S. 8, in which it is compared with the more exact expression (27).

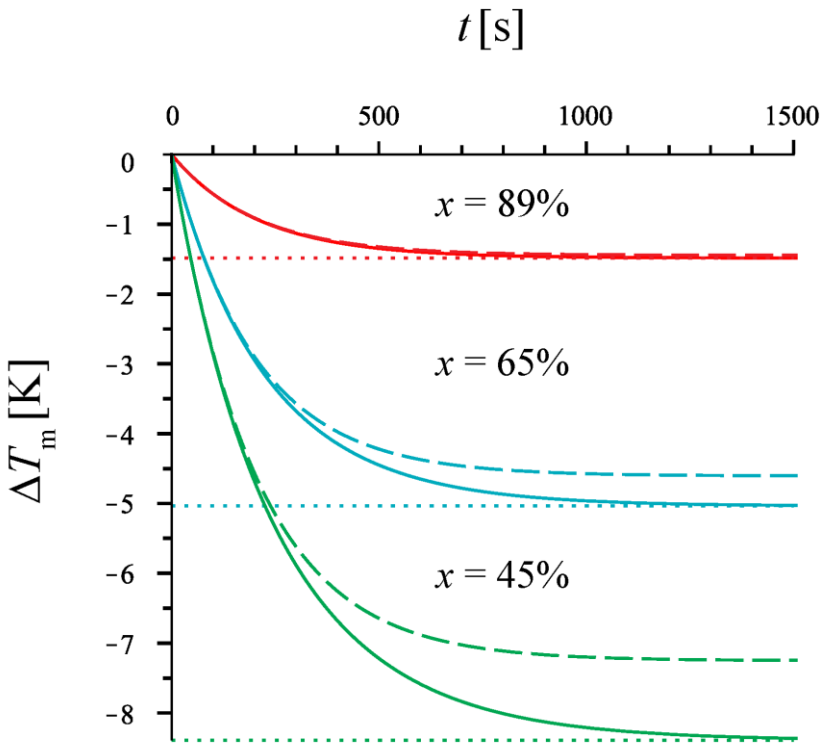

Figure S. 8. Temperature difference ΔT_m between meniscus and air as a function of time for three values of the relative saturation x of the ambient air. The solid lines are calculated according to the exact dependence (27), and the dashed lines represent the approximate analytic eq. (S.133). The stationary temperature $\Delta T_{\mathrm{m,st}}$ at the plateau is marked with dotted lines. The calculations were made for water film in cell of radius R_c = 2 mm, see S1 for the parameter values.

As noted in the main text, the observed decrease of the film lifetime as a function of the time after cell loading, t_{load}, can due to the consecutive formation of several films in the Scheludko cell. This can lead to a significant cooling of the whole capillary cell rather than just the part of it that is in contact with the fluid as we assume in Section 2. In that case, the initial temperature of the meniscus would be lower than the ambient T_{∞}, and the lifetime of the film would be decreased – from eq. (27) in the main text it follows that

$$\tau = -\frac{C_p}{4.57R_{\mathrm{c}}}\int_{\Delta T_{\mathrm{m,initial}}}^{\Delta T_{\mathrm{m,cr}}} \frac{\mathrm{d}\Delta T_{\mathrm{m}}}{\left(\kappa\Delta T_{\mathrm{m}} + h_{\mathrm{e}} D\Delta C_{\mathrm{m}}\right)} < -\frac{C_p}{4.57R_{\mathrm{c}}}\int_{0}^{\Delta T_{\mathrm{m,cr}}} \frac{\mathrm{d}\Delta T_{\mathrm{m}}}{\left(\kappa\Delta T_{\mathrm{m}} + h_{\mathrm{e}} D\Delta C_{\mathrm{m}}\right)}, \qquad \text{(S.134)}$$

where $\Delta T_{\mathrm{m,cr}}$ is the solution to eq. (39) for T_{m} and the initial temperature of the meniscus is T_{∞}+ $\Delta T_{\mathrm{m,initial}}$.

As a final remark on the subject of the cooling down of the meniscus, let us note that we can use the dependence $x(\Delta T_{\mathrm{m,st}})$, eq. (26), to predict the stationary temperature difference $\Delta T_{\mathrm{m,st}}$. Plotting $x(\Delta T_{\mathrm{m,st}})$ on the horizontal axis and $\Delta T_{\mathrm{m,st}}$ on the vertical one, we obtain the stationary temperature difference at different relative saturations; the resulting curve is shown in Figure S. 9.

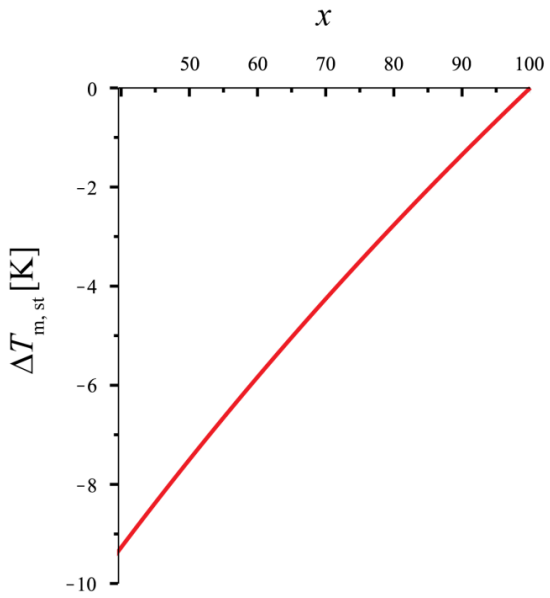

Figure S. 9. Stationary temperature difference $\Delta T_{\mathrm{m,st}}$ between the meniscus and the ambient air as a function of the relative saturation x of the ambient air, according to eq. (26) for the inverse function $x(\Delta T_{\mathrm{m,st}})$. The calculations were made for water, see S1 for the parameter values.

9. Additional experimental data

n-Nonane. *Saturated atmosphere, x* = 1. A photograph of a non-evaporating nonane film is given in Figure 6D in the main text. The lifetime of the non-evaporating nonane films increased with the film radius – for R_f = 50, 62.5 and 100 μm, we observed τ ~ 25, 35 and 50 s respectively. As with water films under saturated conditions, no significant aging effects (such as dependence of τ on t_{load}) were observed, which can be expected in the absence of evaporation-driven cooling. Exceptions were the first 10 films (t_{load} < 30 min): unlike those in Figure 7 from the main text, during their lifetimes (40-50 s), their radii shrunk from the initial R_f = 100 down to 50-80 μm before rupture. Their different behaviour seems related to the initial incomplete saturation.

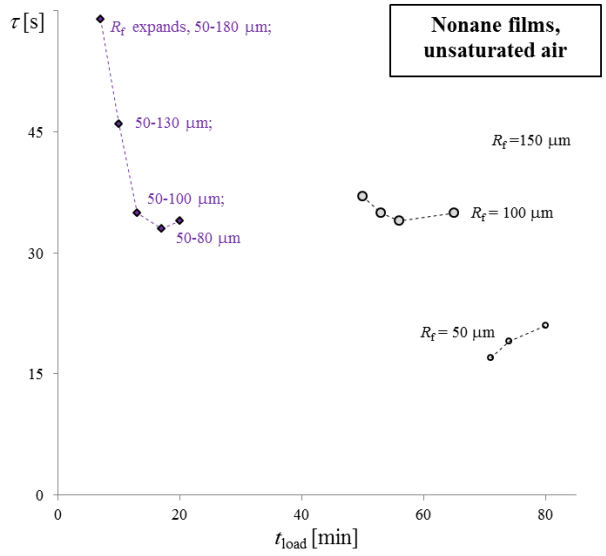

Figure S. 10. Lifetime τ of nonane films formed during one experimental run vs. time after loading the cell, t_{load} (21°C, R_c = 2 mm). Evaporating films formed in a open cell ($x \approx 0$). The first five films expanded during their lifetime; the radii of those formed after 40 min were constant throughout their lifetimes.

Figure S. 10 complements Figure 7 from the main text and shows the dependence of the lifetime of thin nonane films in an unsaturated environment (x ~ 0%) as a function of the time

after cell loading, t_{load}. The first five films expanded during from R_f = 50 μm initially to 80-180 μm at the moment of their rupture; the radii of those formed after 40 min were constant throughout their lifetimes. As noted in the main text, the dependence of film lifetime on R_f agrees qualitatively with the theoretical prediction – films of radius ~50, 100 or 150 μm have $\tau \sim$ 20, 35 and 45 s, whereas the model predicts τ = 0, 14 and 237 s, respectively. Notably, in contrast with the main prediction of our theory, the nonane films formed in a saturated environment were more stable than the evaporating ones – compare Figure 7 from the main text with Figure S. 10.

As explained in the main text, Figure S. 11 presents the comparison between the predictions of our model and the experimental dependence of thickness on time for a thin nonane film situated in an unsaturated environment (x ~ 0 %). The critical thickness of film rupture was ~42.9 nm, whereas the theoretical value is 60.3 nm. The experimental drainage time differs from the theoretical by a factor of ~5, but this is satisfactory agreement given the approximate nature of our expressions for the heat and mass fluxes (19)-(20) and (23)-(24).

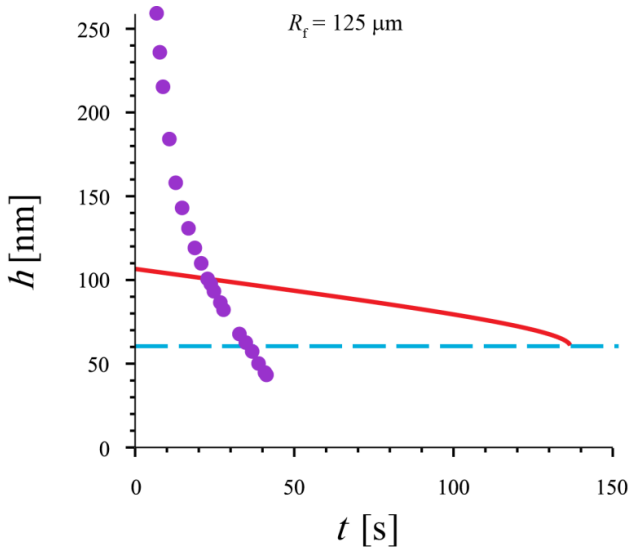

Figure S. 11. Film thickness vs. time for nonane film of radius R_f ~ 125 μm in an unsaturated environment (x ~ 0%).

Reference list

Badam, V.K., Kumar, V., Durst, F., Danov, K., 2007. Experimental and theoretical investigations on interfacial temperature jumps during evaporation. Exp. Therm. Fluid Sci. 32, 276–292. doi:10.1016/j.expthermflusci.2007.04.006

Bergman, T.L., Lavine, A.S., Incropera, F.P., Dewitt, D.P., 2011. Fundamentals of Heat and Mass Transfer, 7th ed. Wiley, Hoboken, N.J.

Butt, H.-J., Kappl, M., 2010. Surface and Interfacial Forces. Wiley-VCH Verlag GmbH & Co. KGaA, Weinheim, Germany. doi:10.1002/9783527629411

Churaev, N.V., Derjaguin, B.V., Muller, V.M., 1987. Surface Forces. Springer Science + Business Media, LLC, New York.

Cussler, E.L., 2009. Diffusion: Mass Transfer in Fluid Systems, 3rd ed. Cambridge University Press, Cambridge.

Dondlinger, M., Margerit, J., Dauby, P.C., 2005. Weakly nonlinear study of Marangoni instabilities in an evaporating liquid layer. J. Colloid Interface Sci. 283, 522–532. doi:10.1016/j.jcis.2004.09.005

Drummond, C.J., Chan, D.Y.C., 1997. van der Waals Interaction, Surface Free Energies, and Contact Angles: Dispersive Polymers and Liquids. Langmuir 13, 3890–3895. doi:10.1021/la962131c

Erdelyi, A. (Ed.), 1954. Tables of integral transforms, Volume I: based, in part, on notes left by Harry Bateman. McGraw-Hill Book Company, Inc., New York.

Erdelyi, A. (Ed.), 1953a. Higher Transcendental Functions, Volume II: based, in part, on notes left by Harry Bateman. McGraw-Hill Book Company, Inc., New York.

Erdelyi, A. (Ed.), 1953b. Higher Transcendental Functions, Volume I: based, in part, on notes left by Harry Bateman. McGraw-Hill Book Company, Inc., New York.

Fuchs, N.A., 1959. Evaporation and Droplet Growth in Gaseous Media. Pergamon Press, London.

Harned, H.S., Davis, R., 1943. The Ionization Constant of Carbonic Acid in Water and the Solubility of Carbon Dioxide in Water and Aqueous Salt Solutions from 0 to 50°. J. Am. Chem. Soc. 65, 2030–2037. doi:10.1021/ja01250a059

Israelachvili, J.N., 2011. Intermolecular and Surface Forces, 3rd ed. Academic Press, London.

Jasper, J.J., Kring, E. V, 1955. The Isobaric Surface Tensions and Thermodynamic Properties of the Surfaces of a Series of n-Alkanes, C5 to C18, 1-Alkenes, C6 to C16, and of n-Decylcyclopentane, n-Decylcyclohexane and n-Dcylbenzene. J. Phys. Chem. 59, 1019–1021. doi:10.1021/j150532a006

Kestin, J., Sokolov, M., Wakeham, W.A., 1978. Viscosity of liquid water in the range −8 °C to 150 °C. J. Phys. Chem. Ref. Data 7, 941–948. doi:10.1063/1.555581

Kralchevsky, P.A., Danov, K.D., Denkov, N.D., 2009. and Interfaces, in: Birdi, K.S. (Ed.), Handbook of Surface and Colloid Chemistry. Boca Raton, FL, p. 197.

Langmuir, I., 1915. The dissociation of hydrogen into atoms. [Part II.] Calculation of the degree of dissociation and the heat of formation. J. Am. Chem. Soc. 37, 417–458. doi:10.1021/ja02168a002

Lee, C.Y., Wilke, C.R., 1954. Measurements of Vapor Diffusion Coefficient. Ind. Eng. Chem. 46, 2381–2387. doi:10.1021/ie50539a046

Levich, V.G., 1962. Physicochemical Hydrodynamics. Prentice-Hall, Inc., Englewood Cliffs, N.J.

Lide, D.R. (Ed.), 2005. CRC Handbook of Chemistry and Physics, Internet Version 2005. CRC Press, Boca Raton, FL.

Lugg, G. a., 1968. Diffusion coefficients of some organic and other vapors in air. Anal. Chem. 40, 1072–1077. doi:10.1021/ac60263a006

Nieto de Castro, C.A., Li, S.F.Y., Nagashima, A., Trengove, R.D., Wakeham, W.A., 1986. Standard Reference Data for the Thermal Conductivity of Liquids. J. Phys. Chem. Ref. Data 15, 1073–1086. doi:10.1063/1.555758

Radoëv, B.P., Dimitrov, D.S., Ivanov, I.B., 1974. Hydrodynamics of thin liquid films effect of the surfactant on the rate of thinning. Colloid Polym. Sci. 252, 50–55. doi:10.1007/BF01381695

Reynolds, O., 1886. On the Theory of Lubrication and Its Application to Mr. Beauchamp Tower's Experiments, Including an Experimental Determination of the Viscosity of Olive Oil. Proc. R. Soc. London 40, 191–203. doi:10.1098/rspl.1886.0021

Růžička, V., Zábranský, M., Majer, V., 1991. Heat capacities of organic compounds in liquid state II. C1 to C18 n-alkanes. J. Phys. Chem. Ref. Data 20, 405–444. doi:10.1063/1.555883

Sabbah, R., Xu-wu, A., Chickos, J.S., Planas Leitão, M.L., Roux, M.V., Torres, L.A., 1999. Reference materials for calorimetry and differential thermal analysis. Thermochim. Acta 331, 93.

Scriven, L.E., Sternling, C. V., 1960. The Marangoni Effects. Nature 187, 186–188. doi:10.1038/187186a0

Sheludko, A., 1967. Thin liquid films. Adv. Colloid Interface Sci. 1, 391–464. doi:10.1016/0001-8686(67)85001-2

Tsoumpas, Y., Dehaeck, S., Rednikov, A., Colinet, P., 2015. Effect of Marangoni Flows on the Shape of Thin Sessile Droplets Evaporating into Air. Langmuir 31, 13334–13340. doi:10.1021/acs.langmuir.5b02673

Vargaftik, N.B., Volkov, B.N., Voljak, L.D., 1983. International Tables of the Surface Tension of Water. J. Phys. Chem. Ref. Data 12, 817–820. doi:10.1063/1.555688

Visser, J., 1972. On Hamaker constants: A comparison between Hamaker constants and Lifshitz-van der Waals constants. Adv. Colloid Interface Sci. 3, 331–363. doi:10.1016/0001-8686(72)85001-2

Wilke, C.R., Lee, C.Y., 1955. Estimation of Diffusion Coefficients for Gases and Vapors. Ind. Eng. Chem. 47, 1253–1257. doi:10.1021/ie50546a056

Yaminsky, V. V., Ohnishi, S., Vogler, E.A., Horn, R.G., 2010a. Stability of Aqueous Films between Bubbles. Part 1. The Effect of Speed on Bubble Coalescence in Purified Water and Simple Electrolyte Solutions. Langmuir 26, 8061–8074. doi:10.1021/la904481d

Yaminsky, V. V., Ohnishi, S., Vogler, E.A., Horn, R.G., 2010b. Stability of Aqueous Films between Bubbles. Part 2. Effects of Trace Impurities and Evaporation. Langmuir 26, 8075–8080. doi:10.1021/la904482n

Yiantsios, S.G., Higgins, B.G., 2006. Marangoni flows during drying of colloidal films. Phys. Fluids 18, 82103. doi:10.1063/1.2336262

Zhu, Q., Kato, S., Murakami, S., Ito, K., 2007. 3D-CFD analysis of diffusion and emission of VOCs in a FLEC cavity. Indoor Air 17, 178–188. doi:10.1111/j.1600-0668.2006.00453.x